

WL-TR-1997-3085

FINITE ELEMENT NONLINEAR RANDOM
RESPONSE OF COMPOSITE PANELS OF
ARBITRARY SHAPE TO ACOUSTIC AND
THERMAL LOADS



CHUH MEI
ROGER R. CHEN

OLD DOMINION UNIVERSITY
PO BOX 6369
NORFOLK VA 23508-0369

OCTOBER 1997

INTERIM REPORT FOR 04/30/1991 - 05/31/1995

APPROVED FOR PUBLIC RELEASE; DISTRIBUTION IS UNLIMITED.

19980727 063

FLIGHT DYNAMICS DIRECTORATE
WRIGHT LABORATORY
AIR FORCE MATERIEL COMMAND
WRIGHT PATTERSON AFB OH 45433-7542

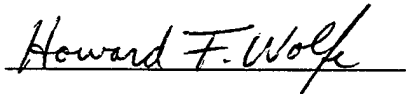
DTIC QUALITY INSPECTED 1

NOTICE

When Government drawings, specifications, or other data are used for any purpose other than in connection with a definitely Government related procurement, the United States Government incurs no responsibility nor any obligation whatsoever. The fact that the government may have formulated, or in any way supplied the said drawings, specifications, or other data, is not to be regarded by implication or otherwise as in any manner construed as licensing the holder or any other persons or corporation, or as conveying any rights or permission to manufacture, use, or sell any patented invention that may in any way be related thereto.

This report is releasable to the National Technical Information Services (NTIS). At NTIS, it will be available to the general public, including foreign nations.

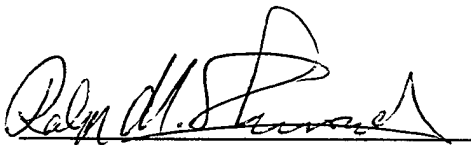
This report has been reviewed and is approved for Publication.



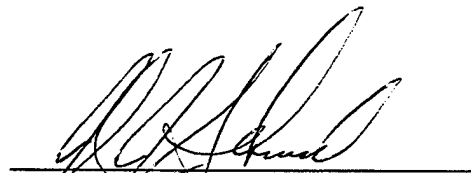
Howard F. Wolfe, PhD.
Senior Aerospace Engineer
Acoustics and Sonic Fatigue Branch



Kenneth R. Wentz
Aerospace Engineer
Acoustics and Sonic Fatigue Branch



Ralph M. Shimovetz
Team Leader
Acoustics and Sonic Fatigue Branch



Capt. Joël J. Schubbe, Ph.D.
Chief, Acoustics and Sonic Fatigue Branch
Air Force Research Lab

If your address has changed, if you wish to be removed from our mailing list, or if the addressee is no longer employed by your organization, please notify AFRL/VASS BLDG 24C, 2145 FIFTH ST STE 2, WRIGHT-PATTERSON AFB, OH 45433-7006 to help maintain a current mailing list.

Copies of this report should not be returned unless security considerations, contractual obligation, or notice on a specified document requires return.

REPORT DOCUMENTATION PAGE			Form Approved OMB No. 0704-0188	
Public reporting burden for this collection of information is estimated to average 1 hour per response, including the time for reviewing instructions, searching existing data sources, gathering and maintaining the data needed, and completing and reviewing the collection of information. Send comments regarding this burden estimate or any other aspect of this collection of information, including suggestions for reducing this burden, to Washington Headquarters Services, Directorate for Information Operations and Reports, 1215 Jefferson Davis Highway, Suite 1204, Arlington, VA 22202-4302, and to the Office of Management and Budget, Paperwork Reduction Project (0704-0188), Washington, DC 20503.				
1. AGENCY USE ONLY (Leave blank)		2. REPORT DATE 31 OCTOBER 1997		3. REPORT TYPE AND DATES COVERED INTERIM - AUG91-OCT 97
4. TITLE AND SUBTITLE Finite Element Nonlinear Random Response of Composite Panels of Arbitrary Shape to Acoustic and Thermal Loads			5. FUNDING NUMBERS CF33615-91-C-3205 PE 62201F PR 2302 TASK N1 WU 07	
6. AUTHOR(S) Professor Chuh Mei and Dr. Roger R. Chen				
7. PERFORMING ORGANIZATION NAME(S) AND ADDRESS(ES) Old Dominion University PO Box 6369 Norfolk, VA 23508-0369			8. PERFORMING ORGANIZATION REPORT NUMBER MDC 97P0075	
9. SPONSORING/MONITORING AGENCY NAME(S) AND ADDRESS(ES) Flight Dynamics Directorate Wright Laboratory Air Force Materiel Command Wright-Patterson Air Force Base, OH 45433-7542 POC: Dr. Howard F. Wolfe (937) 255-5200 X456, AFRL/VASS, WPAFB			10. SPONSORING/MONITORING AGENCY REPORT NUMBER WL-TR-97-3085	
11. SUPPLEMENTARY NOTES				
12a. DISTRIBUTION AVAILABILITY STATEMENT Approved For Public Release; Distribution Unlimited			12b. DISTRIBUTION CODE	
13. ABSTRACT (Maximum 200 words) A finite element formulation in modal coordinates is presented for postbuckling of thin laminated composite plates subjected to combined thermal and mechanical loads. The mechanical load considered is a uniformly distributed transverse load which is to simulate the static pressure differential applied to the aircraft skin panel. A modal participation value is defined and the minimum number of modes for convergence and accurate postbuckling solution can be determined. The modal formulation reduces the number of coupled nonlinear equations in the structure nodal degrees of freedom of hundreds, if not thousands, to a number of coupled nonlinear equations in the modal coordinates of usually ten. This greatly reduces the computation costs. Deflection shape change for a long rectangular plate is observed and investigated.. Three multiple postbuckling solutions or branches are obtained from the modal formulation. The total potential energy and its second variation indicate that there exist only two stable, primary and secondary branches and the third is an unstable peak.				
14. SUBJECT TERMS SONIC FATIGUE, RANDOM RESPONSE, FATIGUE AND ACOUSTICS			15. NUMBER OF PAGES 108	
			16. PRICE CODE	
17. SECURITY CLASSIFICATION OF REPORT UNCLASSIFIED	18. SECURITY CLASSIFICATION OF THIS PAGE UNCLASSIFIED	19. SECURITY CLASSIFICATION OF ABSTRACT UNCLASSIFIED	20. LIMITATION OF ABSTRACT SAR	

TABLE OF CONTENTS

FOREWORD	viii
Chapter 1	INTRODUCTION	1
1.1	Background	1
1.2	Literature Survey	4
1.3	Outline of the study	9
Chapter 2	FORMULATIONS	12
2.1	Element Displacement Functions	13
2.2	Nonlinear Strain-Displacement Relations	15
2.3	Constitutive Law	16
2.4	Resultant Laminate Forces and Moments	17
2.5	The Principle of Virtual Work	18
2.6	Element Equations of Motion	22
2.7	Grazing Acoustic Wave	24
Chapter 3	SOLUTION PROCEDURE	28
3.1	Static Component and Dynamic Component	28
3.2	Thermal Buckling and Large Thermal Deflection	30
3.3	Nonlinear Random Response	31
3.4	Strain Formulas	40

Chapter 4	NUMERICAL RESULTS AND DISCUSSION	42
4.1	Formulation and Computer Program Validation	42
4.2	Thermal Buckling and Postbuckling Results	44
4.3	Nonlinear Random Response	47
4.4	Acoustic-Thermal Response	48
Chapter 5	CONCLUSIONS	83
REFERENCES	86
Appendix A	THE FORMULATIONS FOR $C_{\psi\psi_{ij}}$'s	91
Appendix B	THE ELEMENT MATRICES	93

LIST OF TABLES

Table		Page
4.1	Results for a rhombic cantilever plate	53
4.2	Results of RMS(W_{\max}/h) and micro-strain for simply support plate	53
4.3	Linear natural frequencies of Panel 1	53
4.4	Convergence of RMS(W_{\max}/h) with Number of the Modes	54
4.5	The Natural Frequencies (rad/sec.)	54
4.6	Frequencies for the baseline configuration (rad/sec.)	54

LIST OF FIGURES

Figure		Page
2.1	An Initially Deflected and Stressed Plate	26
2.2	A Typical MIN3 Element	26
2.3	A Mindlin Triangular Plate Element	27
2.4	Grazing Acoustic Wave	27
4.1	Twisted ribbon test via transverse corner forces	55
4.2	Twisted ribbon test via twisting corner moments	55
4.3	Rhombic cantilever plate	56
4.4	W_{max}/h vs. $\Delta T/\Delta T_{ref}$ for (0/90) composite plate	56
4.5	W_{max}/h vs. ΔT for an isosceles triangular plate	57
4.6	Dimensionless critical temperature vs. a/h for a rectangular laminate	57
4.7	W_{max}/h vs. ΔT for various number of layers	58
4.8	W_{max}/h vs. ΔT for a long rectangular laminate	58
4.9	Centerline deflection of a 36X12X0.048 in. angle-ply (60/-60) laminate	59
4.10	W_{max}/h vs. ΔT for a long rectangular laminate with mechanical load 0.01 psi	59
4.11	Centerline deflection of a 36x12X0.048 in. angle-ply (60/-60) laminate with mechanical load 0.01 psi	60
4.12	W_{max}/h vs. skew angle for rectangular plates	60
4.13	RMS W_{max}/h vs. SPL for Panel 1	61
4.14	RMS max. micro strain vs. SPL for Panel 1	61
4.15	The maximum deflection spectrum vs. frequency for Panel 1	62
4.16	RMS W_{max}/h vs. SPL for Panel 2	62
4.17	RMS max. micro strain vs. SPL for Panel 2	63
4.18	The maximum deflection spectrum vs. frequency for Panel 2	63
4.19	Planform of Panel 3	64
4.20	RMS W_{max}/h vs. SPL for Panel 3	64
4.21	RMS max. micro strain vs. SPL for Panel 3	65

4.22	The maximum deflection spectrum vs. frequency for Panel 3	65
4.23	RMS (W_{max}/h) vs. SPL for the baseline configuration	66
4.24	Micro-strain vs. SPL for the baseline configuration	66
4.25	The maximum deflection spectrum vs. frequency for the baseline configuration at SPL = 130 dB	67
4.26	RMS (W_{max}/h) vs. SPL for the simply supported panel	67
4.27	Micro-strain vs. SPL for the simply supported panel	68
4.28	The maximum deflection spectrum vs. frequency for the simply supported panel	68
4.29	The mode shapes of (0/90) clamped panel	69
4.30	The mode shapes of (0/90) clamped panel	72
4.31	The mode shapes of (0/90) clamped panel	75
4.32	RMS (W_{max}/h) vs. SPL for the (0/90) panel	78
4.33	RMS max. micro strain vs. SPL for the (0/90) panel	79
4.34	RMS (W_{max}/h) vs. SPL for a skewed pane	79
4.35	RMS max. micro strain vs. SPL for a skewed panel	80
4.36	Distributions of RMS W/h along the center line of the panel	80
4.37	The maximum deflection spectrum vs. frequency for the simply supported panel subjected to grazing wave	81
4.38	RMS (W_{max}/h) vs. SPL for the simply supported panel with initial deflection W_0	81
4.39	RMS max. Micro-strain vs. SPL for the simply supported plate with initial deflection W_0	82
4.40	RMS max. Micro-strain vs. SPL for the simply supported plate with initial imperfection W_0	82

FOREWORD

The research results contained in this technical report were performed under an Air Force Contract F33615-91-C-3205 entitled, "Finite Element Thermal Acoustic Nonlinear Analysis of Aerospace Structures." The report is based essentially on a Ph. D. dissertation prepared by Roger R. Chen under the supervision of Dr. Chuh Mei. The document presents a finite element formulation and solution procedure for the prediction of nonlinear response of composite plates of arbitrary shape subjected to intense acoustic and thermal loads. The work was conducted at the Department of Aerospace Engineering, Old Dominion University. Mr. Kenneth R. Wentz and Dr. Howard F. Wolfe, WL/FIBGD, Structural Dynamics Branch, Flight Dynamics Directorate, were the technical monitors.

Chapter 1

INTRODUCTION

1.1 Background

“Jet Crash Off Italy Kills 35” The New York Times reported on January 11, 1954. “Rome, Jan. 10 — Thirty-five persons were almost certainly killed when a British Comet jet airliner crashed into the sea this morning about halfway between the islands of Elba and Monte Cristo, off the Italian western coast.” It was Monday, when people went to work, they read this news very sadly. The jet airliner was the Comet, the first propelled by jet turbo engine.

The news surprised the world aircraft designers and manufacturers. After exhaustive investigation and tests on components of the Comet, it was concluded that the accident was caused by fatigue failure of the pressurized cabin. The small fatigue crack originated from a corner of an opening in the fuselage. Since then, extra additional attention has been focused on airframe fatigue design. It has been realized that such failures can substantially increase the maintenance burden and life cycle cost of the aircraft.

In the late 1950's, incidents were reported in which structural components close to high intensity jet exhausts were reaching such high levels of vibration response, due to acoustic excitation, that fatigue cracks could develop and spread quite rapidly. These incidents alerted industry, university and research centers to the possibility of serious design problems as the performance of aircraft and engines increased. Since then, the acoustically induced fatigue failures in aircraft have been one of the major

design considerations. A considerable number of investigations sponsored by USAF and AGARD have been carried out during the 1960's and early 1970's. This series of research lead to design monographs of every type of metal structures. It made it possible for aircraft designers to produce satisfactory structures.

This was the situation towards the middle of 1970's. Although the power of the jet engines was still increasing dramatically, the pressure levels were not increasing because of the use of the higher bypass configurations in engine design which are needed to reduce the community noise. This lead to a great reduction in the research and development activity on sonic fatigue.

In the mid and late 1980s, new interest in random vibration was raised primarily as a result of advances in high speed flight. The missions for these high speed flight vehicles will expose structures to severe acoustic and thermal loads. These include the F-22 advanced tactical fighter (ATF), the supersonic advanced short take-off and vertical landing aircraft (ASTOVL), the national aerospace plane (NASP) and the high speed civil transport (HSCT). The new vectored thrust propulsion systems on ATF and ASTOVL provide short take-off and landing capability, and also increased maneuverability. Most designs feature engine exhaust locations that are positioned near the aircraft mass center, and exhaust jets are directed either onto, or nearly onto, the aircraft structure. Estimates of acoustic loads indicate that for some vectored thrust directions most of the aircraft is immersed in an acoustic field with levels well above 150 dB, with levels much higher near the nozzle (Mixon, 1988). Exhaust temperatures may exceed 1000°F in the region of nozzle, and therefore the structure must withstand high thermal loads. In addition, the HSCT, ATF and NASP will fly at supersonic/hypersonic speeds and will be exposed to intense in-flight acoustic and thermal environments (Pozefsky et al., 1989). Due to

aerodynamic heating, the structures will experience high temperatures with large thermal gradients.

To meet increased performance requirements, new complex, lightweight structures and advanced materials will be required. The complex structures under consideration have significant uncertainties in fatigue behavior due to intense acoustic loads in the presence of high temperatures. The thermal environment can affect acoustic fatigue by introducing thermal inplane forces and thermal bending moments, as well as altering (temperature dependent) material properties. Such thermal effects may also introduce large distortions and snap-through (or oil-canning) behavior, alter buckling loads and modify vibration characteristics. The intense acoustic loads can affect fatigue life by introducing large deflection geometrical nonlinearities, modal coupling and multiple-mode participation (Mei and Wolfe, 1986). Such high sound pressure levels may even drive the structures to have damping nonlinearity (Mei and Prasad, 1987). Because of high costs and difficulties with instrumentation in experiments at high acoustic intensity and elevated temperatures, reliable experimental data is difficult to acquire. Thus, in the design process, greater emphasis will be placed on analytical and computational methods. This brings a tremendous challenge to the analysts for predicting nonlinear response of complex structures subjected to acoustic and thermal loads.

A fundamental challenge of thermo-acoustic random response of aerospace structures is the multi-disciplinary nature of the problem. The thermal environment strongly affects the structural random response because of the development of restraint forces due to thermal expansion and the change of material properties at elevated temperatures. Since the structural response due to high levels of acoustic loads is highly nonlinear and strongly dependent on the thermal effects, the problems are thus inherently multi-disciplinary and

nonlinear. It is, therefore, the purpose of this study to develop an analytical formulation to determine the nonlinear random response of composite laminates to combined acoustic and thermal loads applied simultaneously.

1.2 Literature Survey

A limited number of papers studied the thermal postbuckling of laminated composite plates. Noor and Peters (1983) have investigated the bifurcation buckling and postbuckling response of composite plates subjected to combined axial compression and uniform temperature distribution by the multiple-parameter reduced based technique. Recently, they (Noor et al., 1992) have studied the thermo-mechanical buckling and postbuckling response of composite plates subjected to combined axial and thermal loadings. The analysis is based on a first order and third-order shear deformation, von Karman type of nonlinear plate theory. A mixed formulation is used with the fundamental unknowns consisting of the generalized displacements and the stress resultants of the plate. An efficient multiple-parameter reduction method is used in conjunction with mixed finite element models. Sensitivity derivatives are evaluated and used to study the sensitivity of the postbuckling response to variations in the different lamination and material parameters of the plate. In a paper presented at the 35th SDM conference (Noor et al., 1994), a similar study of the composite plate with cutout was conducted. Huang and Tauchert (1986) used analytical continuum approach and studied the thermal buckling and postbuckling behavior of simply-supported antisymmetric angle-ply plates subjected to uniform temperature change. Their results illustrated the effects of the number of layers, the ply angles and the aspect ratio of the plate upon the thermoelastic response. Chen and Chen (1989, 1991) have studied the thermal postbuckling behaviors of laminated rectangular, antisymmetric angle-ply composite plates subjected to a nonuniform

temperature field by the finite element method. Based on the principle of minimum potential energy, the nonlinear stiffness matrix and geometric stiffness matrix are derived. Their results reveal that the thermal postbuckling behavior of composite laminated plates is influenced by lamination angles, plate aspect ratio, modulus ratio and the number of layers. Their results also revealed that the effect of temperature-dependent mechanical properties on the thermal postbuckling behavior is significant. Librescu et al. (Librescu and Souza, 1991 and Librescu et al. 1994) recently studied the static postbuckling of simply supported flat panels exposed to a stationary nonuniform temperature field and subjected to a system of subcritical in-plane compressive edge loads. The study is performed within a refined theory of composite laminated plates incorporating the effect of transverse shear and the geometric nonlinearities. Meyers and Hyer (1992) have analytically studied thermal buckling and postbuckling of simply supported symmetric composite laminates under uniform temperature change using the Rayleigh-Ritz method. Birman and Bert (1993) investigated the effects of temperature on buckling and postbuckling behavior of reinforced and unstiffened composite plates and cylindrical shells. First, the equilibrium equations are formulated for a shell subjected to the simultaneous action of a thermal field and an axial loading. These equations are used to predict a general form of the algebraic equations describing the postbuckling response of a shell. Conditions for the snap-through of a shell subjected to thermo-mechanical loading are formulated. The theory was also applied to prediction the postbuckling response of flat large-aspect-ratio panels reinforced in the direction of their short edges.

There are many survey articles which review analysis techniques and experiments of nonlinear random structural responses. Mei and Wolfe (1986) have presented a discussion on analytical and experimental techniques to predict the acoustic fatigue life of aircraft

structures. They discussed the problem and the steps taken to solve the problem and reviewed the analytical approaches to single degree-of-freedom (SDOF) and multi-degree-of-freedom (MDOF) linear and nonlinear systems under random excitations. They also reported the advances of analytical prediction and experiments. To (1987) has also presented a comprehensive survey paper on the analysis of nonlinear systems subjected to random excitation. Methods reported to be applicable to both SDOF and MDOF systems include equivalent linearization techniques (EL), the Fokker-Planck-Kolmogorov equation (FPK) and moment approaches. Clarkson (1994) has recently presented a very comprehensive sonic fatigue technology review report. He reported that: " From the early-1960s until the mid-1980s, there was very little theoretical development for sonic fatigue prediction." The design monographs for most common aircraft structures were made based on simple theoretical models and results of specially designed tests. The use of advanced composites in the 1980s generated an increasing interest in development of more sophisticated theoretical models, because the much wider range of parameters of composite panels made creation of nomograph based on tests not possible.

A limited amount of investigations on structural response subjected to intense acoustic and thermal loads exists in the literature. Seide and Adami (1983) were the first who studied large deflection random response of a thermally buckled simply supported beam. The thermal load and the acoustic pressure are thus considered to be applied in sequence. The well-known classic Woinowsky-Krieger large amplitude beam vibration equation is used. The Galerkin's method and time domain numerical simulation are then applied to obtain random response.

The papers by Mei and Prasad (1987 and 1989) aim to explain the observed broadening of the response peak and its increase in frequency by including nonlinear

damping as well as large amplitude displacements in the theory. This is a very valuable formulation because damping is inherently nonlinear and its behavior and magnitude is one of the major unknowns in the work to date. In their work a single mode analysis is used and the results show the expected broadening and increase in frequency.

Most recently, the Galerkin/numerical simulation approach was applied to simply supported metal and orthotropic composite rectangular plates by Vaicaitis and Arnold (1990) and Vaicaitis (1991), the thermal and acoustic loads are considered to be applied simultaneously. The classic von Karman large deflection plate equations including temperature and orthotropic property effects are employed. The thermal effects on rectangular isotropic plate random response have also been investigated thoroughly by Lee (1993). The three thermal effects: (i) global expansion by uniform plate temperature, (ii) local expansion by temperature variation over the plate, and (iii) thermal moment induced by temperature gradient across the plate thickness are included in the investigation. The single mode Galerkin method and the EL (Roberts and Spanos, 1990) technique are used. The analytical continuum approaches have been so far limited to uniform or linear temperature distributions and to beams and rectangular plates of either simply supported or clamped edges.

For over three decades, the finite element method has been the predominant method for structural mechanics. However, there are only few studies on nonlinear random response of structures using the finite element method. Hwang and Pi (1972) have investigated a simply supported rectangular isotropic plate subjected to rain-drop type uniform intensity random acoustic loads. The high precision 18 degree-of-freedom (DOF) triangular plate bending element developed by Cowper et al. was used. Both first and second-order nonlinear stiffness matrices are developed to account for large deflections.

The finite element nonlinear equations of motion were treated as a linearized eigenvalue problem with an iterative scheme. The acceleration spectra at the plate center were obtained at three pressure levels. No comparison was made with other approximate solutions.

Busby and Weingarton (1973) used the finite element method only to obtain the nonlinear differential equations of motion which are expressed in terms of the normal mode coordinates. The EL method is then used for the solution of these equations. Mean square deflections at the midspan are obtained for beams with both ends simply supported and both ends clamped. However, comparisons with other solutions were not made.

Chiang (1988) has presented a finite element method for large deflection random response of beams, plates and built-up panels subjected to acoustic loads. Geometrical stiffness matrices to account for the induced inplane forces due to large deflections were developed for an isotropic beam element and an isotropic rectangular plate element. Root-mean-square (RMS) maximum deflections and RMS maximum strains are obtained for beams and rectangular plates with simply supported and clamped boundary conditions. The finite element results are in good agreement with single-mode Fokker-Planck-Kolmogorov (FPK) equation and analytical equivalent linearization solutions.

Locke (1988) and Locke and Mei (1990) extended the finite element method to isotropic beam and rectangular plate structures subjected to thermal and acoustic loads applied in sequence. The thermal load considered is a steady-state temperature distribution $\Delta T(x,y)$. The thermal postbuckling structural problem is solved first to obtain the deflection and thermal stresses. The deflection and thermal stresses are then treated as initial deflection and initial stresses in the subsequent random vibration analysis. The Newton-Raphson iterative method is used in the thermal postbuckling analysis. For the

nonlinear random vibration, the linear mode shapes of the thermally buckled structure are used to reduce the order of the system equations of motion to a set of nonlinear modal equations of a much smaller order. The EL technique is then used to iteratively obtain for RMS responses. Excellent agreement has been obtained between the finite element and the Galerkin/numerical simulation results by Seide and Adami.

Jay Robison (1990, 1991) has derived a numerical integration routine from a set of unified single step integration algorithms using a weighted satisfaction of the equilibrium equation governing the large deflection random response of laminated composite plates. The equilibrium equations are derived using large deflection finite element formulations. The in-plane inertia terms are considered in the formulation, however, rotary inertia terms are assumed negligible. Probability density, spectral density and autocorrelation functions of the maximum displacement and strain responses are presented for three acoustic excitation levels. Classical thin plate boundary conditions and pseudo white noise excitation are used in this investigation.

Chen (1990) and Chen and Yang (1991) have presented a finite element formulation combined with stochastic linearization and normal mode methods, including the geometrical nonlinearity for the study of random vibration responses of beams, frames and composite plates subjected to simultaneously spatial and temporal Gaussian stationary nonwhite and nonzero mean random excitations.

Chen and Mei(1993) presented a finite element formulation, solution procedure and results of a study attempted to analyze nonlinear random response of beams subjected to acoustic and thermal loads applied simultaneously.

1.3 Outline of the study

The acoustic fatigue life prediction problem is very important to military and civil

aircraft. The problem consists of three major parts: (1) acoustic loading analysis; (2) determination of the response of structures; and (3) estimation of the fatigue life of the materials. In this study, only the second part is concerned.

Since the structural response due to intense acoustic pressure levels is extremely nonlinear and strongly dependent on the thermal environment, the method of superposition is not applicable. Rather the thermal effects must be integrated and coupled directly into the acoustic-structural analysis. The finite element formulations by Chiang, C. T. Chen and Robinson did not consider temperature effects. The formulation by Locke treated the two loads in sequence; thus there is no inter-dependence between the thermal effects and the acoustic-structural response. In the aforementioned literature survey, it appears that studies of the nonlinear random response of structures subjected to simultaneously applied acoustic and thermal loads using finite element method are not available in the literature.

In addition, only normal incidence acoustic pressure loads have been considered in all the existing investigations. It appears that studies of the nonlinear random response of plates subjected to a grazing incidence acoustic wave using finite element method are not available in the literature.

Therefore, this dissertation will develop a finite element formulation and solution procedure which is believed to be the first attempt to analyze nonlinear random response of complex composite panels subjected to simultaneous acoustic and thermal loads, and the acoustic pressure can be either normal incidence or grazing incidence.

In Chapter 2, the formulation for the problem is derived. The formulation is based on von Karman large deflection theory and the first order shear deformation theory. In Chapter 3, the solution procedure is described. Using linear vibration modes of the thermally buckled structure, the governing equations are reduced to a set of nonlinear

coupled modal equations. The equivalent linearization technique is employed, because satisfactory results have been obtained using this technique. Finally, in order to uncouple the linearized modal equations of motion, the modal transformation is utilized once more. In Chapter 4, the numerical results are presented. It includes thermal buckling and postbuckling results, random response and acoustic-thermal combined response. Chapter 5 is concerned with conclusion and further work suggestions.

Chapter 2

FORMULATIONS

In this chapter, the governing nonlinear equations of motion are derived for a plate of arbitrary shape subjected to a set of simultaneously applied thermal and acoustic loads. The thermal load is taken to be an arbitrary distribution, but steady-state, i.e., $\Delta T = \Delta T(x, y, z)$. The acoustic loading is considered to be a stationary Gaussian pressure wave, with the extension such that in order to include in the travelling wave a combination of wavelengths, the pressure at any one point is random but the whole pattern moves in the direction λ (normal incidence $\lambda=0^\circ$ and grazing incidence $\lambda=90^\circ$) with wave traveling speed c .

The following features are considered in the formulation:

- (a). Initial imperfection deflection $w_o(x, y)$,
- (b). In-plane initial forces $\{N_o\}$,
- (c). Arbitrary temperature distribution $\Delta T(x, y, z)$,
- (d). Large deflections in von Karman sense,
- (e). Composite materials with transverse shear deformation, and
- (f). Acoustic waves directed with an inclination angle λ .

The assumption regarding temperature independent material properties is utilized in this study.

The three-node triangular Mindlin (MIN3) plate element with improved transverse shear is extended and employed in this study. The element was initially developed by Tessler and Hughes (1985). This simple plate element of five degrees of freedom per node in large-scale finite element structural analysis and, especially, in nonlinear analysis, has great computational advantage. Tessler and Hughes have found that the transverse shear energy was the major cause of difficulty, therefore a special interpolation scheme, anisoparametric interpolation, was devised. In addition, the element transverse shear energy was further enhanced by a suitable (element appropriate) shear correction factor. Based on extensive numerical testing, MIN3 is an excellent element. They concluded: "Due to its reliability, economy, and good stress recovery, it may be regarded as a viable candidate for extension to shell, laminated composite and nonlinear analyses." The finite element formulation is described as follows for the nonlinear random response of composite panels.

2.1 Element Displacement Functions

A typical triangular plate element is shown in Figs. 2.1 and 2.2 to discretize a rectangular panel. The element displacement functions used in the derivation of the equations of motion are:

$$\begin{aligned} u_x &= u(x, y, t) + z\psi_y(x, y, t) \\ u_y &= v(x, y, t) + z\psi_x(x, y, t) \\ u_z &= w(x, y, t) \end{aligned} \tag{2.1}$$

where u_x, u_y, u_z are the three displacement components at any point in the element; u, v, w are the displacements of the middle surface; and ψ_x and ψ_y are the rotations of the normal around the x and y axes due to bending only.

The node displacement vector is defined as follows:

$$\begin{aligned}
\{w\}^T &= [w_b, \psi, w_m] \\
&= [w_1, w_2, w_3, \psi_{x1}, \psi_{x2}, \psi_{x3}, \psi_{y1}, \psi_{y2}, \psi_{y3}, \\
&\quad u_1, u_2, u_3, v_1, v_2, v_3]
\end{aligned} \tag{2.2}$$

The interpolation functions for the MIN3 element are

$$\begin{aligned}
w(x, y, t) &= [H_w] \{w_b\} + [H_{w\psi}] \{\psi\} \\
&= [\xi_1, \xi_2, \xi_3] \{w_b\} + [L_1, L_2, L_3, M_1, M_2, M_3] \{\psi\}
\end{aligned} \tag{2.3}$$

$$\psi_x(x, y, t) = [H_{\psi_x}] \{\psi\} = [\xi_1, \xi_2, \xi_3, 0, 0, 0] \{\psi\} \tag{2.4}$$

$$\psi_y(x, y, t) = [H_{\psi_y}] \{\psi\} = [0, 0, 0, \xi_1, \xi_2, \xi_3] \{\psi\} \tag{2.5}$$

$$u(x, y, t) = [H_u] \{w_m\} = [\xi_1, \xi_2, \xi_3, 0, 0, 0] \{w_m\} \tag{2.6}$$

$$v(x, y, t) = [H_v] \{w_m\} = [0, 0, 0, \xi_1, \xi_2, \xi_3] \{w_m\} \tag{2.7}$$

where ξ_1, ξ_2, ξ_3 are the area coordinates, and the transformation between x, y and ξ_i is

$$\begin{aligned}
\begin{Bmatrix} 1 \\ x \\ y \end{Bmatrix} &= \begin{bmatrix} 1 & 1 & 1 \\ x_1 & x_2 & x_3 \\ y_1 & y_2 & y_3 \end{bmatrix} \begin{Bmatrix} \xi_1 \\ \xi_2 \\ \xi_3 \end{Bmatrix} \\
\begin{Bmatrix} \xi_1 \\ \xi_2 \\ \xi_3 \end{Bmatrix} &= \frac{1}{2A} \begin{bmatrix} x_2 y_3 - x_3 y_2 & y_2 - y_3 & x_3 - x_2 \\ x_3 y_1 - x_1 y_3 & y_3 - y_1 & x_1 - x_3 \\ x_1 y_2 - x_2 y_1 & y_1 - y_2 & x_2 - x_1 \end{bmatrix} \begin{Bmatrix} 1 \\ x \\ y \end{Bmatrix}
\end{aligned} \tag{2.8}$$

where $2A = (x_2 - x_1)(y_3 - y_1) - (x_3 - x_1)(y_2 - y_1)$, A is the area of the triangular element, (x_i, y_i) is the coordinates of the node i ; and

$$\begin{aligned} L_1 &= \frac{1}{8}(b_3N_4 - b_2N_6), \quad L_2 = \frac{1}{8}(b_1N_5 - b_3N_4) \\ L_3 &= \frac{1}{8}(b_2N_6 - b_1N_5), \quad M_1 = \frac{1}{8}(a_2N_6 - a_3N_4) \\ M_2 &= \frac{1}{8}(a_3N_4 - a_1N_5), \quad M_3 = \frac{1}{8}(a_1N_5 - a_2N_6) \\ N_4 &= 4\xi_1\xi_2, \quad N_5 = 4\xi_2\xi_3, \quad N_6 = 4\xi_3\xi_1 \end{aligned} \quad (2.9)$$

$$a_1 = x_{32}, \quad a_2 = x_{13}, \quad a_3 = x_{21},$$

$$b_1 = y_{23}, \quad b_2 = y_{31}, \quad b_3 = y_{12}$$

$$x_{ij} = x_i - x_j, \quad y_{ij} = y_i - y_j$$

$$\int_A \xi^k \xi^l \xi^m dA = 2A \frac{k!l!m!}{(2+k+l+m)!} \quad (2.10)$$

2.2 Nonlinear Strain-Displacement Relations

The von Karman strain-displacement relations are given as

$$\{\epsilon\} = \begin{Bmatrix} \epsilon_x \\ \epsilon_y \\ \gamma_{xy} \end{Bmatrix} = \{\epsilon^o\} + z\{\kappa\} \quad (2.11)$$

where $\{\epsilon^o\}$ is the in-plane strain vector, and $\{\kappa\}$ is the curvature vector such that

$$\{\epsilon^o\} = \begin{Bmatrix} u_{,x} \\ v_{,y} \\ u_{,y} + v_{,x} \end{Bmatrix} + \frac{1}{2} \begin{Bmatrix} w_{,x}^2 \\ w_{,y}^2 \\ 2w_{,x}w_{,y} \end{Bmatrix} + \begin{Bmatrix} w_{,x}w_{o,x} \\ w_{,y}w_{o,y} \\ w_{,x}w_{o,y} + w_{,y}w_{o,x} \end{Bmatrix} \quad (2.12)$$

$$= \{\epsilon_m^o\} + \{\epsilon_b^o\} + \{\epsilon_o^o\}$$

$$\{\kappa\} = \begin{Bmatrix} \psi_{y,x} \\ \psi_{x,y} \\ \psi_{y,y} + \psi_{x,x} \end{Bmatrix} \quad (2.13)$$

where subscripts m , b and o denote that the inplane strain components are due to membrane, bending and initial imperfection deflection respectively. The shear strain-

displacement relations are given by

$$\{\gamma\} = \begin{Bmatrix} \gamma_{yz} \\ \gamma_{xz} \end{Bmatrix} = \begin{Bmatrix} w_{,y} \\ w_{,x} \end{Bmatrix} + \begin{Bmatrix} \psi_x \\ \psi_y \end{Bmatrix} \quad (2.14)$$

where the subscript “,” denotes the derivative.

2.3 Constitutive Law

For the k-th layer of an orthotropic material with an orientation ϕ , the stress-strain relations are

$$\begin{aligned} \{\sigma\}_k &= \begin{Bmatrix} \sigma_x \\ \sigma_y \\ \tau_{xy} \end{Bmatrix}_k = \begin{bmatrix} \bar{Q}_{11} & \bar{Q}_{12} & \bar{Q}_{16} \\ \bar{Q}_{12} & \bar{Q}_{22} & \bar{Q}_{26} \\ \bar{Q}_{16} & \bar{Q}_{26} & \bar{Q}_{66} \end{bmatrix}_k (\{\epsilon\} - \{\epsilon_{\Delta T}\}_k) + \{\sigma_{No}\} \\ &= [\bar{Q}]_k (\{\epsilon\} - \{\epsilon_{\Delta T}\}_k) + \{\sigma_{No}\} \\ \{\tau\}_k &= \begin{Bmatrix} \tau_{yz} \\ \tau_{xz} \end{Bmatrix}_k = \begin{bmatrix} \bar{Q}_{44} & \bar{Q}_{45} \\ \bar{Q}_{45} & \bar{Q}_{55} \end{bmatrix}_k \begin{Bmatrix} \gamma_{yz} \\ \gamma_{xz} \end{Bmatrix} = [\bar{Q}_s]_k \{\gamma\} \end{aligned} \quad (2.15)$$

where the free-expansion thermal strain vector is

$$\{\epsilon_{\Delta T}\}_k = \begin{Bmatrix} \alpha_x \\ \alpha_y \\ \alpha_{xy} \end{Bmatrix}_k \Delta T = \begin{bmatrix} c^2 & s^2 & -2cs \\ s^2 & c^2 & 2cs \\ 2cs & -2cs & 2(c^2 - s^2) \end{bmatrix}_k \begin{Bmatrix} \alpha_1 \\ \alpha_2 \\ 0 \end{Bmatrix}_k \Delta T \quad (2.16)$$

$c = \cos \phi, \quad s = \sin \phi$

where $[\bar{Q}]_k$ is the transformed reduced stiffness matrix for the k-th lamina, and $\{\sigma_{No}\}$ is the initial stress vector corresponding to $\{N_o\}$.

2.4 Resultant Laminate Forces and Moments

The resultant forces, moments and shear forces per unit length acting on a laminate are obtained by integration of the stresses in each layer through the laminate thickness

$$(\{N\}, \{M\}) = \int_{-\frac{h}{2}}^{\frac{h}{2}} \{\sigma\}_k(1, z) dz \quad (2.17)$$

and

$$\{R\} = \int_{-\frac{h}{2}}^{\frac{h}{2}} \left\{ \begin{matrix} \tau_{yz} \\ \tau_{xz} \end{matrix} \right\}_k dz \quad (2.18)$$

where $\{N\}$ is the resultant force, $\{M\}$ is the moment and $\{R\}$ is the shear force vector.

The laminae shear stiffness is

$$[A_s] = \int_{-\frac{h}{2}}^{\frac{h}{2}} \begin{bmatrix} \bar{Q}_{44} & \bar{Q}_{45} \\ \bar{Q}_{54} & \bar{Q}_{55} \end{bmatrix} dz \quad (2.19)$$

For a lamina in the material axes, the so-called reduced stiffnesses are

$$\begin{aligned} Q_{11} &= \frac{E_1}{1 - \nu_{12}\nu_{21}} \\ Q_{12} &= \frac{\nu_{12}E_2}{1 - \nu_{12}\nu_{21}} = \frac{\nu_{21}E_1}{1 - \nu_{12}\nu_{21}} \\ Q_{22} &= \frac{E_2}{1 - \nu_{12}\nu_{21}} \\ Q_{66} &= G_{12} \\ Q_{44} &= G_{23} \\ Q_{55} &= G_{13} \end{aligned} \quad (2.20)$$

where G_{23}, G_{13} are the shear modulus of the materials. Then the transformed reduced stiffnesses are

$$\begin{aligned} [\bar{Q}] &= [T]^{-1}[Q][T]^{-T} \\ [T] &= \begin{bmatrix} c^2 & s^2 & 2sc \\ s^2 & c^2 & -2sc \\ -sc & sc & c^2 - s^2 \end{bmatrix} \\ s &= \sin \varphi, \quad c = \cos \varphi \end{aligned} \quad (2.21)$$

The above equations can be written as

$$\begin{Bmatrix} N \\ M \end{Bmatrix} = \begin{bmatrix} A & B \\ B & D \end{bmatrix} \begin{Bmatrix} \epsilon^o \\ \kappa \end{Bmatrix} - \begin{Bmatrix} N_{\Delta T} \\ M_{\Delta T} \end{Bmatrix} + \begin{Bmatrix} N_o \\ 0 \end{Bmatrix} \quad (2.22)$$

$$\{R\} = [A_s]\{\gamma\}$$

where $[A]$, $[B]$ and $[D]$ are the laminate extensional, extension-bending and bending stiffness, respectively, and $[A_s]$ is the laminate shear stiffness. And the free-expansion thermal resultant force and moment vectors are

$$(\{N_{\Delta T}\}, \{M_{\Delta T}\}) = \int_{-\frac{h}{2}}^{\frac{h}{2}} [\bar{Q}]_k \{\epsilon_{\Delta T}\}_k(1, z) dz \quad (2.23)$$

and $\{N_o\}$ is a known initial force vector.

2.5 The Principle of Virtual Work

The virtual works done by internal and external forces are

$$\delta W_{\text{int}} = \int_A \left(\{\delta \epsilon^o\}^T \{N\} + \{\delta \kappa\}^T \{M\} + \alpha \{\delta \gamma\}^T \{R\} \right) dA \quad (2.24)$$

and

$$\begin{aligned} \delta W_{\text{ext}} = \int_A & [\delta w(p(x, y, t; \lambda) - \rho h w_{,tt}) \\ & + \delta u(-\rho h u_{,tt}) + \delta v(-\rho h v_{,tt})] dA \end{aligned} \quad (2.25)$$

where $p(x, y, t; \lambda)$ is the acoustic excitation, λ is an incidence angle for normal or grazing acoustic wave, ρ is the mass density of the laminate, and α is a shear correction factor,

$$\alpha = \frac{1}{1 + 0.5 \frac{\sum_{i=4,9} k_{sii}}{\sum_{i=4,9} k_{bii}}} \quad (2.26)$$

It is assumed that the rotatory inertia effect is neglected for relative thin plate ($a/h > 50$).

Some geometric matrices are given below:

$$\begin{aligned}
 [\theta] &= \begin{bmatrix} w_{,x} & 0 \\ 0 & w_{,y} \\ w_{,y} & w_{,x} \end{bmatrix}, \quad [\theta_o] = \begin{bmatrix} w_{o,x} & 0 \\ 0 & w_{o,y} \\ w_{o,y} & w_{o,x} \end{bmatrix} \\
 \{G\} &= \begin{Bmatrix} w_{,x} \\ w_{,y} \end{Bmatrix} = [C_{\psi b}]\{w_b\} + [C_{\psi\psi}]\{\psi\} \\
 \{\epsilon_b^o\} &= \frac{1}{2}[\theta]\{G\}, \quad \{\delta\epsilon_b^o\} = \frac{1}{2}\delta([\theta]\{G\}) = [\theta]\{\delta G\}
 \end{aligned} \tag{2.27}$$

$$[C_m] = \begin{bmatrix} \frac{\partial}{\partial x}[H_u] \\ \frac{\partial}{\partial y}[H_v] \\ \frac{\partial}{\partial x}[H_v] + \frac{\partial}{\partial y}[H_u] \end{bmatrix} = \frac{1}{2A} \begin{bmatrix} y_{23} & y_{31} & y_{12} & 0 & 0 & 0 \\ 0 & 0 & 0 & x_{32} & x_{13} & x_{21} \\ x_{32} & x_{13} & x_{21} & y_{23} & y_{31} & y_{12} \end{bmatrix} \tag{2.28}$$

$$[C_{\psi b}] = \begin{bmatrix} \frac{\partial}{\partial x}[H_w] \\ \frac{\partial}{\partial y}[H_w] \end{bmatrix} = \frac{1}{2A} \begin{bmatrix} y_{23} & y_{31} & y_{12} \\ x_{32} & x_{13} & x_{21} \end{bmatrix} \tag{2.29}$$

$$[C_{\psi\psi}] = \begin{bmatrix} \frac{\partial}{\partial x}[H_{w\psi}] \\ \frac{\partial}{\partial y}[H_{w\psi}] \end{bmatrix} = \frac{1}{2A} \begin{bmatrix} C_{\psi\psi 11} & C_{\psi\psi 12} & C_{\psi\psi 13} & C_{\psi\psi 14} & C_{\psi\psi 15} & C_{\psi\psi 16} \\ C_{\psi\psi 21} & C_{\psi\psi 22} & C_{\psi\psi 23} & C_{\psi\psi 24} & C_{\psi\psi 25} & C_{\psi\psi 26} \end{bmatrix} \tag{2.30}$$

where the 12 $C_{\psi\psi ij}$'s are related to the area coordinates and the coordinates of the three nodes, and they are listed in the Appendix A.

$$[C_b] = \begin{bmatrix} \frac{\partial}{\partial x}[H_{\psi_y}] \\ \frac{\partial}{\partial y}[H_{\psi_x}] \\ \frac{\partial}{\partial x}[H_{\psi_x}] + \frac{\partial}{\partial y}[H_{\psi_y}] \end{bmatrix} = \frac{1}{2A} \begin{bmatrix} 0 & 0 & 0 & y_{23} & y_{31} & y_{12} \\ x_{32} & x_{13} & x_{21} & 0 & 0 & 0 \\ y_{23} & y_{31} & y_{12} & x_{32} & x_{13} & x_{21} \end{bmatrix} \tag{2.31}$$

$$[C_{\gamma b}] = \begin{bmatrix} \frac{\partial}{\partial y}[H_w] \\ \frac{\partial}{\partial x}[H_w] \end{bmatrix} = \frac{1}{2A} \begin{bmatrix} x_{32} & x_{13} & x_{21} \\ y_{23} & y_{31} & y_{12} \end{bmatrix} \tag{2.32}$$

$$\begin{aligned}
[C_{\gamma\psi}] &= \begin{bmatrix} \frac{\partial}{\partial y} [H_{w\psi}] + [H_{\psi_x}] \\ \frac{\partial}{\partial x} [H_{w\psi}] + [H_{\psi_y}] \end{bmatrix} \\
&= \begin{bmatrix} C_{\psi\psi 21} + \xi_1 & C_{\psi\psi 22} + \xi_2 & C_{\psi\psi 23} + \xi_3 & C_{\psi\psi 24} & C_{\psi\psi 25} & C_{\psi\psi 26} \\ C_{\psi\psi 11} & C_{\psi\psi 12} & C_{\psi\psi 13} & C_{\psi\psi 14} + \xi_1 & C_{\psi\psi 15} + \xi_2 & C_{\psi\psi 16} + \xi_3 \end{bmatrix} \quad (2.33)
\end{aligned}$$

Substituting Eqs. (2.28)-(2.33) into Eqs. (2.12)-(2.14), one obtains

$$\begin{aligned}
\{\delta\epsilon^o\}^T &= \{\delta w_m\}^T [C_m]^T + \{\delta w_b\}^T [C_{\psi b}]^T [\theta]^T + \{\delta\psi\}^T [C_{\psi\psi}]^T [\theta]^T \\
&\quad + \{\delta w_b\}^T [C_{\psi b}]^T [\theta_o]^T + \{\delta\psi\}^T [C_{\psi\psi}]^T [\theta_o]^T \quad (2.34)
\end{aligned}$$

$$\begin{aligned}
\{N\} &= [A]\{\epsilon^o\} + [B]\{\kappa\} - \{N_{\Delta T}\} + \{N_o\} \\
&= [A][C_m]\{w_m\} + \frac{1}{2}[A][\theta]([C_{\psi b}]\{w_b\} + [C_{\psi\psi}]\{\psi\}) + [A][\theta][C_{\psi b}]\{w_{bo}\} \quad (2.35)
\end{aligned}$$

$$\begin{aligned}
&+ [A][\theta][C_{\psi\psi}]\{\psi_o\} + [B][C_b]\{\psi\} - \{N_{\Delta T}\} + \{N_o\} \\
\{\delta\kappa\}^T &= \{\delta\psi\}^T [C_b]^T \quad (2.36)
\end{aligned}$$

$$\begin{aligned}
\{M\} &= [B]\{\epsilon^o\} + [D]\{\kappa\} - \{M_{\Delta T}\} \\
&= [B][C_m]\{w_m\} + \frac{1}{2}[B][\theta]([C_{\psi b}]\{w_b\} + [C_{\psi\psi}]\{\psi\}) + [B][\theta][C_{\psi b}]\{w_{bo}\} \quad (2.37)
\end{aligned}$$

$$\begin{aligned}
&+ [B][\theta][C_{\psi\psi}]\{\psi_o\} + [D][C_b]\{\psi\} - \{M_{\Delta T}\} \\
\{\delta\gamma\}^T &= \{\delta w_b\}^T [C_{\gamma b}]^T + \{\delta\psi\}^T [C_{\gamma\psi}]^T \quad (2.38)
\end{aligned}$$

$$\{R\} = [A_s][C_{\gamma b}]\{w_b\} + [A_s][C_{\gamma\psi}]\{\psi\} \quad (2.39)$$

The virtual work principle gives

$$\delta W_{int} = \delta W_{ext} \quad (2.40)$$

Finally, from Eq. (2.24):

$$\begin{aligned}
\delta W_{int} &= \int_A \left(\{\delta \epsilon^o\}^T \{N\} + \{\delta \kappa\}^T \{M\} + \alpha \{\delta \gamma\}^T \{R\} \right) dA \\
&= \int_A \left\{ \{\delta w_m\}^T [C_m]^T \left([A][C_m] \{w_m\} + \frac{1}{2} [A][\theta] [C_{\psi b}] \{w_b\} + \frac{1}{2} [A][\theta] [C_{\psi \psi}] \{\psi\} \right. \right. \\
&\quad \left. \left. + [A][\theta] [C_{\psi b}] \{w_{bo}\} + [A][\theta] [C_{\psi \psi}] \{\psi_o\} + [B][C_b] \{\psi\} - \{N_{\Delta T}\} + \{N_o\} \right) \right. \\
&\quad \left. + \{\delta w_b\}^T [C_{\psi b}]^T [\theta]^T \left([A][C_m] \{w_m\} + \frac{1}{2} [A][\theta] [C_{\psi b}] \{w_b\} + \frac{1}{2} [A][\theta] [C_{\psi \psi}] \{\psi\} \right. \right. \\
&\quad \left. \left. + [A][\theta] [C_{\psi b}] \{w_{bo}\} + [A][\theta] [C_{\psi \psi}] \{\psi_o\} + [B][C_b] \{\psi\} - \{N_{\Delta T}\} + \{N_o\} \right) \right. \\
&\quad \left. + \{\delta \psi\}^T [C_{\psi \psi}]^T [\theta]^T \left([A][C_m] \{w_m\} + \frac{1}{2} [A][\theta] [C_{\psi b}] \{w_b\} + \frac{1}{2} [A][\theta] [C_{\psi \psi}] \{\psi\} \right. \right. \\
&\quad \left. \left. + [A][\theta] [C_{\psi b}] \{w_{bo}\} + [A][\theta] [C_{\psi \psi}] \{\psi_o\} + [B][C_b] \{\psi\} - \{N_{\Delta T}\} + \{N_o\} \right) \right. \\
&\quad \left. + \{\delta w_b\}^T [C_{\psi b}]^T [\theta_o]^T \left([A][C_m] \{w_m\} + \frac{1}{2} [A][\theta] [C_{\psi b}] \{w_b\} + \frac{1}{2} [A][\theta] [C_{\psi \psi}] \{\psi\} \right. \right. \\
&\quad \left. \left. + [A][\theta] [C_{\psi b}] \{w_{bo}\} + [A][\theta] [C_{\psi \psi}] \{\psi_o\} + [B][C_b] \{\psi\} - \{N_{\Delta T}\} + \{N_o\} \right) \right. \\
&\quad \left. + \{\delta \psi\}^T [C_{\psi \psi}]^T [\theta_o]^T \left([A][C_m] \{w_m\} + \frac{1}{2} [A][\theta] [C_{\psi b}] \{w_b\} + \frac{1}{2} [A][\theta] [C_{\psi \psi}] \{\psi\} \right. \right. \\
&\quad \left. \left. + [A][\theta] [C_{\psi b}] \{w_{bo}\} + [A][\theta] [C_{\psi \psi}] \{\psi_o\} + [B][C_b] \{\psi\} - \{N_{\Delta T}\} + \{N_o\} \right) \right. \\
&\quad \left. + \{\delta \psi\}^T [C_b]^T \left([B][C_m] \{w_m\} + \frac{1}{2} [B][\theta] [C_{\psi b}] \{w_b\} + \frac{1}{2} [B][\theta] [C_{\psi \psi}] \{\psi\} \right. \right. \\
&\quad \left. \left. + [B][\theta] [C_{\psi b}] \{w_{bo}\} + [B][\theta] [C_{\psi \psi}] \{\psi_o\} + [D][C_b] \{\psi\} - \{M_{\Delta T}\} \right) \right. \\
&\quad \left. + \alpha \{\delta w_b\}^T [C_{\gamma b}]^T \left([A_s][C_{\gamma b}] \{w_b\} + [A_s][C_{\gamma \psi}] \{\psi\} \right) \right. \\
&\quad \left. + \alpha \{\delta \psi\}^T [C_{\gamma \psi}]^T \left([A_s][C_{\gamma b}] \{w_b\} + [A_s][C_{\gamma \psi}] \{\psi\} \right) \right\} dA
\end{aligned} \tag{2.41}$$

and from Eq. (2.25):

$$\begin{aligned}
\delta W_{ext} = & \int_A \left\{ \left(\{\delta w_b\}^T \{H_w\} + \{\delta \psi\}^T \{H_{w\psi}\} \right) \right. \\
& \left(p(x, y, t; \lambda) - \rho h \left([H_w] \{\ddot{w}_b\} + [H_{w\psi}] \{\ddot{\psi}\} \right) \right) \\
& \left. - \{\delta w_m\}^T (\{H_u\} [H_u] \{\ddot{w}_m\}) - \{\delta w_m\}^T (\{H_v\} [H_v] \{\ddot{w}_m\}) \right\} dA
\end{aligned} \tag{2.42}$$

2.6 Element Equations of Motion

The application of the principle of virtual work to derive the element equations of motion and the element matrices is lengthy and tedious. There are total 56 terms in the expressions of virtual work. The equations of motion for the MIN3 plate element can be written in the matrix form as

$$\begin{aligned}
& \left(\begin{bmatrix} 0 & 0 & 0 \\ 0 & [k]_{\psi} & [k]_{\psi m} \\ 0 & [k]_{m\psi} & [k]_m \end{bmatrix} + \begin{bmatrix} [k_o]_b & [k_o]_{b\psi} & [k_o]_{bm} \\ [k_o]_{\psi b} & [k_o]_{\psi} & [k_o]_{\psi m} \\ [k_o]_{mb} & [k_o]_{m\psi} & 0 \end{bmatrix} \right) \begin{Bmatrix} w_b \\ \psi \\ w_m \end{Bmatrix} \\
& - \left(\begin{bmatrix} [k_{N\Delta T}]_b & [k_{N\Delta T}]_{b\psi} & 0 \\ [k_{N\Delta T}]_{\psi b} & [k_{N\Delta T}]_{\psi} & 0 \\ 0 & 0 & 0 \end{bmatrix} - \begin{bmatrix} [k_{No}]_b & [k_{No}]_{b\psi} & 0 \\ [k_{No}]_{\psi b} & [k_{No}]_{\psi} & 0 \\ 0 & 0 & 0 \end{bmatrix} \right) \begin{Bmatrix} w_b \\ \psi \\ w_m \end{Bmatrix} \\
& + \frac{1}{2} \left(\begin{bmatrix} 0 & [n1]_{b\psi} & [n1]_{bm} \\ [n1]_{\psi b} & [n1]_{\psi} & [n1]_{\psi m} \\ [n1]_{mb} & [n1]_{m\psi} & 0 \end{bmatrix} + \begin{bmatrix} [n1_o]_b & [n1_o]_{b\psi} & 0 \\ [n1_o]_{\psi b} & [n1_o]_{\psi} & 0 \\ 0 & 0 & 0 \end{bmatrix} \right) \begin{Bmatrix} w_b \\ \psi \\ w_m \end{Bmatrix} \\
& + \frac{1}{2} \left(\begin{bmatrix} [n1Nm]_b & [n1Nm]_{b\psi} & 0 \\ [n1Nm]_{\psi b} & [n1Nm]_{\psi} & 0 \\ 0 & 0 & 0 \end{bmatrix} + \begin{bmatrix} [n1Nb]_b & [n1Nb]_{b\psi} & 0 \\ [n1Nb]_{\psi b} & [n1Nb]_{\psi} & 0 \\ 0 & 0 & 0 \end{bmatrix} \right) \begin{Bmatrix} w_b \\ \psi \\ w_m \end{Bmatrix} \quad (2.43) \\
& + \frac{1}{3} \begin{bmatrix} [n2]_b & [n2]_{b\psi} & 0 \\ [n2]_{\psi b} & [n2]_{\psi} & 0 \\ 0 & 0 & 0 \end{bmatrix} \begin{Bmatrix} w_b \\ \psi \\ w_m \end{Bmatrix} + \alpha \begin{bmatrix} [k_s]_b & [k_s]_{b\psi} & 0 \\ [k_s]_{\psi b} & [k_s]_{\psi} & 0 \\ 0 & 0 & 0 \end{bmatrix} \begin{Bmatrix} w_b \\ \psi \\ w_m \end{Bmatrix} \\
& + \begin{bmatrix} [m]_b & [m]_{b\psi} & 0 \\ [m]_{\psi b} & [m]_{\psi} & 0 \\ 0 & 0 & [m]_m \end{bmatrix} \begin{Bmatrix} \ddot{w}_b \\ \ddot{\psi} \\ \ddot{w}_m \end{Bmatrix} \\
& = \begin{Bmatrix} \{p_p\}_b \\ \{p_p\}_{\psi} \\ 0 \end{Bmatrix} + \begin{Bmatrix} 0 \\ \{p_{\Delta T}\}_{\psi} \\ \{p_{\Delta T}\}_m \end{Bmatrix} + \begin{Bmatrix} \{p_{\Delta T_o}\}_b \\ \{p_{\Delta T_o}\}_{\psi} \\ 0 \end{Bmatrix} + \begin{Bmatrix} 0 \\ 0 \\ \{p_{No}\}_m \end{Bmatrix} + \begin{Bmatrix} \{p_{Noo}\}_b \\ \{p_{Noo}\}_{\psi} \\ 0 \end{Bmatrix}
\end{aligned}$$

or in the short form,

$$\begin{aligned}
& ([k] + [k_o] - [k_{N\Delta T}] + [k_{No}])\{w\} \\
& + \frac{1}{2}([n1] + [n1_o] + [n1_{Nm}] + [n1_{Nb}])\{w\} \\
& + \frac{1}{3}[n2]\{w\} + \alpha[k_s]\{w\} + [m]\{\ddot{w}\} \\
& = \{p_p(t)\} + \{p_{\Delta T}\} + \{p_{\Delta To}\} + \{p_{No}\} + \{p_{Noo}\}
\end{aligned} \tag{2.44}$$

where $[m]$, $[k]$ and $\{p\}$ denote the element mass, linear stiffness matrices and load vector, respectively, and $[n1]$ and $[n2]$ denote the first and second-order nonlinear stiffness matrices, respectively. The subscripts b, ψ and m denote the transverse, rotation and in-plane components, respectively. The subscripts s, o, No, $N\Delta T$, Nm, Nb denote the stiffness matrices which are due to transverse shear, $w_o(x,y)$, $\{No\}$, $\{N_{\Delta T}\}$, $\{N_m\}([A]\{\epsilon_m^o\})$, and $\{N_b\}([B]\{\kappa\})$, respectively. The expressions for element stiffness, nonlinear stiffness, mass matrices and load vectors are given in the Appendix B.

2.7 Grazing Acoustic Wave

The grazing incidence acoustic wave applied on a plate can be treated as an extension of the plane wave which includes in the travelling wave a combination of wavelengths such that the pressure at any one point is random but the whole pattern moves in the direction λ with wave traveling speed c . The pressure distribution on a plate is then given by [Clarkson]

$$p(x, y, t) = \frac{1}{2\pi} \int_{-\infty}^{\infty} P(\omega) e^{i\omega(t - \frac{x}{c} \sin \lambda)} d\omega \tag{2.45}$$

where x is the coordinate along the wave travelling direction, and assume that the pressure distribution is independent of y . This model is suitable to represent the waves in the progressive-wave test facility.

For a random plane wave, the pressure at a point can be written in the Fourier integral form:

$$\bar{p}(t) = \frac{1}{2\pi} \int_{-\infty}^{\infty} \bar{P}(\omega) e^{i\omega t} d\omega \quad (2.46)$$

Physically, this is equivalent to representing the oncoming wave as the sum of an infinite number of waves of different wavelength.

The nodal force vector of an element can be calculated as:

$$\begin{aligned} \{p_p(t)\} &= \int_A \{H_w\} p(x, y, t; \lambda) dA \\ &= \frac{1}{2\pi} \int_{-\infty}^{\infty} P(\omega) e^{i\omega t} \int_A e^{-\frac{i\omega x \sin \lambda}{c}} \{H_w\} dA d\omega \end{aligned} \quad (2.47)$$

Let

$$\{Y(\omega)\} = \int_A e^{-\frac{i\omega x \sin \lambda}{c}} \{H_w\} dA \quad (2.48)$$

then we have

$$\{p_p(t)\} = \frac{1}{2\pi} \int_{-\infty}^{\infty} P(\omega) \{Y(\omega)\} e^{i\omega t} d\omega \quad (2.49)$$

where $\{H_w\}$ is defined in Eq. (2.3) as

$$w(x, y, t) = \{H_w\}^T \begin{Bmatrix} \{w_b\} \\ \{\psi\} \end{Bmatrix} = \{H_w(x, y)\}^T \{w_b\} + \{H_{w\psi}\}^T \{\psi\} \quad (2.50)$$

and the nodal displacement components $\{w_b\}$ and $\{\psi\}$ are defined in Eq. (2.2). Therefore, $P(\omega)\{Y(\omega)\}$ is the Fourier transform of $\{p_p(t)\}$. The spectrum density of $\{p_p(t)\}$ is (Clarkson, 1986)

$$\begin{aligned} \{S_f(\omega)\} &= \lim_{T \rightarrow \infty} \frac{\pi}{T} |P(\omega) \{Y(\omega)\}|^2 \\ &= S_p(\omega) |\{Y(\omega)\}|^2 \end{aligned} \quad (2.51)$$

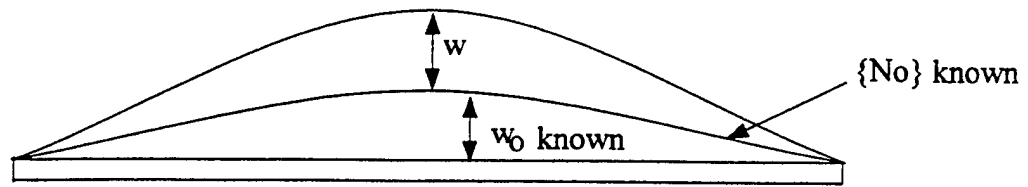


Fig. 2.1 An Initially Deflected and Stressed Plate

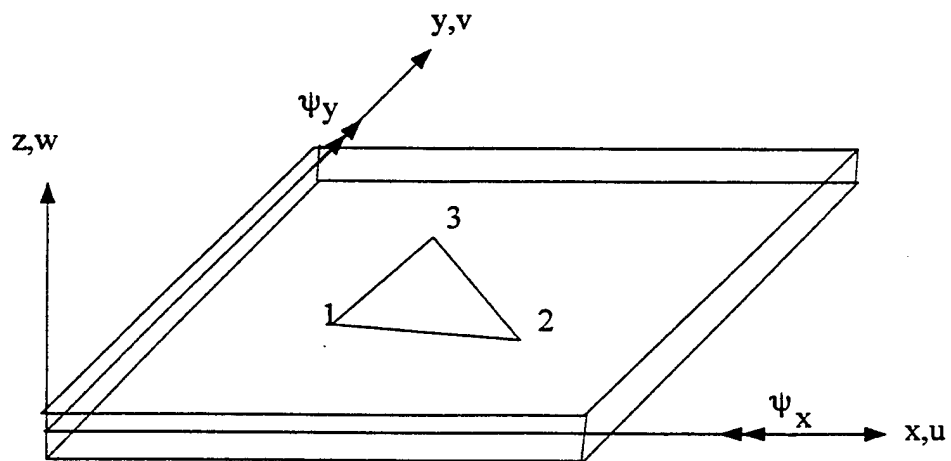


Fig. 2.2 A Typical MIN3 Element.

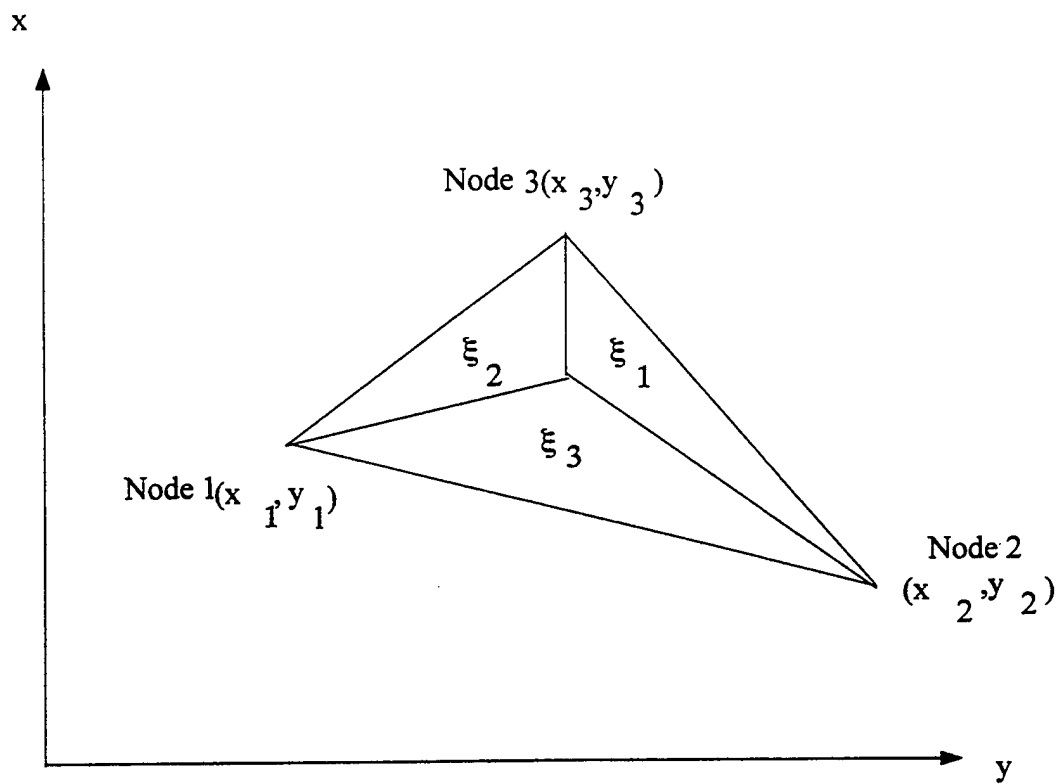


Fig. 2.3 A Mindlin Triangular Plate Element

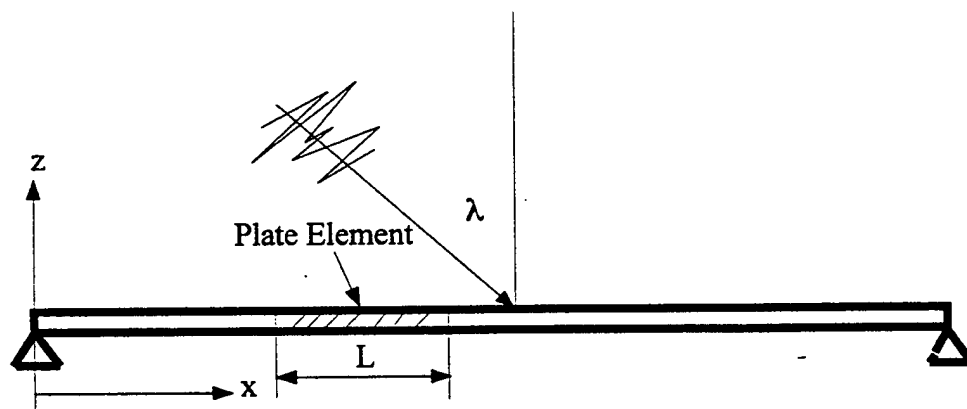


Fig. 2.4 Grazing Acoustic Wave

Chapter 3

SOLUTION PROCEDURE

3.1 Static Component and Dynamic Component

The system equation of motion can be written as

$$\begin{aligned}
 [M]\{\ddot{W}\} + ([K] + [K_o] - [K_{N\Delta T}] + [K_{No}])\{W\} \\
 + \frac{1}{2}[N1]\{W\} + \frac{1}{3}[N2]\{W\} + \alpha[K_s]\{W\} \\
 = \{P_p(t)\} + \{P_{\Delta T}\} + \{P_{\Delta T_o}\} + \{P_{No}\} + \{P_{No_o}\}
 \end{aligned} \tag{3.1}$$

where $\{W\}^T = [W_b, \Psi, W_m]$. The subscripts s, o, No, $N\Delta T$, Nm, Nb denote the stiffness matrices which are due to transverse shear, $w_o(x,y)$, $\{No\}$, $\{N_{\Delta T}\}$, $\{N_m\}([A]\{\epsilon_m^o\})$, and $\{N_b\}([B]\{\kappa\})$, respectively. And

$$[N1] = \sum_{assembly} ([n1] + [n1_{Nm}] + [n1_{Nb}] + [n1_o]) \tag{3.2}$$

In order to solve the system equation of motion Eq. (3.1), an innovative solution procedure is described as follows. First, the response is assumed to be the sum of $\{W\}_s$ and $\{W\}_t$, i.e. $\{W\} = \{W\}_s + \{W\}_t$, where $\{W\}_s$ denotes the time-independent or static component and $\{W\}_t$ the time-dependent or dynamic component. The displacement $\{W\}_s$ represents a stable static equilibrium position due to thermal load and the mean of the random excitation $E[\{P_p(t)\}]$; while $\{W\}_t$ represents the zero-mean random response. Substituting $\{W\}$ into Eq. (3.1) and regrouping the terms, the equation is of the form $F(\{W\}_s) = G(\{W\}_t)$ with

$$\begin{aligned}
 F(\{W\}_s) = ([K] + \alpha[K_s] + [K_o] - [K_{N\Delta T}] + [K_{No}])\{W\}_s \\
 + \frac{1}{2}[N1]_s\{W\}_s + \frac{1}{3}[N2]_{ss}\{W\}_s - \{P_{\Delta T}\} - E[\{P_p(t)\}]
 \end{aligned} \tag{3.3}$$

$$\begin{aligned}
G(\{W\}_t) = & [M]\{\ddot{W}\}_t + ([K] + \alpha[K_s] + [K_o] - [K_{N\Delta T}] + [K_{No}])\{W\}_t \\
& + \frac{1}{2}\left([N1]_s + \frac{2}{3}[N2]_{ss}\right)\{W\}_t + \frac{1}{2}[N1]_t\{W\}_s \\
& + \frac{1}{2}[N1]_t\{W\}_t + \frac{1}{3}([N2]_{st} + [N2]_{ts} + [N2]_{tt})(\{W\}_s + \{W\}_t) \\
& - \{P_p(t)\} + E[\{P_p(t)\}]
\end{aligned} \tag{3.4}$$

In Eq. (3.3), the load vectors $\{P_{\Delta T o}\}$, $\{P_{No}\}$ and $\{P_{Noo}\}$ are temporarily dropped. The left-hand-side of the equation, $F(\{W\}_s)$, is independent of time t ; while the right-hand-side, $G(\{W\}_t)$, is time dependent. Therefore, the only possibility for both F and G to exist is that both F and G equal to zero, and the following two equations are thus obtained:

$$\begin{aligned}
& ([K] + \alpha[K_s] + [K_o] - [K_{N\Delta T}] + [K_{No}])\{W\}_s \\
& + \frac{1}{2}[N1]_s\{W\}_s + \frac{1}{3}[N2]_{ss}\{W\}_s = \{P_{\Delta T}\} + E[\{P_p(t)\}]
\end{aligned} \tag{3.5}$$

$$\begin{aligned}
& [M]\{\ddot{W}\}_t + ([K] + \alpha[K_s] + [K_o] - [K_{N\Delta T}] + [K_{No}])\{W\}_t \\
& + \left(\frac{1}{2}[N1]_s + \frac{1}{3}[N2]_{ss}\right)\{W\}_t + \frac{1}{2}[N1]_t\{W\}_s \\
& + \frac{1}{2}[N1]_t\{W\}_t + \frac{1}{3}([N2]_{st} + [N2]_{ts} + [N2]_{tt})(\{W\}_s + \{W\}_t) \\
& = \{P_p(t)\} - E[\{P_p(t)\}]
\end{aligned} \tag{3.6}$$

where the subscript $[]_s$ denotes that the corresponding stiffness matrix is evaluated with the static deflection, and $[]_t$ is evaluated with the dynamic deflection.

Examination of Eqs. (3.5) and (3.6) reveals that both equations are nonlinear. The Newton-Raphson iterative method is used to determine $\{W\}_s$ from Eq. (3.5). Combined normal mode method and equivalent linearization technique are then applied to Eq. (3.6) to obtain $\{W\}_t$.

In Eq. (3.6), the matrix $[N1]_s$ which is ignored in the reference (Locke, 1988) is due to the membrane component of thermally postbuckling displacement $\{W_{\Delta T}\}$. The term $[N2]_{ss}\{W\}_t$ is due to the combined effect of $\{W_{\Delta T}\}$ and $\{W_{\Delta T}\}$, which has a different coefficient in Locke's formulation(1988).

When comparing with the Sequential Load method(SQL)(Locke, 1988), this Simultaneous Load method(SML) is much logical mathematically and straightforward, it is then easier to formulate nonlinear problems with combined loading. The solution procedure itself can take care of the inter-dependence between the thermal effects and the acoustic-structural response. In the SQL method engineering judgment is essential, otherwise some terms might be missed.

3.2 Thermal Buckling and Large Thermal Deflection

To obtain the critical buckling temperature change $\Delta T_{cr}(x, y)$ for a plate, it is assumed that the prebuckling configuration is flat and without coupling between bending and extension, then the linear system equation in membrane

$$[K_m]\{W_m\} = \{P_m \Delta T\} \quad (3.7)$$

is solved for an assumed temperature distribution ΔT first. Once $\{W_m\}$ is obtained, one can calculate the first-order nonlinear stiffness matrix $[N1_{Nm}]$. Because the nonlinear term due to transverse deflection does not exist, the stability equation of the investigated plate becomes

$$([K_b] - [K_{N\Delta T}] + [N1_{Nm}]) \begin{Bmatrix} \Delta W_b \\ \Delta \Psi \end{Bmatrix} = 0 \quad (3.8)$$

where

$$[K_b] = \begin{bmatrix} 0 & 0 \\ 0 & K_\psi \end{bmatrix} + \alpha \begin{bmatrix} K_{sb} & K_{sb\psi} \\ K_{s\psi b} & K_{s\psi\psi} \end{bmatrix} \quad (3.9)$$

Examination of Eq. (3.8) reveals that $[K_b]$ is independent of temperature change, and $(-[K_{N\Delta T}] + [N1_{Nm}])$ is proportional to temperature change. Therefore Eq. (3.8) describes an eigenvalue problem. The critical buckling temperature change is

$$\Delta T_{cr} = \lambda_1 \Delta T \quad (3.10)$$

where λ_1 is the lowest eigenvalue. For a non-symmetrically laminated plate, the ΔT_{cr} from Eq. (3.10) is referred as reference temperature, ΔT_{ref} .

The iterative solution scheme is to seek a solution $\{W\}_s$ of $F(\{W\}_s) = 0$. The Newton-Raphson iterative method is a well established procedure for solving time-independent nonlinear problems. This method involves a repeated solution of the equation for the i -th iteration

$$[K]_{T,i} \{\Delta W\}_{s,i+1} = \{\Delta P\}_{s,i} \quad (3.11)$$

Then $[K]_{T,i+1}$ and $\{\Delta P\}_{s,i+1}$ are updated by using $\{W\}_{s,i+1} = \{W\}_{s,i} + \{\Delta W\}_{s,i+1}$. The solution process seeks to reduce the load imbalance, and consequently $\{\Delta W\}_s$, to a specified small quantity. The tangent-stiffness matrix is determined from

$$[K]_T = \left[\frac{dF(\{W\}_s)}{d(\{W\}_s)} \right] = [K] + \alpha[K_s] + [K_o] + [K_{No}] - [K_{N\Delta T}] + [N1]_s + [N2]_{ss} \quad (3.12)$$

and the load imbalance vector is

$$\{\Delta P\}_s = \{P\}_s - ([K] + \alpha[K_s] + [K_o] + [K_{No}] - [K_{N\Delta T}] + \frac{1}{2}[N1]_s + \frac{1}{3}[N2]_{ss})\{W\}_s \quad (3.13)$$

where $\{P\}_s = \{P_{\Delta T}\} + E[\{P_p(t)\}]$. The linear buckling mode shape from Eq.(3.8) multiplying a scale factor is usually taken to be the initial trial solution of Eq. (3.11).

3.3 Nonlinear Random Response

After solving $\{W\}_s$ from Eq. (3.5) and evaluating the matrices $[N1]_s$ and $[N2]_{ss}$, Eq. (3.6) is ready to be solved. Firstly, Eq. (3.6) will be reduced to a system of coupled nonlinear modal equations with reduced degree-of-freedom. The linear vibration modes of the deformed structure are used to transform the system equation of motion to modal coordinates. The resulting nonlinear modal equations of motion are then linearized using the equivalent linearization method. Finally, in order to uncouple the linearized equations of motion, a modal transformation is used once more.

Coupled nonlinear modal equations

From Eq.(3.6), the linear frequencies and mode shapes of the deformed structure can be obtained by solving the eigenvalue problem

$$([K] + \alpha[K_s] + [K_o] - [K_{N\Delta T}] + [K_{No}] + [N1]_s + [N2]_{ss})\{\phi\}_n = \omega_n^2[M]\{\phi\}_n \quad (3.14)$$

where it is assumed that

$$[N1]_s\{W\}_t = \frac{1}{2}[N1]_s\{W\}_t + \frac{1}{2}[N1]_t\{W\}_s \quad (3.15)$$

and

$$[N2]_{ss}\{W\}_t = \frac{1}{3}[N2]_{ss}\{W\}_t + \frac{1}{3}[N2]_{st}\{W\}_s + \frac{1}{3}[N2]_{ts}\{W\}_s \quad (3.16)$$

Actually, from numerical test this assumption doesn't introduce significant error. Solving Eq. (3.14), the truncated modal matrix is given by

$$[\phi] = [\{\phi\}_1, \{\phi\}_2, \dots, \{\phi\}_N] \quad (3.17)$$

where N is the number of modes to be used for the analysis of Eq. (3.6). Now $\{W\}_t$ can be written in terms of the modal amplitudes as

$$\{W\}_t = [\phi]\{q\} = \sum_{n=1}^N \{\phi\}_n q_n \quad (3.18)$$

Using Eq. (3.18), the first-order nonlinear system stiffness matrix can be written in terms of $\{q\}$ as the sum of first-order nonlinear system modal stiffness matrices

$$[N1]_t = \sum_{n=1}^N q_n [N1]_t^{(n)} \quad (3.19)$$

and

$$[N1]_t^{(n)} = \sum_{assembly} ([n1] + [n1_{Nm}] + [n1_o] + [n1_{Nb}])^{(n)} \quad (3.20)$$

$$\frac{1}{2}[N1]_t\{W\}_s = \frac{1}{2}[K1]_s\{q\} \quad (3.21)$$

$$\frac{1}{3}([N2]_{st} + [N2]_{ts})\{W\}_s = \frac{1}{3}[K2]_{st}\{q\} \quad (3.22)$$

$$\frac{1}{3}[N2]_{tt}\{W\}_s = \frac{1}{3}\sum_{n=1}^N q_n [K2]_{tt}^{(n)}\{q\} \quad (3.23)$$

where the i th column in $[K1]_s$, $[K2]_{st}$ and $[K2]_{tt}^{(n)}$ are

$$\begin{aligned} \{K1\}_{si} &= [N1]_t^{(i)}\{W\}_s; \{K2\}_{sti} = ([N2]_{st} + [N2]_{ts})^{(i)}\{W\}_s \\ \{K2\}_{tti}^{(n)} &= [N2]_{tti}^{(n)}\{W\}_s \end{aligned} \quad (3.24)$$

The second-order nonlinear system stiffness matrices as the sum of second-order nonlinear system modal stiffness matrices are

$$[N2]_{st} = \sum_{n=1}^N q_n [N2]_{st}^{(n)} \quad (3.25)$$

and

$$[N2]_{st}^{(n)} = \sum_{assembly} [n2]_{st}^{(n)} \quad (3.26)$$

$$[N2]_{ts} = \sum_{n=1}^N q_n [N2]_{ts}^{(n)} \quad (3.27)$$

$$[N2]_{ts}^{(n)} = \sum_{assembly} [n2]_{ts}^{(n)} \quad (3.28)$$

similarly

$$[N2]_{tt} = \sum_{n=1}^N \sum_{r=1}^N q_n q_r [N2]_{tt}^{(nr)} \quad (3.29)$$

$$[N2]_{tt}^{(nr)} = \sum_{assembly} [n2]_{tt}^{(nr)} \quad (3.30)$$

where superscripts $[]^{(n)}$ and $[]^{(nr)}$ denote the corresponding nonlinear modal stiffness matrix is evaluated with the modes $\{\phi\}_n$ and $\{\phi\}_r$.

Substituting these nonlinear modal stiffness matrices into Eq. (3.6), a set of nonlinear coupled modal equations of motion can be expressed as

$$\begin{aligned}
[\phi]^T G(\{W\}_t) &= [M]\{\ddot{q}\} + [K]_{linear}\{q\} \\
&+ [\phi]^T \left(\frac{1}{2}[K1]_s + \frac{1}{3}[K2]_{st} \right) \{q\} + \frac{1}{3}[\phi]^T \sum_{n=1}^N q_n [K2]_{tt}^{(n)} \{q\} \\
&+ [\phi]^T \sum_{n=1}^N q_n \left(\frac{1}{2}[N1]_t^{(n)} + \frac{1}{3}[N2]_{st}^{(n)} + \frac{1}{3}[N2]_{ts}^{(n)} \right) [\phi]\{q\} \\
&+ [\phi]^T \left(\frac{1}{3} \sum_{n=1}^N \sum_{r=1}^N q_n q_r [N2]_{tt}^{(nr)} \right) [\phi]\{q\} - \{f\} = 0
\end{aligned} \tag{3.31}$$

where the modal force vector and the diagonal modal mass and linear stiffness matrices are

$$\{f\} = [\phi]^T \{P\}_t \tag{3.32}$$

$$[M] = [\phi]^T [M] [\phi] = \begin{bmatrix} m_1 & & 0 \\ & \ddots & \\ 0 & & m_N \end{bmatrix} \tag{3.33}$$

$$\begin{aligned}
[K]_{linear} &= [\phi]^T \left([K] + \alpha[K_s] + [K_o] - [K_{N\Delta T}] + [K_{No}] + \frac{1}{2}[N1]_s + \frac{1}{3}[N2]_{ss} \right) [\phi] \\
&= \begin{bmatrix} \omega_1^2 m_1 & & 0 \\ & \ddots & \\ 0 & & \omega_N^2 m_N \end{bmatrix}
\end{aligned} \tag{3.34}$$

$$\{P\}_t = \{P_p(t)\} - E[\{P_p(t)\}] \tag{3.35}$$

and $[]$ denotes a diagonal matrix. Equation (3.31), is a set of coupled nonlinear modal equations, it is then linearized by using the equivalent linearization method (Atalik and Utku, 1976, and Roberts and Spanos, 1990).

Equivalent linearization and coupled linearized modal equations

Rewriting Eq. (3.31) in the form

$$\{g(\{q\})\} + [M]\{\ddot{q}\} = \{f\} \tag{3.36}$$

The corresponding linear form of Eq. (3.31) can be expressed as

$$[\bar{K}]\{q\} + [M]\{\ddot{q}\} = \{f\} \quad (3.37)$$

where $[\bar{K}]$ is an equivalent linear modal stiffness matrix. The error vector involved in using Eq. (3.37) instead of Eq. (3.36) is given by the difference between the two equations as

$$\{e\} = \{g(\{q\})\} - [\bar{K}]\{q\} \quad (3.38)$$

The equivalent linear stiffness matrix $[\bar{K}]$ can be found by requiring that the mean square value of error be a minimum, thus we have

$$\frac{\partial E[\{e\}^T \{e\}]}{\partial \bar{K}_{nr}} = 0 \quad n, r = 1, 2, \dots, N \quad (3.39)$$

Substituting $\{e\}$ and $\{g(\{q\})\}$ into Eq. (3.39), the equivalent stiffness matrix $[\bar{K}]$ can be determined from the equation

$$E[\{q\}\{q\}^T][\bar{K}] = E[\{q\}\{g\}^T] \quad (3.40)$$

The right-hand side of Eq. (3.40) can be evaluated as

$$\begin{aligned} E[\{q\}\{g\}^T] &= E[\{q\}\{q\}^T][K]_{linear} + E[\{q\}\{q\}^T] \left[[\phi]^T \left(\frac{1}{2}[K1]_s + \frac{1}{3}[K2]_{st} \right) \right]^T \\ &\quad + \frac{1}{3} \sum_n E[q_n \{q\}\{q\}^T] \left[[\phi]^T [K2]_{tt}^{(n)} \right]^T \\ &\quad + \sum_n E[q_n \{q\}\{q\}^T] \left[[\phi]^T \left(\frac{1}{2}[N1]_t^{(n)} + \frac{1}{3}[N2]_{st}^{(n)} + \frac{1}{3}[N2]_{ts}^{(n)} \right) [\phi] \right]^T \\ &\quad + \frac{1}{3} \sum_n \sum_r E[q_n q_r \{q\}\{q\}^T] \left[[\phi]^T [N2]_{tt}^{(nr)} [\phi] \right]^T \\ &= E[\{q\}\{q\}^T][K]_{linear} + E[\{q\}\{q\}^T] \left[[\phi]^T \left(\frac{1}{2}[K1]_s + \frac{1}{3}[K2]_{st} \right) \right]^T \\ &\quad + \frac{1}{3} \sum_n \sum_r E[q_n q_r \{q\}\{q\}^T] \left([K2]^{(nr)} \right)^T \end{aligned} \quad (3.41)$$

since $E[q_n\{q\}\{q\}^T] = 0$ for Gaussian process, and

$$[K2]^{(nr)} = \frac{1}{3}[\phi]^T[N2]_{tt}^{(nr)}[\phi] \quad (3.42)$$

If the covariance matrix $E[\{q\}\{q\}^T]$ is known, the equivalent linear stiffness matrix $[\bar{K}]$ can be determined from Eq. (3.41). However, $\{q\}$ has to be obtained first from Eq. (3.37) and $[\bar{K}]$ is not known. In order to solve Eq. (3.37), modal coordinate transform is used once again with an iterative scheme.

Uncoupled linear modal equations

The modal transformation is used once more and it is determined from the equation

$$[\bar{K}]\{\tilde{\phi}\} = \Omega^2[M]\{\tilde{\phi}\} \quad (3.43)$$

and the modal transformation matrix is defined as

$$\{q\} = [\{\tilde{\phi}\}_1, \{\tilde{\phi}\}_2, \dots, \{\tilde{\phi}\}_N]\{\eta\} = [\tilde{\phi}]\{\eta\} \quad (3.44)$$

Equation (3.37) thus becomes a set of uncoupled modal equations

$$\ddot{\eta}_j + \xi\dot{\eta}_j + \Omega_j^2\eta_j = \tilde{f}_j \quad j = 1, 2, \dots, N \quad (3.45)$$

where

$$\tilde{f}_j = \frac{\{\tilde{\phi}\}_j^T\{f\}}{\tilde{m}_j} \quad (3.46)$$

$$\tilde{m}_j = \{\tilde{\phi}\}_j^T[M]\{\tilde{\phi}\}_j \quad (3.47)$$

and $\xi\dot{\eta}_j = 2\zeta\omega_{l1}\dot{\eta}_j$ is the modal damping term which has been added to Eq. (3.45), and ω_{l1} is the first linear frequency of the deformed system, which is obtained from Eq. (3.14).

Solutions for the uncoupled modal equation of motion Eq. (3.45) for the case of Gaussian white noise uniform random load $p(t)$ are given in the following form

$$E[\eta_j\eta_k] = S_P\tilde{f}_j\tilde{f}_kI_{jk} \quad (3.48)$$

where

$$I_{jk} = \int_{-\infty}^{\infty} H_j(\omega) H_k(-\omega) d\omega = \frac{4\pi\xi}{(\Omega_j^2 - \Omega_k^2)^2 + 2\xi^2(\Omega_j^2 + \Omega_k^2)} \quad (3.49)$$

where

$$H_j(\omega) = \frac{1}{\Omega_j^2 - \omega^2 + i\xi\omega} \quad (3.50)$$

and S_P is the double sided loading spectrum density. Using Eq. (3.44), the covariance matrix of the coupled modal amplitude becomes

$$\begin{aligned} E[\{q\}\{q\}^T] &= E\left[\left[\tilde{\phi}\right]\{\eta\}\{\eta\}^T\left[\tilde{\phi}\right]^T\right] \\ &= \left[\tilde{\phi}\right] E[\{\eta\}\{\eta\}^T] \left[\tilde{\phi}\right]^T \end{aligned} \quad (3.51)$$

The deflection spectrum density is as follows:

$$\begin{aligned} G_{\eta_j\eta_k} &= S_P \tilde{f}_j \tilde{f}_k H_j(\omega) H_k(-\omega) \\ [G_w] &= [\phi] \left[\tilde{\phi}\right] [G_{\eta_j\eta_k}] \left[\tilde{\phi}\right]^T [\phi]^T \end{aligned} \quad (3.52)$$

For grazing incidence, the covariance terms for the case of ideal white noise excitation can be expressed as

$$E[\eta_j\eta_k] = 2 \int_0^{\infty} S_P(\omega) |Z_j(\omega) Z_k(\omega)| |H_j(\omega) H_k(-\omega)| d\omega \quad (3.53)$$

where

$$Z_j(\omega) = \frac{1}{\tilde{m}_j} \left\{ \tilde{\phi} \right\}_j^T [\phi]^T \{Y(\omega)\} \quad (3.54)$$

and

$$\{Y(\omega)\} = \sum_{element} \int_A \left[\cos\left(\frac{\omega x \sin \theta}{c}\right) - i \sin\left(\frac{\omega x \sin \theta}{c}\right) \right] \begin{Bmatrix} H_w \\ H_{w\psi} \end{Bmatrix} dA \quad (3.55)$$

In order to calculate $E[\eta_j\eta_k]$ from Eq. (3.53), a simple numerical integration method is used, the cut off frequency is $1.5 * \Omega_N$.

Iterative solution procedure

Therefore, Eqs. (3.40), (3.41) and (3.51) can be used to determine $[\bar{K}]$ and $E[\{q\}\{q\}^T]$. However, since each of these quantities is dependent on the other and these equations are nonlinear, consequently, they must be solved by an iterative method.

The first approximation of $[\bar{K}]$ and $E[\{q\}\{q\}^T]$ is obtained by neglecting the cross terms in $E[\{q\}\{q\}^T]$, (i.e. $E[q_n q_r] = 0$ for $n \neq r$), and assuming all the equations in Eq.(3.37) are uncoupled. The diagonal terms in the equivalent linear stiffness matrix $[\bar{K}]$ can be expressed from Eqs. (3.40) and (3.41) as

$$\bar{K}_{nn} = K_n + 3(K2_{nn})^{(nn)} E[q_n^2] \quad (3.56)$$

where $(K2_{nn})^{(nn)}$ are the diagonal terms of the second-order nonlinear stiffness matrix, the subscript nn denotes the diagonal term and the superscript (nn) denotes the term is due to the n -th mode $\{\phi\}_n$. From Eq. (3.43) Ω_n^2 can be written as

$$\Omega_n^2 = \frac{\bar{K}_{nn}}{\tilde{m}_n} = \omega_n^2 + 3(K2_{nn})^{(nn)} E[q_n^2] / \tilde{m}_n \quad (3.57)$$

and $E[q_n^2]$ can be found from Eq. (3.48) for this uncoupled first approximation ($\eta_n = q_n$, $\tilde{f}_n = f_n/m_n$) to be

$$E[q_n^2] = S_P \frac{f_n^2}{m_n^2} \left(\frac{\pi}{\xi \Omega_n^2} \right) \quad (3.58)$$

Using Eqs. (3.57) and (3.58), $E[q_n^2]$ can be determined to be

$$E[q_n^2] = \left(\sqrt{B^2 + 4C} - B \right) / 2 \quad (3.59)$$

where

$$\begin{aligned} B &= K_n / 3(K2_{nn})^{(nn)} \\ C &= S_P f_n^2 \pi / 3 \xi m_n (K2_{nn})^{(nn)} \end{aligned} \quad (3.60)$$

To begin the iteration process for the cross terms are no longer neglected, the cross correlation terms $E[q_n q_r]$ can be evaluated using Eq. (3.48) with Eq. (3.49) and (3.51). Using Eqs. (3.40) and (3.41), the equivalent linear stiffness can be computed. After obtaining $[\bar{K}]$, a new iterative cycle begins. The iterative process goes on, until some convergence criteria are satisfied, $\frac{|E[q_n^2]_{i+1} - E[q_n^2]_i|}{E[q_n^2]_i} \leq 10^{-6}$ for all n, then the iteration is terminated. The covariance matrix can be found from

$$E[\{W\}_t \{W\}_t^T] = [\phi] E[\{q\} \{q\}^T] [\phi]^T \quad (3.61)$$

3.4 Strain Formulas

After the displacements for a given combination of thermal and acoustic load condition are known, the element strains can be calculated using Eqs. (2.11), (2.12), (2.13) and (2.14). Because the displacements consist of two parts, dynamic and static. The strains can be expressed as

$$\{\epsilon\} = \{\epsilon^o\} + z\{\kappa\} = \{\epsilon\}_s + \{\epsilon\}_t \quad (3.62)$$

$$\{\gamma\} = \{\gamma\}_s + \{\gamma\}_t \quad (3.63)$$

where

$$\begin{aligned} \{\epsilon\}_s = & [C_m]\{w_m\}_s + \frac{1}{2}[\theta]_s([C_{\psi b}]\{w_b\}_s + [C_{\psi\psi}]\{\psi\}_s) \\ & + [\theta]_s([C_{\psi b}]\{w_{bo}\} + [C_{\psi\psi}]\{\psi_o\}) + z[C_b]\{\psi\}_s \end{aligned} \quad (3.64)$$

and

$$\{\epsilon\}_t = \sum_{j=1}^N \{\epsilon\}_{1j} q_j + \sum_{j=1}^N \sum_{k=1}^N \{\epsilon\}_{2jk} q_j q_k \quad (3.65)$$

where

$$\{\epsilon\}_{1j} = [C_m]\{\phi_m\}_j + [\theta]_j([C_{\psi b}]\{w_{bo}\} + [C_{\psi\psi}]\{\psi_o\}) + z[C_b]\{\phi_\psi\}_j \quad (3.66)$$

$$\{\epsilon\}_{2jk} = \frac{1}{2}[\theta]_j([C_{\psi b}]\{\phi_b\}_k + [C_{\psi\psi}]\{\phi_\psi\}_k) \quad (3.67)$$

$$[\theta]_j = \begin{bmatrix} \phi_{bj,x} & 0 \\ 0 & \phi_{bj,y} \\ \phi_{bj,y} & \phi_{bj,x} \end{bmatrix} \quad (3.68)$$

For the shear strain,

$$\{\gamma\}_s = [C_{\gamma b}]\{w_b\}_s + [C_{\gamma\psi}]\{\psi\}_s \quad (3.69)$$

and

$$\{\gamma\}_t = \sum_{j=1}^N ([C_{\gamma b}]\{\phi_b\}_j + [C_{\gamma\psi}]\{\phi_\psi\}_j) q_j = \sum_{j=1}^N \{\gamma\}_{1j} q_j \quad (3.70)$$

Using the above $\{\epsilon\}_s$ and $\{\epsilon\}_t$ formulation, the stain vector can be expressed as

$$E\left[\{\epsilon\}_t\{\epsilon\}_t^T\right] = \sum_{i=1}^N \sum_{j=1}^N \left(2\{\epsilon_s\}\{\epsilon_{2ij}\}^T + \{\epsilon\}_{1i}\{\epsilon\}_{1j}\right) E[q_i q_j] \\ + \sum_{i=1}^N \sum_{j=1}^N \sum_{k=1}^N \sum_{l=1}^N \{\epsilon\}_{2ij}\{\epsilon\}_{2kl}^T E[q_i q_j q_k q_l] \quad (3.71)$$

and

$$E\left[\{\gamma\}_t\{\gamma\}_t^T\right] = \sum_{i=1}^N \sum_{j=1}^N \{\gamma\}_{1i}\{\gamma\}_{1j}^T E[q_i q_j] \quad (3.72)$$

where

$$E[q_i q_j q_k q_l] = E[q_i q_j] E[q_k q_l] + E[q_i q_k] E[q_j q_l] + E[q_i q_l] E[q_j q_k] \quad (3.73)$$

Chapter 4

NUMERICAL RESULTS AND DISCUSSION

4.1 Formulation and Computer Program Validation

4.1.1. Twisted Ribbon Tests

A cantilevered, thin rectangular plate subject to a twisting moment at the free end is regarded as a severe test for plate bending elements under large aspect ratio distortions (Robinson, 1979). Herein, the mesh A (Figs. 4.1 and 4.2) results has been repeated. The tip deflection results are compared with the results produced by the popular nine degrees-of-freedom, thin triangles, namely, BCIZ1, HSM, HCT and DKT, are shown in Figs. 4.1 and 4.2. In this comparison, the MIN3 which is adopted for the present random analysis appears to outperform the other triangular elements.

4.1.2. Static Analysis of a Rhombic Cantilever

This problem deals with the analysis of a rhombic cantilevered plate subjected to a uniform load. The geometry and material properties are given in Figure 4.3. Experimental results of this problem are available for comparison (Clough and Tocher, 1965). A 4 by 4 mesh (32 elements) is used and the results obtained with MIN3 and test are given in Table 4.1. It is observed that even with this coarse mesh, the MIN3 element gives results in good agreement with the experimental values (Batoz et al., 1980).

4.1.3. Thermal Buckling and Post Buckling

For this problem, a square plate with two boundary conditions is calculated, one is simply supported and the other is clamped. The results are compared with the results by Paul (1982) and Singh (1993), the agreement is very good.

For the simply supported square plate, the results are given below:

$$\begin{aligned}\Delta T_{cr} &= 1.777^\circ F \\ \frac{\Delta T}{\Delta T_{cr}} &= 2.0 \quad \frac{W_{\Delta T}}{h} = 0.852\end{aligned}\tag{4.1}$$

For the clamped support square plate, the following is obtained:

$$\begin{aligned}\Delta T_{cr} &= 4.67^\circ F \\ \frac{\Delta T}{\Delta T_{cr}} &= 1.19 \quad \frac{W_{\Delta T}}{h} = 0.58 \\ \frac{\Delta T}{\Delta T_{cr}} &= 1.40 \quad \frac{W_{\Delta T}}{h} = 0.852 \\ \frac{\Delta T}{\Delta T_{cr}} &= 1.62 \quad \frac{W_{\Delta T}}{h} = 1.054\end{aligned}\tag{4.2}$$

4.1.4. Random Response and Strain Validation

The plate used by Chiang (1988) was analyzed as a validation example. The plate is of the following dimension and material properties:

Young's modulus	$E = 10.5 \times 10^6 psi$
mass density	$\rho = 0.2588 \times 10^{-3} lbsec^2/in^4$
damping ratio	$\zeta = 0.01$
length	$a = 15in$
width	$b = 12in$
thickness	$h = 0.04in$
Poisson's ratio	$\nu = 0.33$

The results obtained by the present study and Chiang are shown in Table 4.2. Because the elements used are different, the difference of strain values for N=4 is relatively large. The others are close.

4.2 Thermal Buckling and Postbuckling Results

In order to understand the response of a plate to combined acoustic and thermal load better, the thermal buckling and postbuckling behavior of a composite plate is studied in this section. Seven cases are investigated. The graphite-epoxy material properties are taken as:

Young's moduli	$E_1 = 22.5 \times 10^6, E_2 = 1.17 \times 10^6 \text{ psi}$
Shear moduli	$G_{23} = 0.4 \times 10^6, G_{12} = G_{13} = 0.66 \times 10^6 \text{ psi}$
Poisson's ratio	$\nu_{12} = 0.22$
Therm. expan. coeff.	$\alpha_1 = -0.04 \times 10^{-6}/F^\circ, \alpha_2 = 16.7 \times 10^{-6}/F^\circ$

The finite element results are presented as follows:

4.2.1. Effect of Extension and Bending Coupling

The bending and extension coupling is studied first. A two-layer Gr/Ep rectangular laminate (15×12×0.048 in.) with the stacking sequence of (0/90) is considered. For this case the extension and bending coupling matrix [B] is not equal to zero, therefore the critical buckling temperature does not exist. When the laminate is subjected to the temperature change, the bending deflection occurred immediately. The postbuckling deflection is shown in Fig. 4.4 for the simply supported boundary condition. The ΔT_{ref} used in the figure is $13.37F^\circ$ only for reference purpose, and it has no physical meaning. In the calculation, the full plate is discretised to 128 elements or 8×8×2 mesh. From the figure one can see that there is no bifurcation critical temperature.

4.2.2. Isosceles Triangular Plate

The second problem investigated is an isosceles right triangular plate with symmetrical stacking sequence of $(0/45/-45/90)_s$, the length of two perpendicular sides is 12 in. The plate is simulated by 144 elements. In Fig. 4.5, the postbuckling behavior is shown for simply supported and clamped boundary conditions. These two conditions are theoretically idealized, the boundary conditions in the real world are somewhere between them, therefore they can be considered as the upper and lower bounds.

4.2.3. Effect of Shear Deformation

The plates studied are the same as the first case, i.e. 15×12 in., but the stacking sequence is $(0/45/-45/90)_s$. The ratio of length to thickness investigated are $a/h=312.5, 200, 100, 50$ and 20 . The critical buckling temperature is shown in Fig. 4.6. As expected, the results show that when a/h is greater than 100 , the shear deformation can be neglected. But for thick laminates the shear deformation is important.

4.2.4. Effect of Number of Layers

The dimension of the plate studied in this problem is $15 \times 12 \times 0.08$ in., and the mesh used is $8 \times 8 \times 2$ (128 elements). The boundary support condition is simply supported. The plate consists of $(45/-45)_n$. In Fig. 4.7, it is shown that the increase of number of layers reduces the response due to the reduction of the extension and bending coupling.

4.2.5. Postbuckling Mode Change

The fifth problem studied is a $36 \times 12 \times 0.048$ in. long rectangular laminate, the stacking sequence is $(60/-60)$. The full plate is modeled by a $18 \times 6 \times 2$ mesh i.e. 216

elements. The results are shown in Figs. 4.8 and 4.9. The laminate is subjected only to a uniform temperature change without transverse mechanical load. For this load case, the postbuckling deflection is close to a (3,1) mode shape at low temperature. When the temperature change ΔT is greater than 20°F, there is a mode shape change and the deflection is close to a (4,1) mode.

4.2.6. Thermo-Mechanical Postbuckling

The plate investigated in the sixth problem has the same dimension and stacking sequence as the previous problem. The mechanical load of uniformly distributed 0.01 psi is applied simultaneously with the uniform temperature change. Figures 4.10 and 4.11 show the thermo-mechanical deflection and the deflection shapes. It is interesting to note that the maximum deflection exhibits slightly soften behavior at low temperature change due to increasing in thermal compressive in-plane forces. The deflection shape at this low temperature is a combination of (1,1) and (3,1) modes due to the presence of mechanical load. However, the deflection at the high temperature is changed to a (5,1) dominated mode shape. The mechanical load is to simulate the static pressure difference applied to the aircraft skin panels.

4.2.7. Effect of the Skew Angle of the Plate

In this problem, the skew angle β (see Fig. 4.12) of the plate varies, but the height (12 in.) of the parallelogram keeps the same. The length of the plate is 15 in. and the thickness is 0.048 in. The height of the plates studied is equal to 12 in. Fig. 4.12 shows the postbuckling response. When the skew angle β increases the deflection reduces, this is due to that the length of 90° fibers are relatively shorter thus making the plate stiffer.

4.2.8. Conclusions

Seven problems were studied in this section. The extension and bending coupling stiffness matrix makes the plate bending out-of-plane immediately when the plate is heated without prebuckling stage. The most interesting thing in this study is the mode shape change and the described solution procedure can automatically obtain the mode changing of postbuckling deflection as long as the incremental step of temperature change is small enough regardless of the presence of mechanical load. This study demonstrated that the finite element method can deal with different planforms, various boundary conditions as expected.

4.3 Nonlinear Random Response

The numerical results of random response to acoustic pressure only are presented in this section. A eight-layer rectangular laminate (15×12 in.) with the stacking sequence of (0/45/-45/90)_s is considered first. The plate is clamped at all four edges and with immovable inplane boundary conditions. Hereafter it is referred to as Panel 1. The material properties, mass density, and damping ratio are taken as:

Young's moduli	$E_1 = 22.5 \times 10^6, E_2 = 1.17 \times 10^6 psi$
Shear moduli	$G_{23} = 0.4 \times 10^6, G_{12} = G_{13} = 0.66 \times 10^6 psi$
Poisson's ratio	$\nu_{12} = 0.22$
mass density	$\rho = 1.45 \times 10^{-4} lb - sec^2/in.^4$
damping ratio	$\zeta = 0.02$

The root mean square (RMS) of the maximum deflection response to a normal incidence is shown in Fig. 4.13. The corresponding RMS maximum micro strain is shown in Fig.

4.14. The response consists of symmetrical modes, for this laminate the 2nd, 3rd and 4th modes are anti-symmetric, they are not appeared in the response. The frequencies are shown in Table 4.3. Figure 4.15 shows the spectrum density distribution of response vs. frequencies. When the applied acoustic load is low, the response is linear. The peak of curve is very close to the natural frequencies. But at high pressure levels the peaks are shifted up, when the SPL reaches 130 dB, the first peak appears at 358 Hz.

The second example is the same as the first one except the stacking sequence, it is a (0/90) two-layer laminate. This panel is referred to as Panel 2. The root mean square of the maximum response to a normal incidence is shown in Fig. 4.16. The corresponding RMS micro strain is shown in Fig. 4.17. Fig. 4.18 shows the spectrum density distribution of response vs. frequencies.

The third example is a swept rectangular plate as shown in Fig. 4.19. The plate consists of eight-layer laminate as same as the first one. It is referred as Panel 3. The root mean square of the maximum response to a normal incidence is shown in Fig. 4.20. The corresponding RMS micro strain is shown in Fig. 4.21. Figure 4.22 shows the spectrum density distribution of response vs. frequencies.

4.4 Acoustic-Thermal Response

The numerical results presented in this section concern with the response to combined acoustic and thermal loads.

4.4.1. Effect of Number of Modes

In order to evaluate the convergence characteristics of the present modal analysis formulation and determine the required number of modes for reasonable accuracy, an eight-layer Gr/Ep rectangular laminate (15×12 in.) with the stacking sequence of (0/45/-45/90)_s is analyzed by mode number N=1, N=2, N=3 and N=4. Anti-symmetrical modes

are not included. The plate is clamped at all four edges and with immovable inplane boundary conditions ($u=v=0$ at all four edges). The full plate is modeled with $8 \times 8 \times 2$ mesh or 128 MIN3 elements. For convenience, this plate is referred to as the baseline configuration. The material properties, mass density, and damping ratio are taken as:

Young's moduli	$E_1 = 22.5 \times 10^6, E_2 = 1.17 \times 10^6 \text{ psi}$
Shear moduli	$G_{23} = 0.4 \times 10^6, G_{12} = G_{13} = 0.66 \times 10^6 \text{ psi}$
Poisson's ratio	$\nu_{12} = 0.22$
mass density	$\rho = 1.45 \times 10^{-4} \text{ lb} - \text{sec}^2/\text{in.}^4$
damping ratio	$\zeta = 0.02$

The result of RMS(W_{\max}/h) without temperature is shown in Table 4.4. The first 12 mode characteristics are (1,1), (1,2), (2,1), (2,2), (1,3), (3,1), (2,3), (3,2), (1,4), (4,1), (4,3) and (3,3). The first 12 frequencies are shown in Table 4.5. The critical buckling temperature change is 37.38°F. The result shows that use of three modes obtained satisfied displacement results. Therefore, in the following calculation, three modes are used.

4.4.2. Effect of Thermal Load

The above configuration is analyzed again with $\Delta T/\Delta T_{cr} = 0.0, 2.0, 3.0$. For simplicity, this panel is called the baseline configuration. The root mean square (RMS) of the maximum deflection response to a normal incidence and temperature change is shown in Fig. 4.23. The corresponding RMS maximum micro strain is shown in Fig. 4.24. The response consists of symmetrical modes. For this laminate the 2nd, 3rd and 4th modes are antisymmetric, and they do not appear in the response. The frequencies are shown in Table 4.4. Figure 4.25 shows the spectrum density distribution of response vs. frequencies at $\Delta T/\Delta T_{cr} = 0.0$ and 3.0 and 130 dB. When the applied acoustic load is low, the response is linear. The thermal loads increase the nonlinear stiffness and the response is reduced due to the large temperature rise. The peak of the curve is very close

to the natural frequencies. But at high pressure levels the peaks are shifted up, when the SPL reaches 130 dB and $\Delta T/\Delta T_{cr} = 3.0$, the first peak appears at 2248 rad/sec.

For the simply supported boundary condition, the displacement response is much larger than clamped case, but the strain is kept at about the same amount. the results for the simply supported condition are shown in Figs. 4.26, 4.27 and 4.28. The strain with temperature (Figs. 4.24 and 4.27) could be smaller or larger than the one without temperature. It illustrates that two effects are occurred. The thermal postbuckling increases the nonlinear stiffness which reduces the RMS deflection, the strain component due to the RMS deflection is thus also reduced. On the other hand, the thermal strain increases the strain component.

4.4.3 Antisymmetric Cross-ply Laminate

The material properties and dimension of this clamped antisymmetric cross-ply laminate (0/90) are the same as the baseline configuration. Figures 4.29 4.30 and 4.31 show the mode shapes of this panel at $\Delta T=0$, 97.972 and 149.688°F, respectively. In these figures two features should be noticed: the mode sequence is changed with temperature rise; and some mode shapes are not exactly symmetric or antisymmetric as in the case of isotropic material. Figure 4.32 shows the displacement response while Figure 4.33 shows the micro strain distribution vs. sound pressure level.

4.4.4. Skewed Panel and Non-uniform Temperature

The planform of this panel is shown in Fig. 4.19. the material property is the same as the baseline configuration. The non-uniform temperature change is that at the edge grid points the temperature change is zero, at interior grids is uniform. The boundary condition is clamped. The results are shown in Figs. 4.34 and 4.35. The critical buckling temperature changes for uniform and non-uniform temperature distributions are 67.36°F and 76.32°F , respectively. It can be seen from the figures that the responses and strains for uniform temperature and nonuniform temperature have very little difference. This illustrates that the temperature gradient along the edge has little influence on random responses.

4.4.5. Grazing Incidence Wave

The plate studied in this case is the same as the baseline configuration. But the boundary condition is simply supported for transverse displacement and immovable for in-plane displacements. The thickness of the plate is 0.048 in. The dimension is 15 in. by 12 in. The stacking sequence is (0/45/-45/90)s.

The result of this example is very interesting. Because the acoustic wave is travelling along the positive direction of x axis with a speed c , the acoustic pressure on the plate along the x-axis is not uniform and the antisymmetric modes about y-axis participates in the response of the plate. Therefore the maximum deflection point moves forward slightly as shown in Fig. 4.36. The deflection spectrum density is shown in Fig. 4.37.

4.4.6 Effect of Initial Imperfection

If the plate has some initial imperfection in deflection, the nonlinear stiffness due to initial deflection reduces the response as compared to flat plate. It is also stiffer than thermal postbuckling deflection, assuming that they have the same maximum deflection

as shown in Fig. 4.26. For thermal postbuckling, the panel is also subjected to certain thermal stress. For initial deflection, the plate has only geometric stiffness which reduces the random response; while thermal postbuckling plate has thermal stresses and thermal deflection. The results are shown in Figs. 4.38, 4.39 and 4.40.

Table 4.1 Results for a rhombic cantilever plate

	Deflection at locations (in.)					
	1	2	3	4	5	6
MIN 3 result	0.263	0.178	0.108	0.103	0.048	0.019
Experiment value	0.297	0.204	0.121	0.129	0.056	0.022

Table 4.2 Results of RMS (Wmax/h) and Micro-strain for simply supported plate
(N=number of modes)

SSL	Present:N=1		resent:N=2		present:N=4		Chiang:N=1		Chiang:N=4	
	RMS	Micro	RMS	Micro	RMS	Micro	RMS	Micro	RMS	Micro
(dB)	W	strain	W	strain	W	strain	W	strain	W	strain
110	1.04	64.5	1.04	80.5	1.07	77.7	1.030	87.4	1.031	112.0
120	1.89	213.2	1.89	274.5	1.96	259.2	1.902	256.5	1.905	361.0

Table 4.3 Linear Natural Frequencies(Hz) of Panel 1

1st	2nd	3rd	4th	5th	6th	7th
100.3	184.9	210.4	286.0	321.0	360.8	413.6

The 2nd, 3rd and 4th are antisymmetrical modes.

Table 4.4 Convergence of RMS(Wmax/h) with Number of the Modes

No. of Modes	N=1	N=2	N=3	N=4
RMS(Wmax/h)	2.0252	1.9626	1.8676	1.8695

Table 4.5 The Natural Frequencies (rad/sec.)

1st	2nd	3rd	4th	5th	6th
629.95	1161.6	1322.0	1796.8	2016.6	2267.0
7th	8th	9th	10th	11th	12th
2598.7	2758.1	3125.7	3393.4	3526.6	3734.8

Table 4.6 Frequencies for the baseline configuration (rad/sec.)

$\Delta T/\Delta T_{cr}$	1st	2nd	3rd	4th	5th	6th
0.0	630.0	1161.6	1322.0	1796.8	2016.6	2267.0
2.0	811.9	848.3	1135.6	1406.0	1784.2	2122.8
3.0	1046.2	1100.7	1265.0	1421.6	1940.2	2251.4

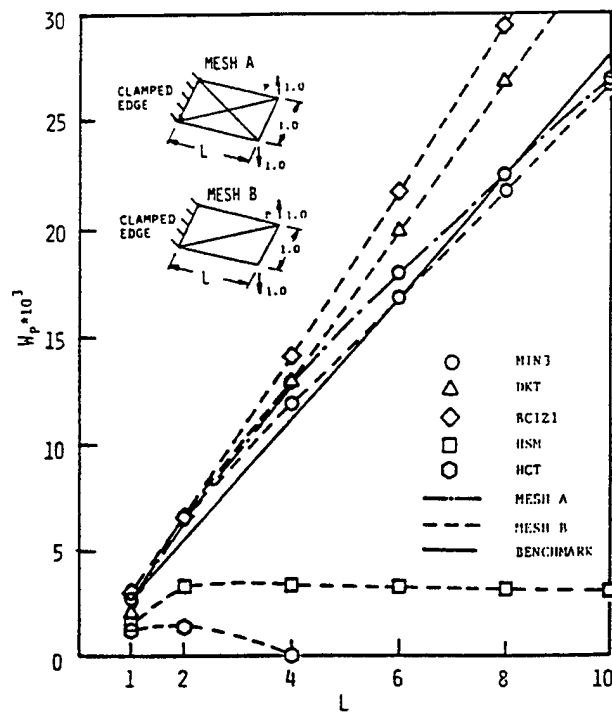


Fig. 4.1 Twisted ribbon test via transverse corner forces ($E=10^7$, $\nu=0.25$, $h=0.05$) (From Tessler and Hughes, 1985)

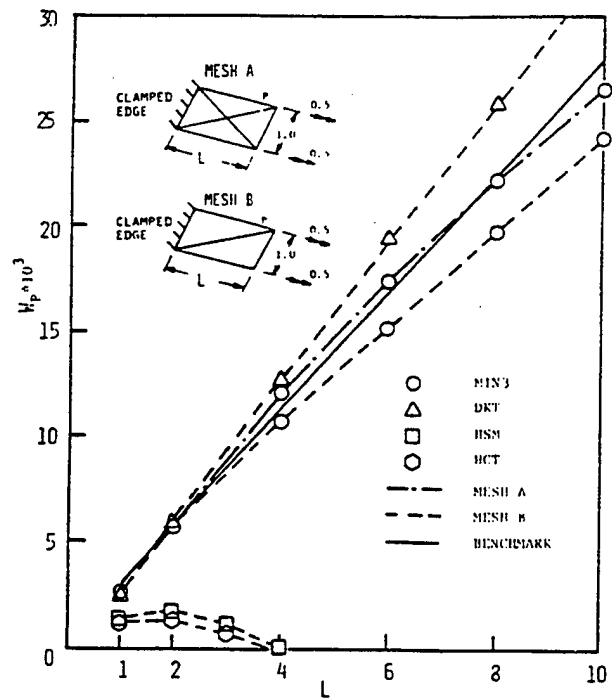


Fig. 4.2 Twisted ribbon test via twisting corner moments ($E=10^7$, $\nu=0.25$, $h=0.05$) (From Tessler and Hughes, 1985)

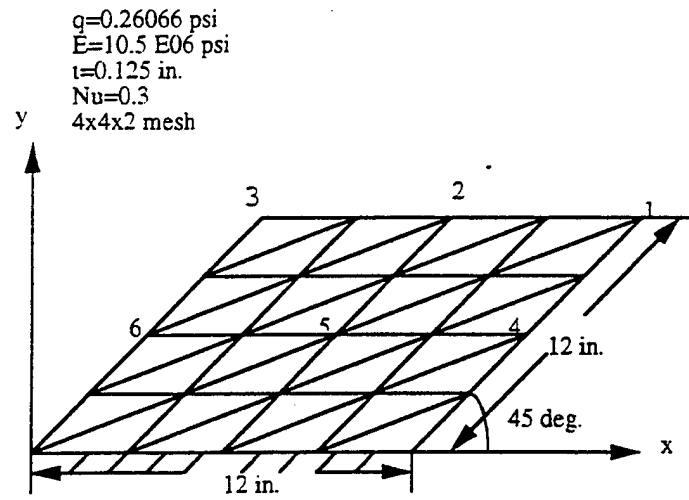


Fig. 4.3 Rhombic cantilever plate

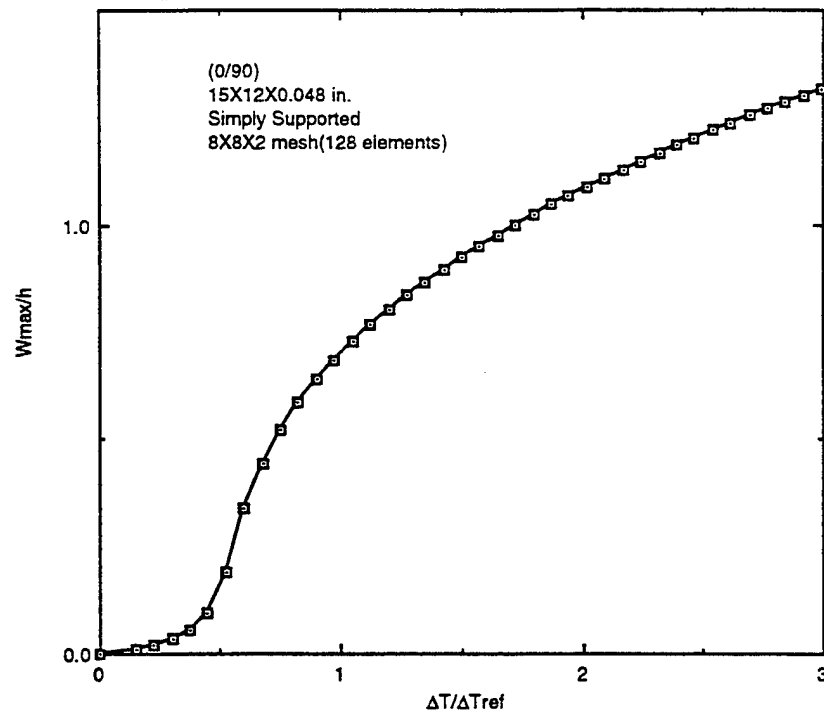


Fig. 4.4 W_{max}/h vs. $\Delta T/\Delta T_{ref}$. for $(0/90)$ composite plate

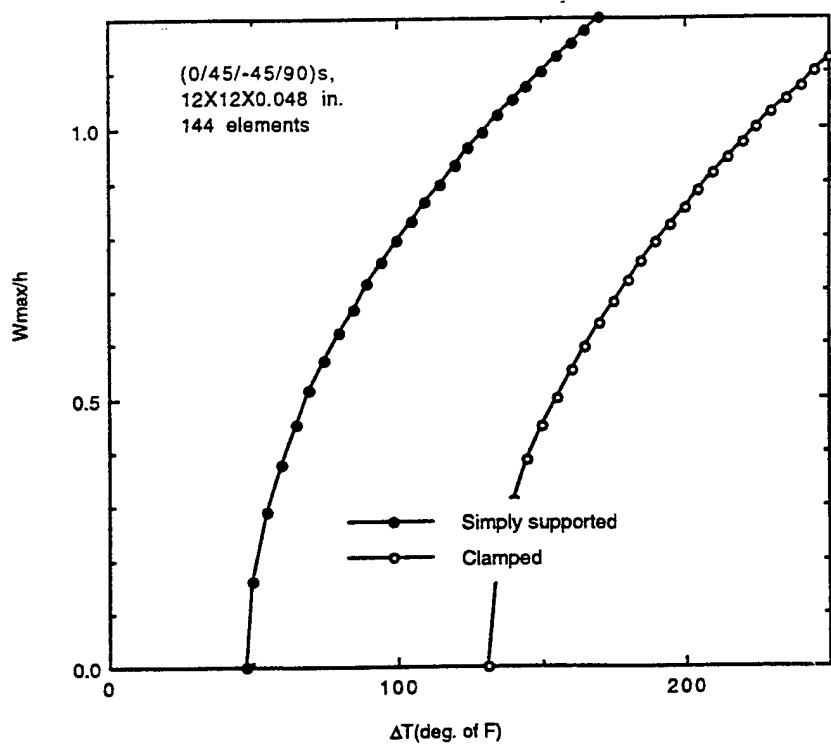


Fig. 4.5 W_{max}/h vs. ΔT for an isosceles triangular plate

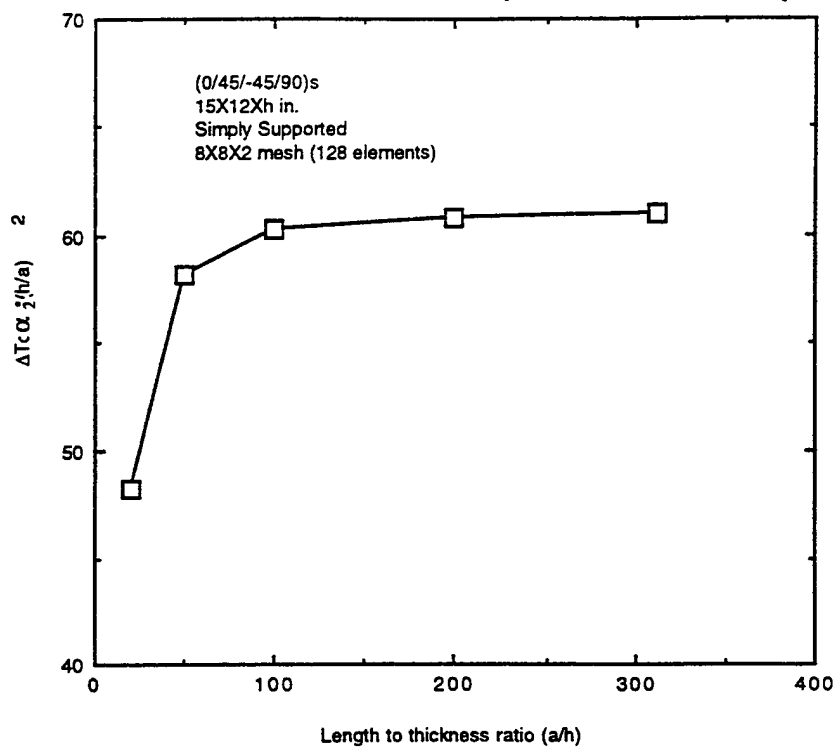


Fig. 4.6 Dimensionless critical temperature vs. a/h for a rectangular laminate

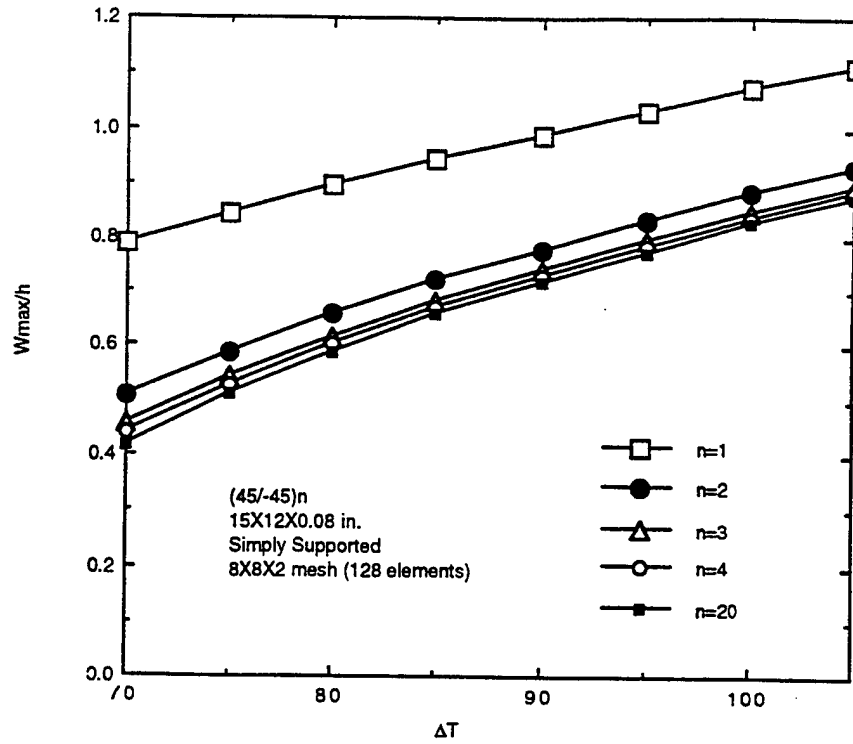


Fig. 4.7 W_{max}/h vs. ΔT for various number of layers

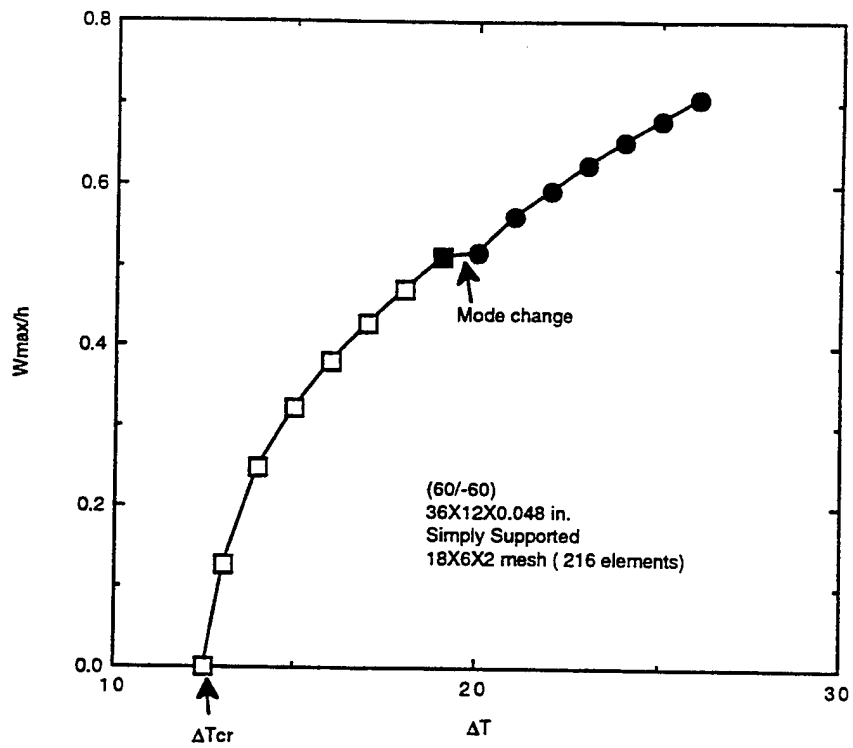


Fig. 4.8 W_{max}/h vs. ΔT for a long rectangular laminate

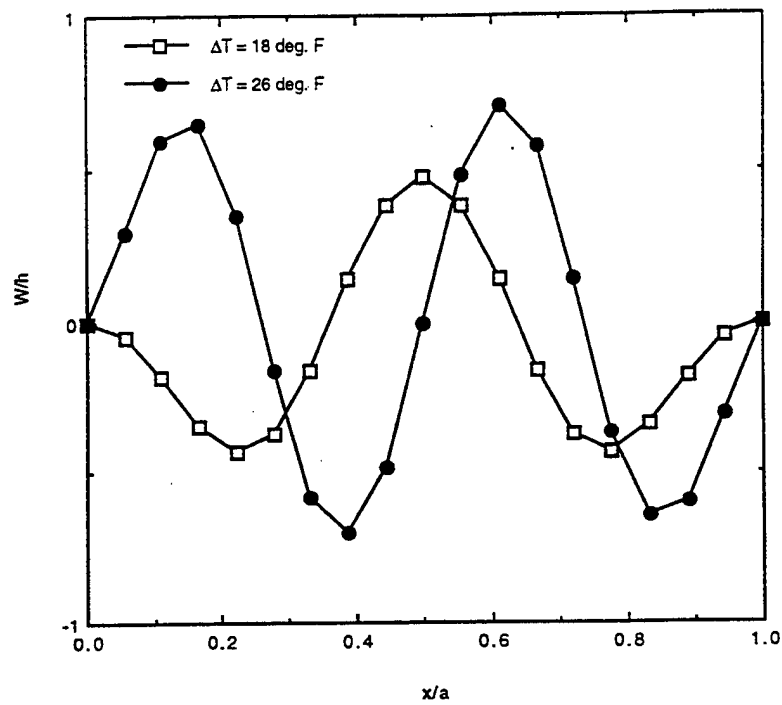


Fig. 4.9 Centerline deflection of a 36x12x0.048 in. angle-ply (60/-60) laminate

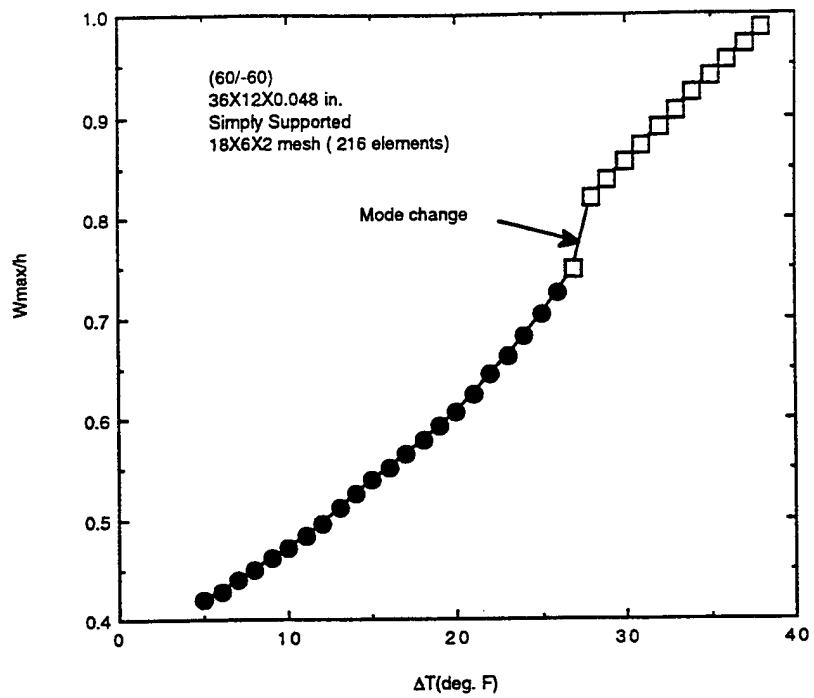


Fig. 4.10 W_{max}/h vs. ΔT for a long rectangular laminate with mechanical load 0.01 psi

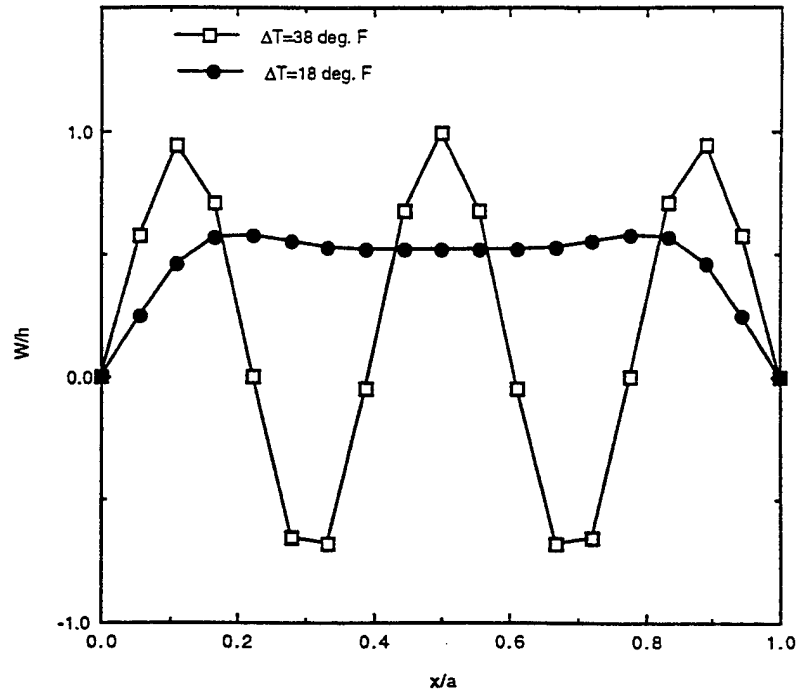


Fig. 4.11 Centerline deflection of a 36x12x0.048 in. angle-ply (60/-60) laminate with mechanical load 0.01 psi

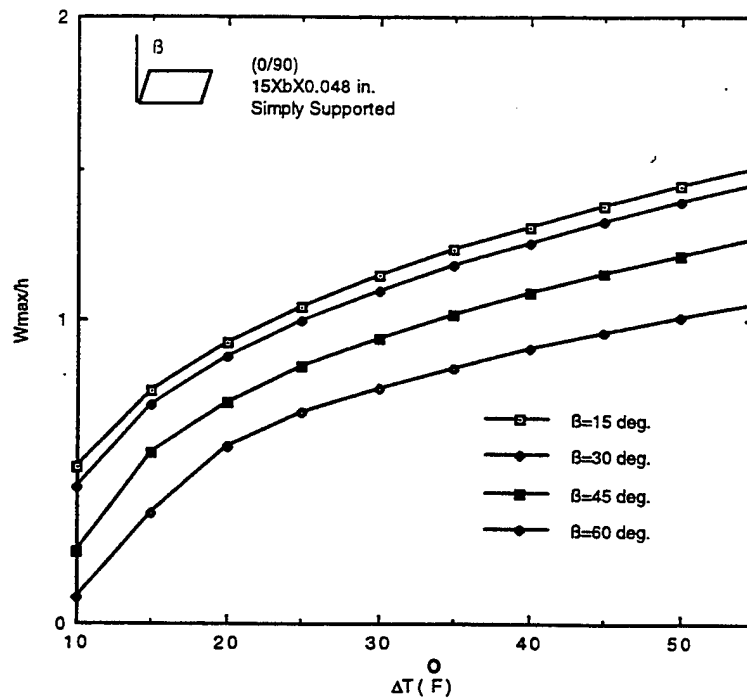


Fig. 4.12 W_{max}/h vs. skew angle for rectangular plates

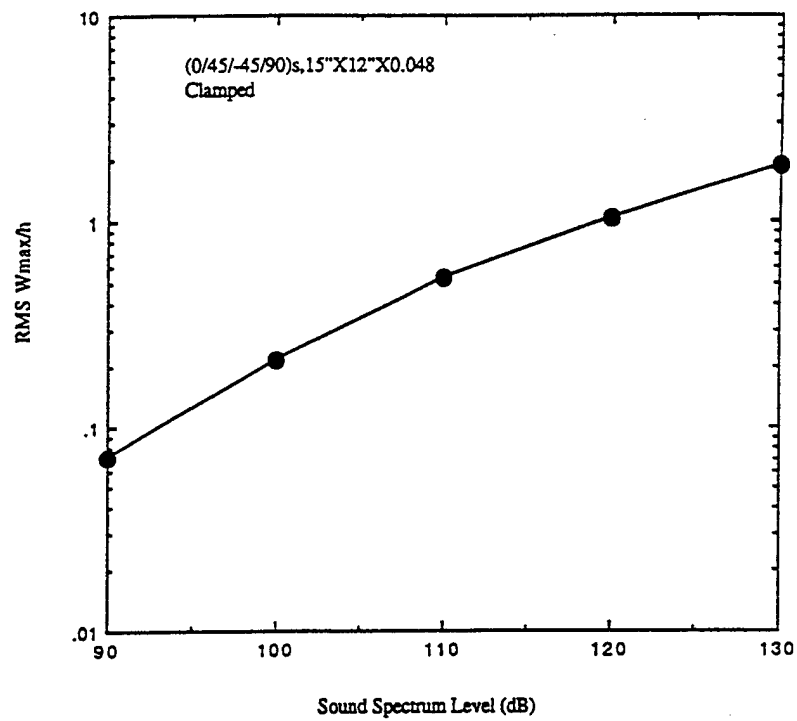


Fig. 4.13 RMS W_{max}/h vs. SPL for Panel 1

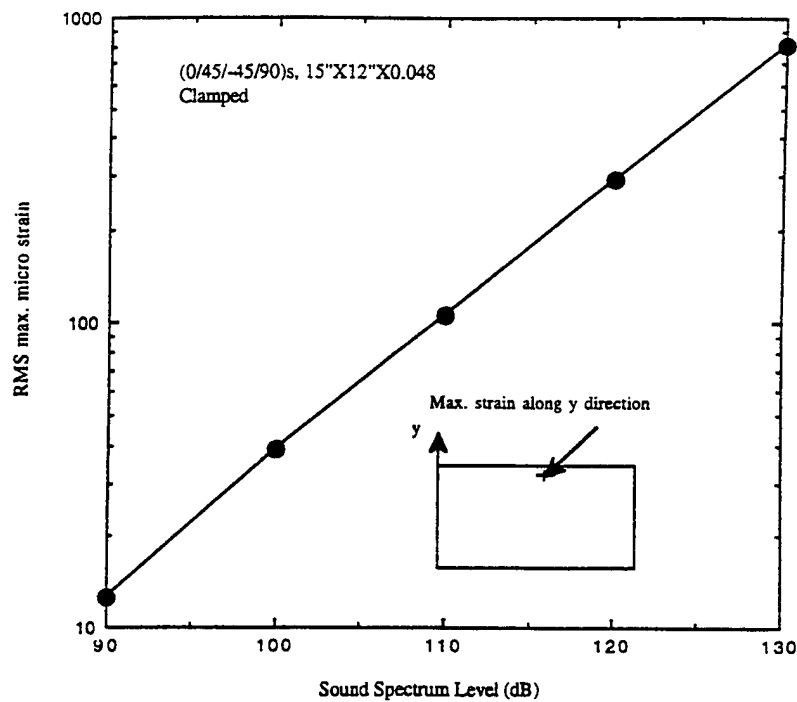


Fig. 4.14 RMS max. micro strain vs. SPL for Panel 1

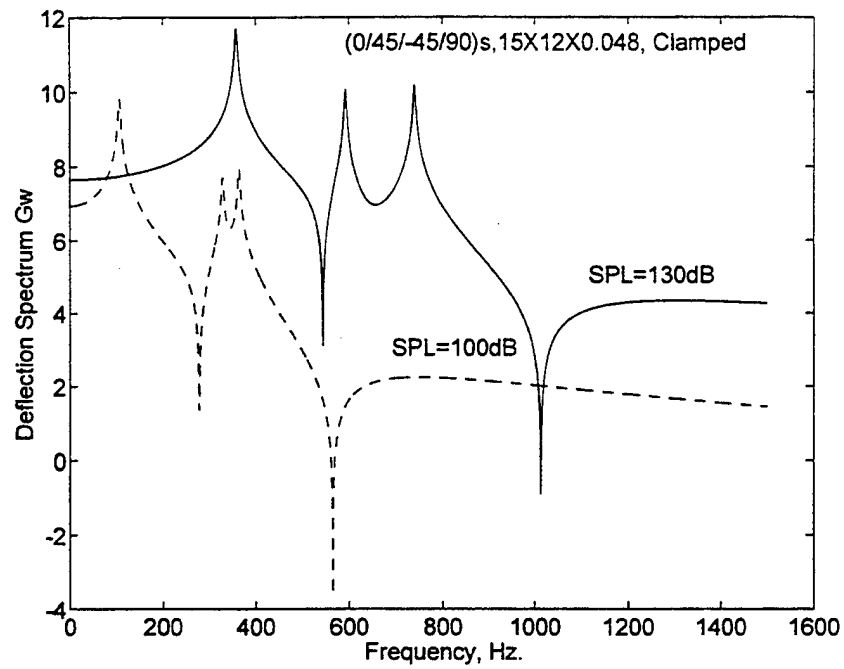


Fig. 4.15 The maximum deflection spectrum vs. frequency for Panel 1

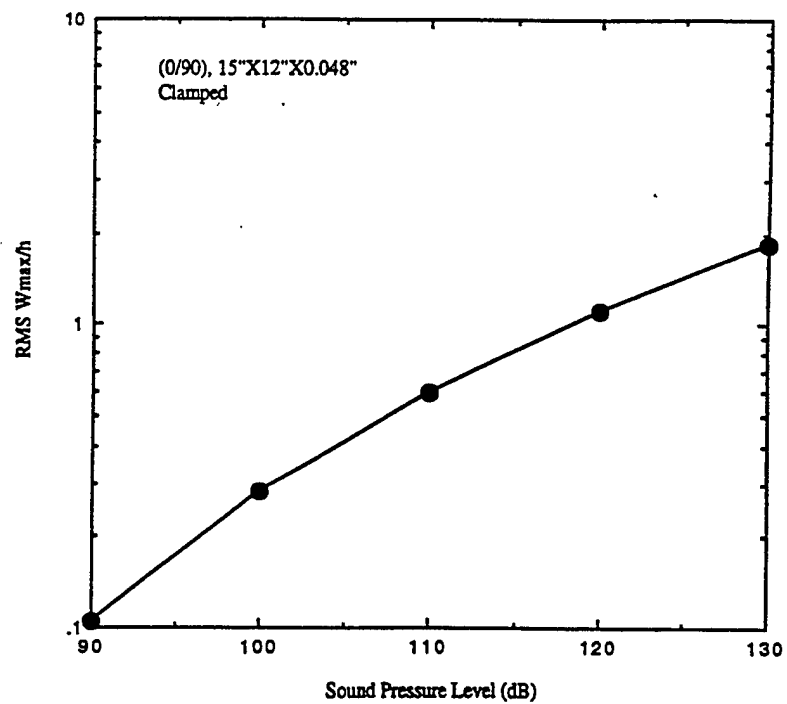


Fig. 4.16 RMS max. micro strain vs. SPL for Panel 2

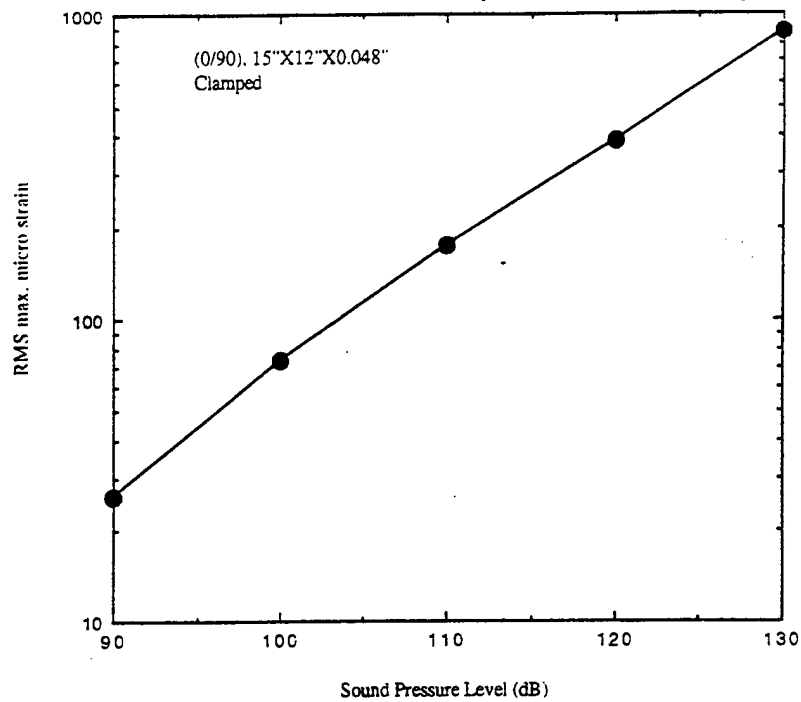


Fig. 4.17 RMS max. micro strain vs. SPL for Panel 2

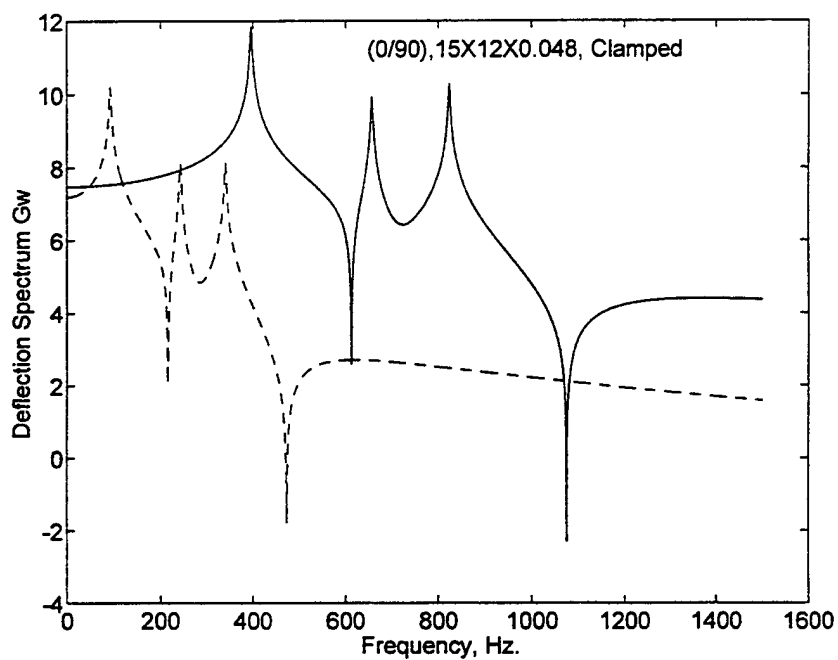


Fig. 4.18 The maximum deflection spectrum vs. frequency for Panel 2

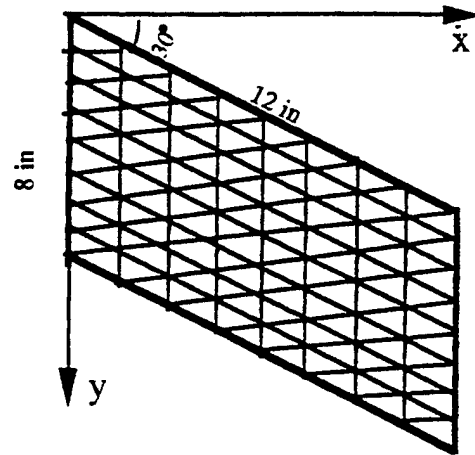


Fig. 4.19 Planform of Panel 3

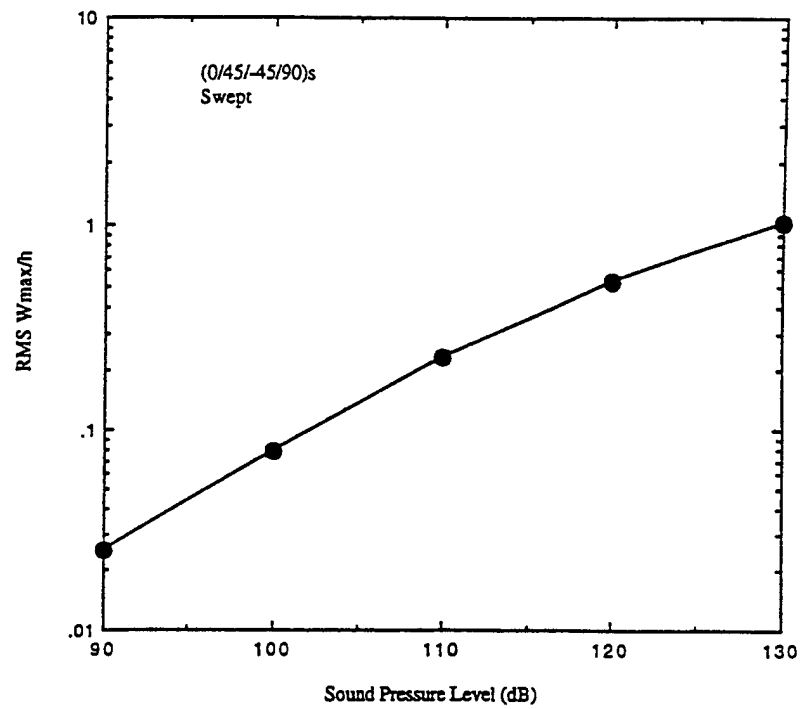


Fig. 4.20 RMS W_{max}/h vs. SPL for Panel 3

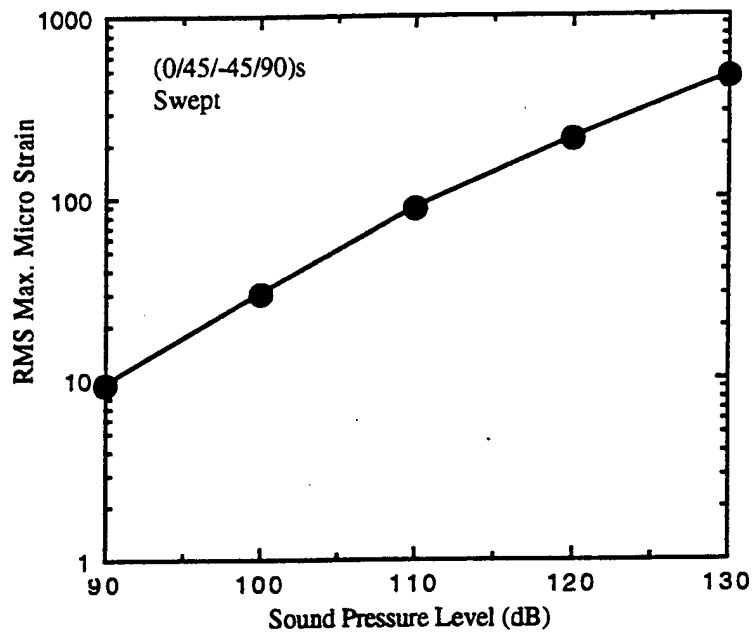


Fig. 4.21 RMS max. micro strain vs. SPL for Panel 3

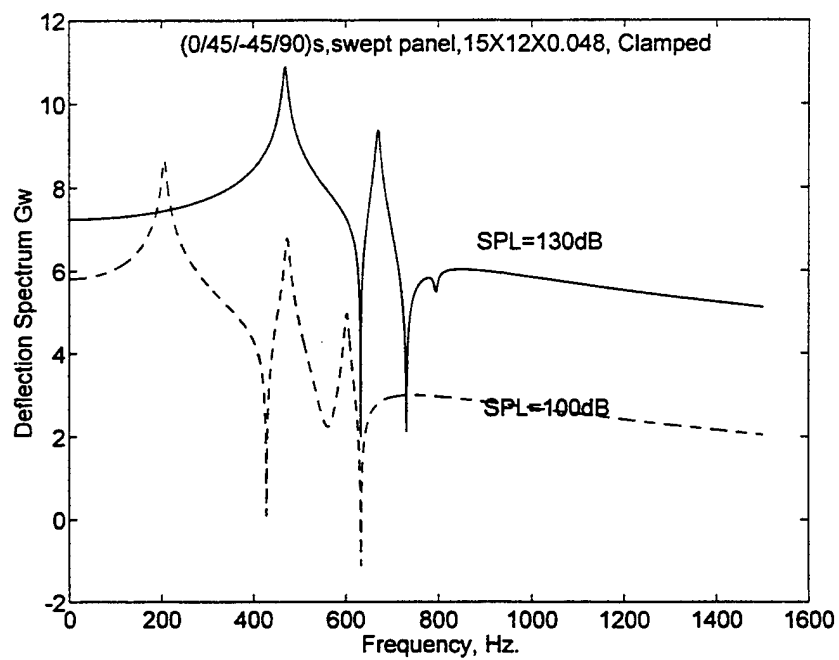


Fig. 4.22 The maximum deflection spectrum vs. frequency for Panel 3

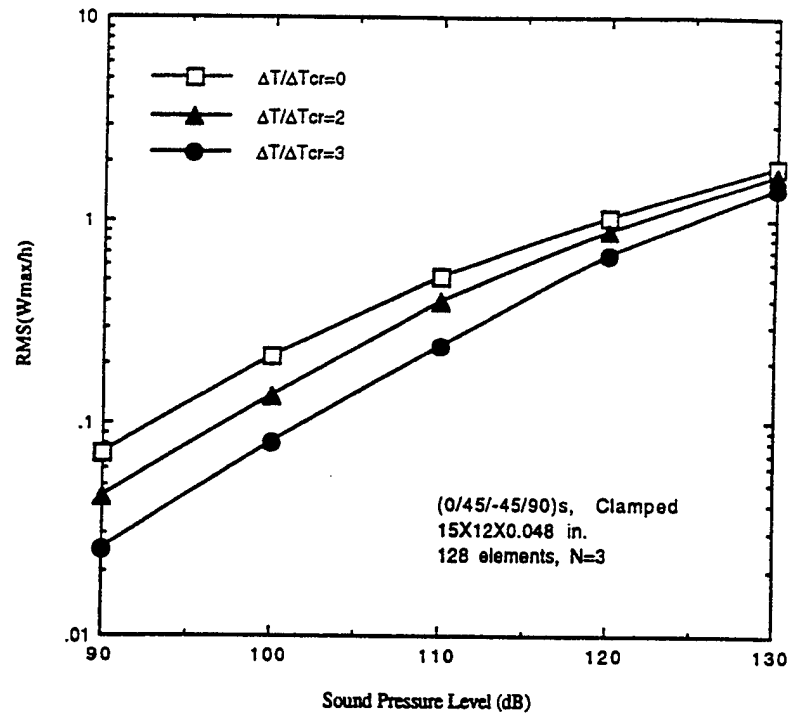


Fig. 4.23 RMS (Wmax/h) vs. SPL for the baseline configuration

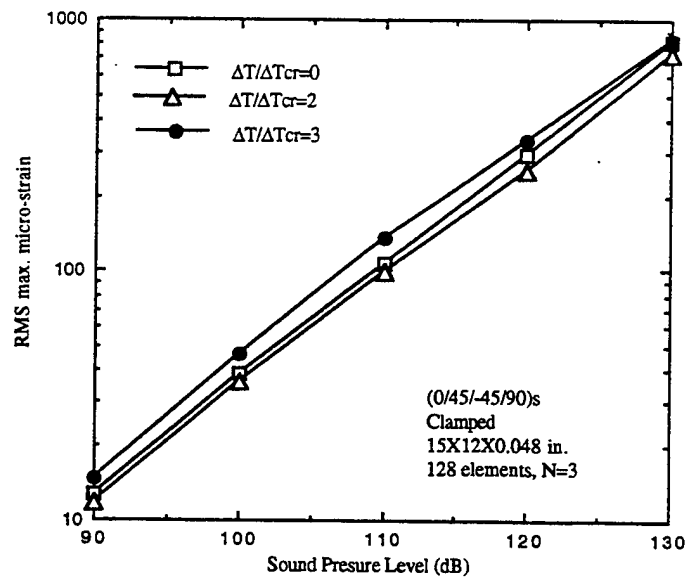


Fig. 4.24 Micro-strain vs. SPL for the baseline configuration

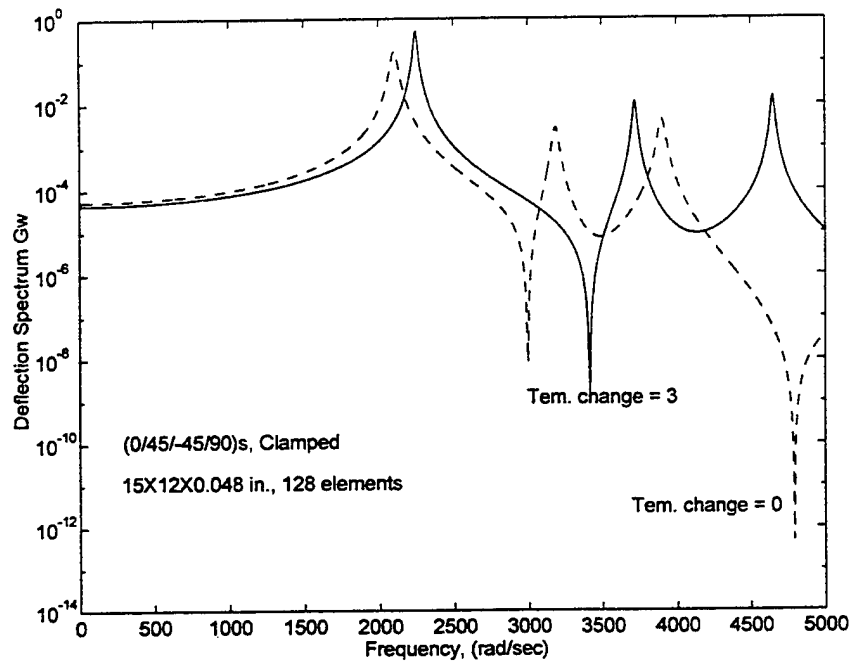


Fig. 4.25 The maximum deflection spectrum vs. frequency for the baseline configuration at SPL = 130 dB

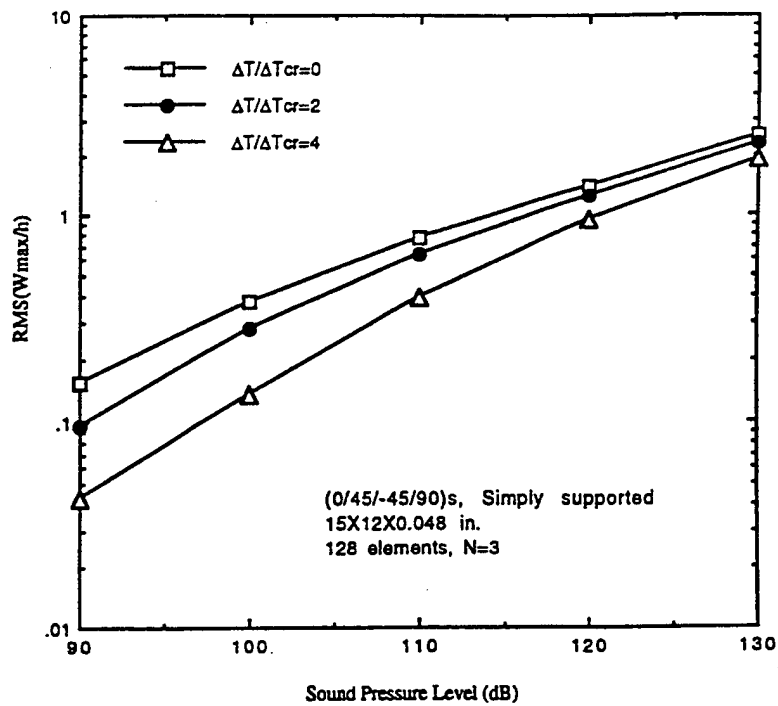


Fig. 4.26 RMS (W_{\max}/h) vs. SPL for the simply supported panel

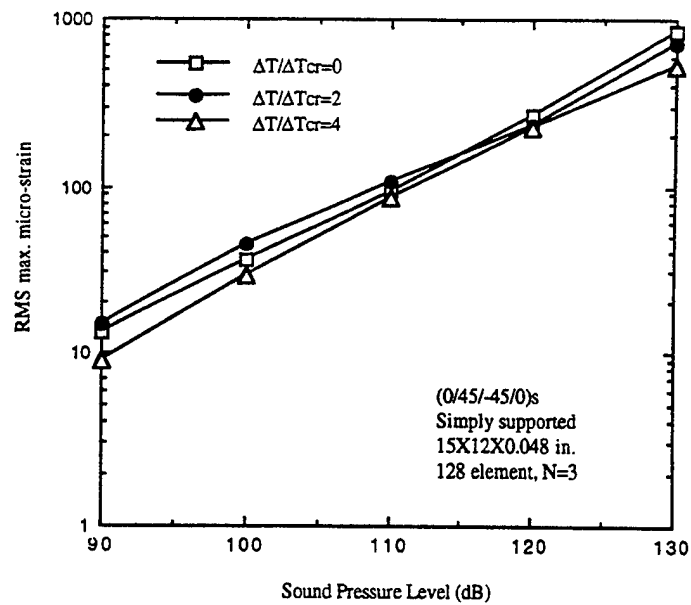


Fig. 4.27 Micro-strain vs. SPL for the simply supported panel

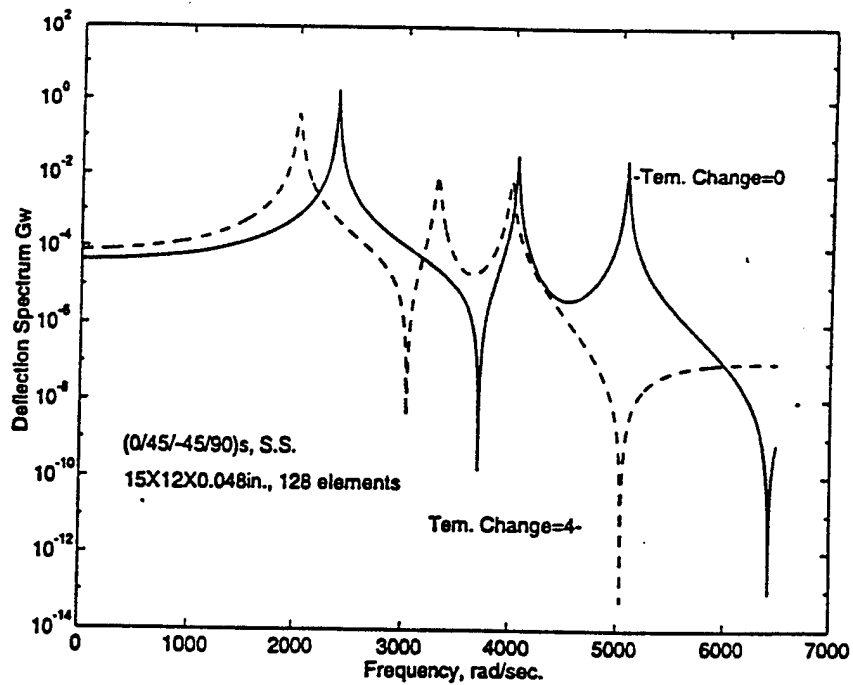


Fig. 4.28 The maximum deflection spectrum vs. frequency for the simply supported panel

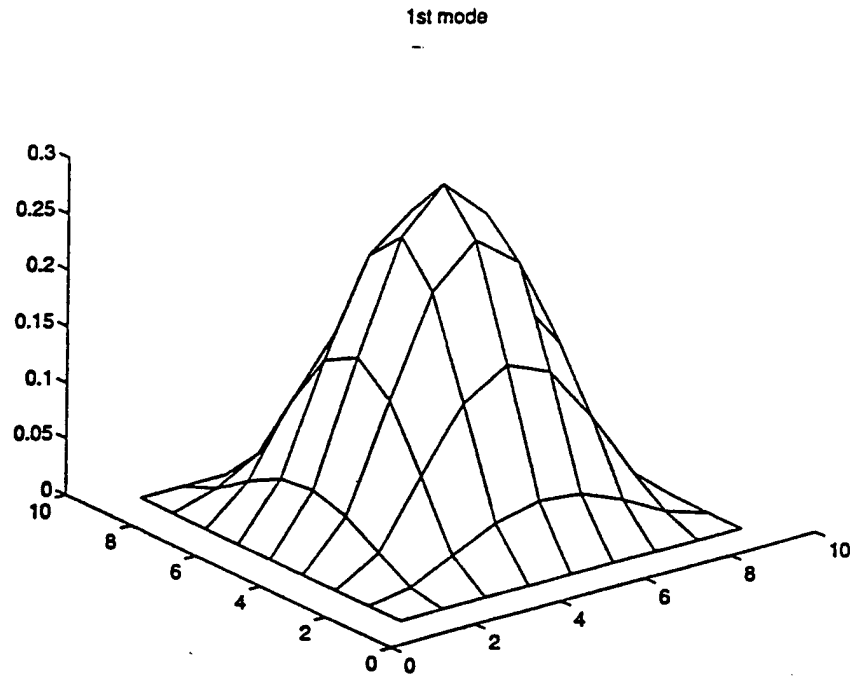


Fig. 4.29 The mode shapes of (0/90) clamped panel

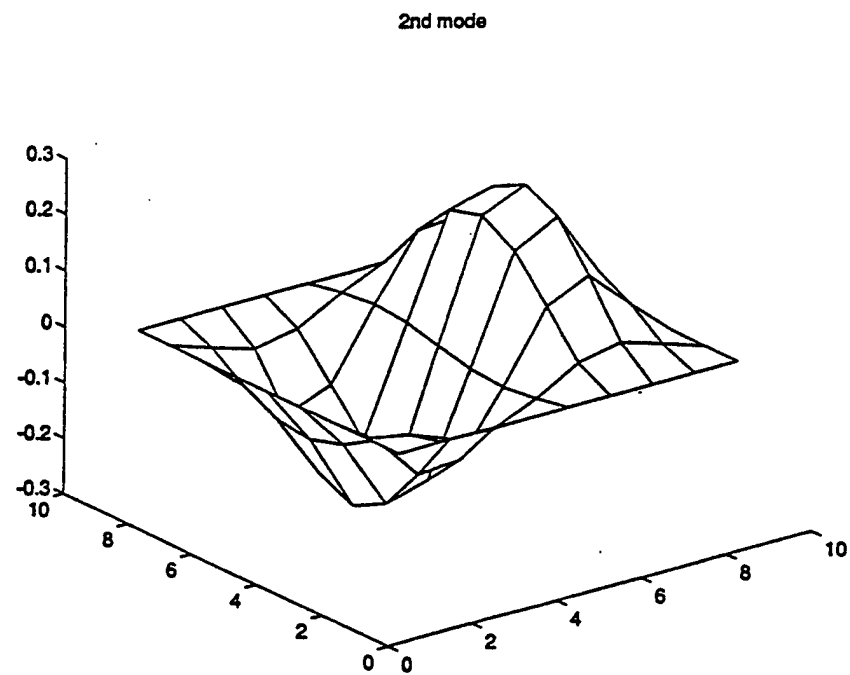


Fig. 4.29 Continued

3rd mode

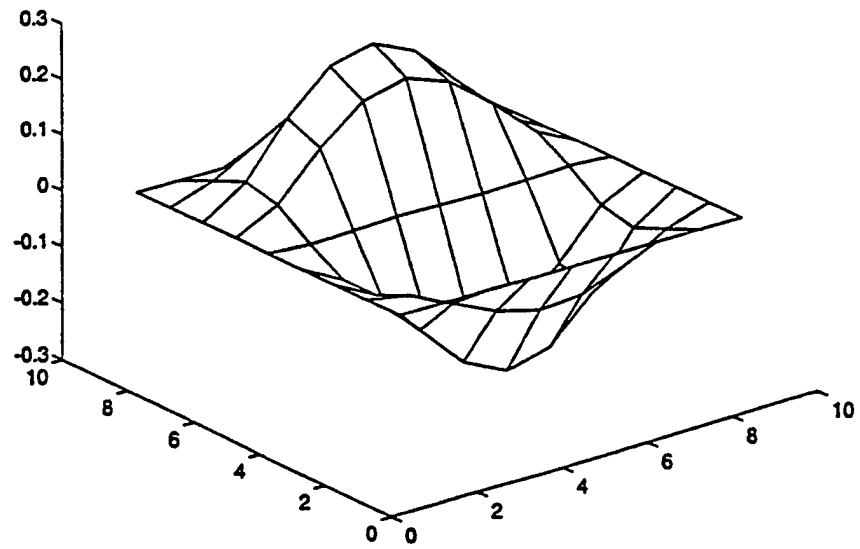


Fig. 4.29 Continued

4th mode

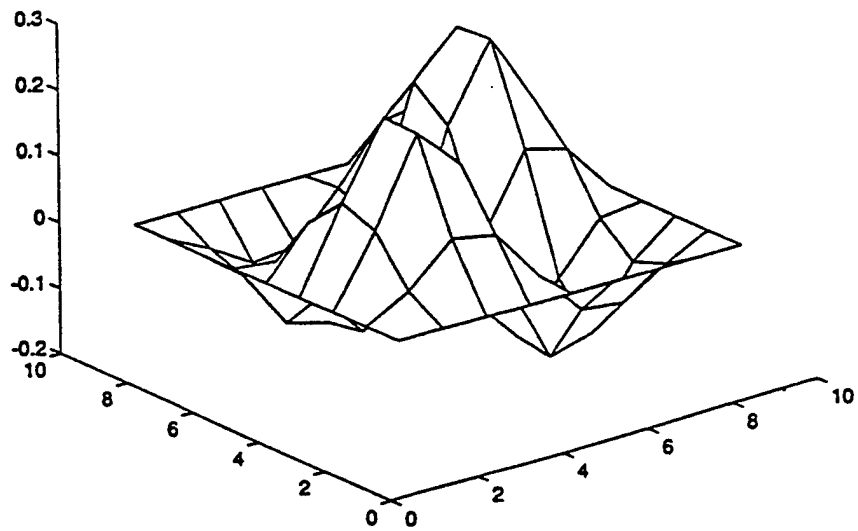


Fig. 4.29 Continued

5th mode

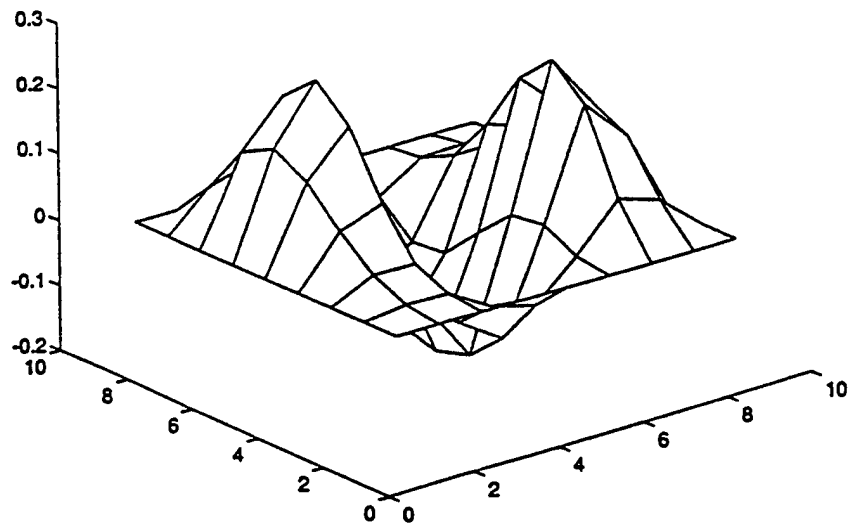


Fig. 4.29 Continued

6th mode

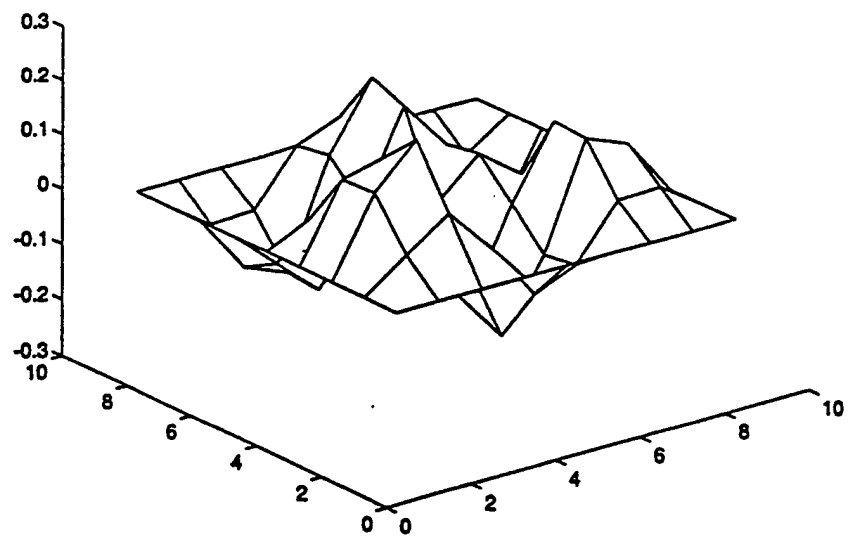


Fig. 4.29 Continued

7th mode

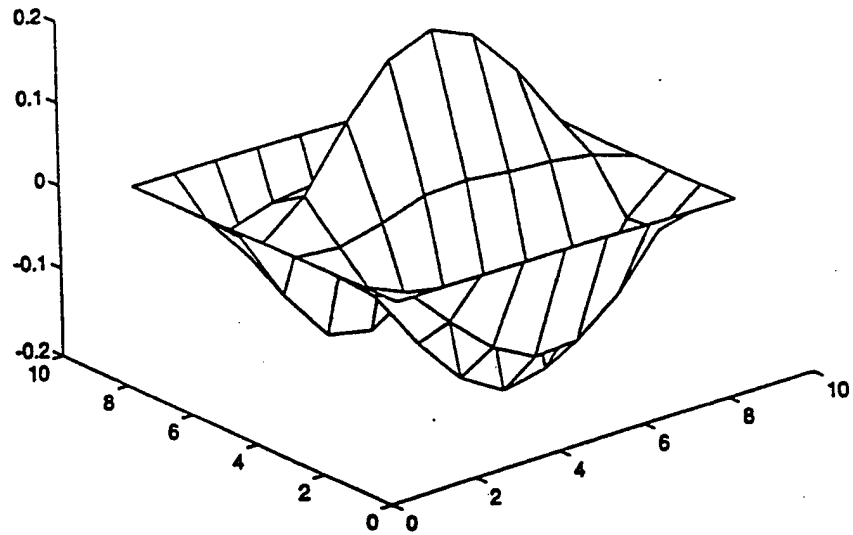


Fig. 4.29 Continued

1st mode, Tem. Change=97.792 (deg. F)

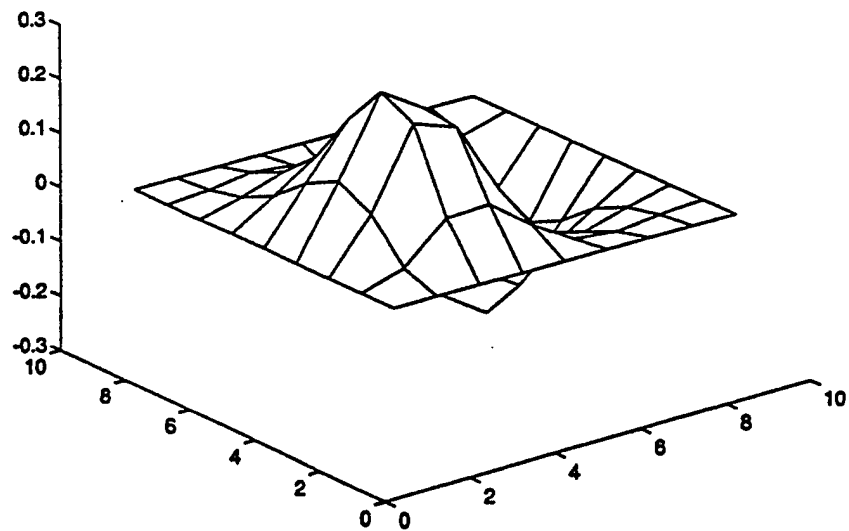


Fig. 4.30 The mode shapes of (0/90) clamped panel

2nd mode, Tem. Change=97.792 (deg. F)

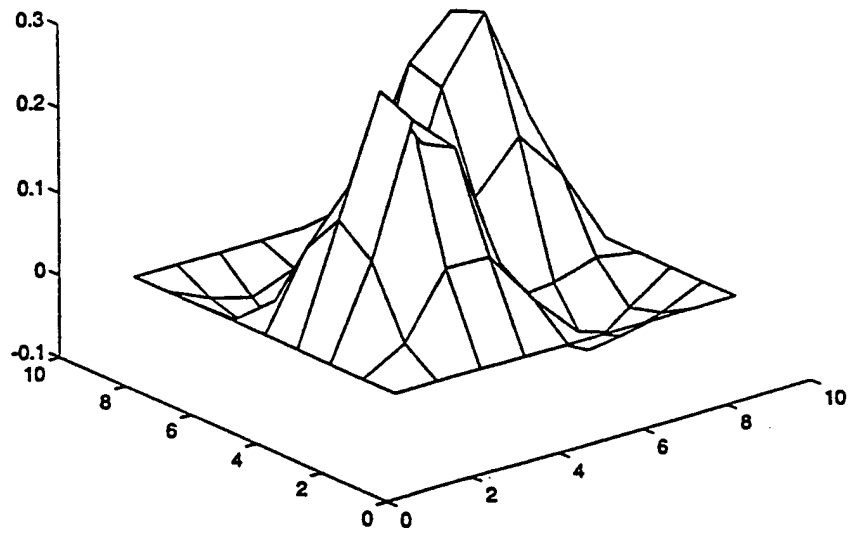


Fig. 4.30 Continued

3rd mode, Tem. Change=97.792 (deg. F)

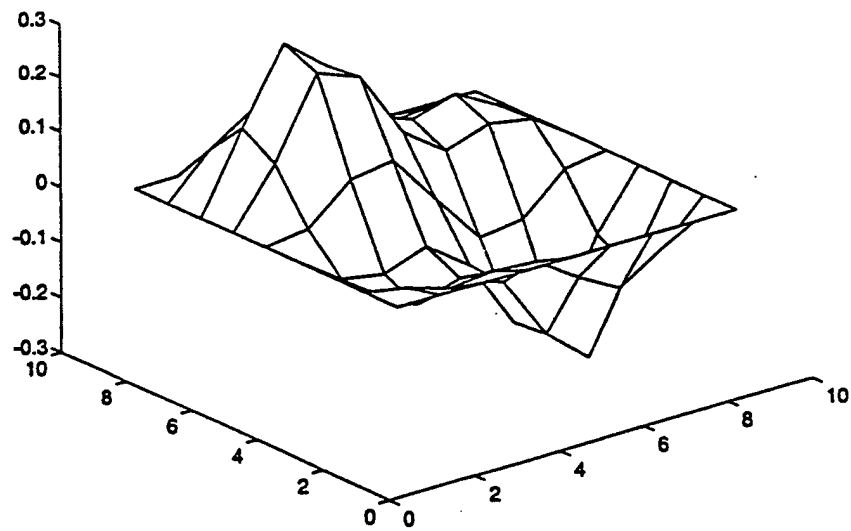


Fig. 4.30 Continued

4th mode, Tem. Change=97.792 (deg. F)

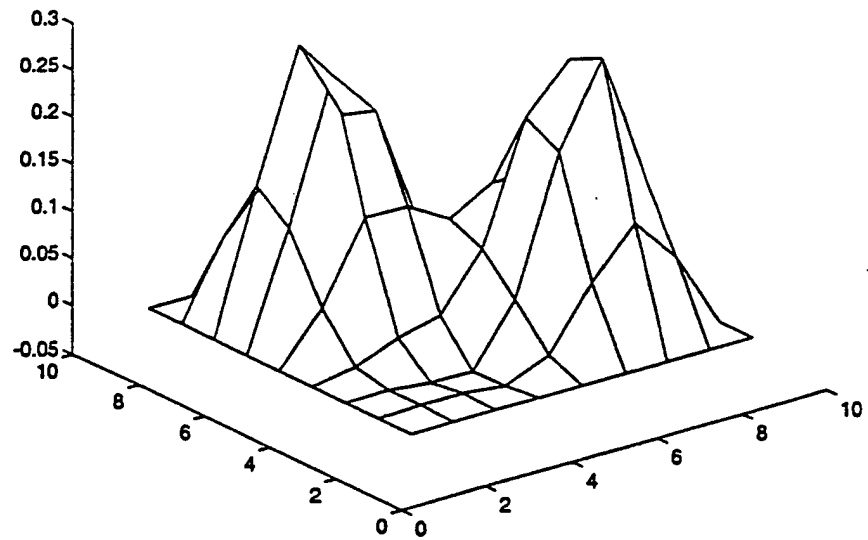


Fig. 4.30 Continued

5th mode, Tem. Change=97.792 (deg. F)

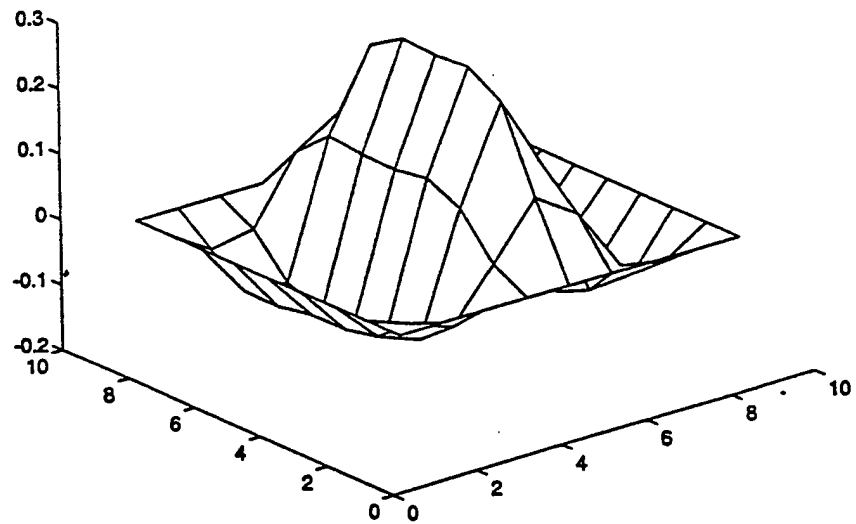


Fig. 4.30 Continued

6th mode, Tem. Change=97.792 (deg. F)

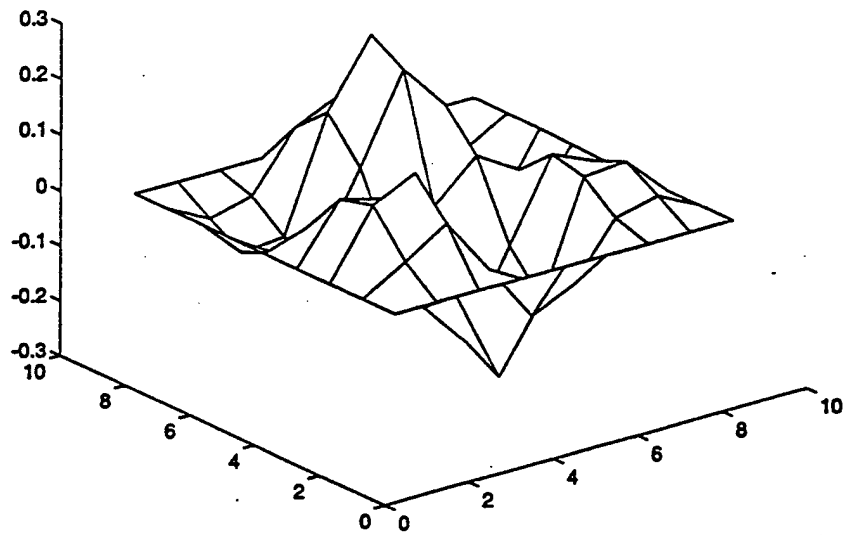


Fig. 4.30 Continued

1st mode, Tem. Change=149.688 (deg. F)

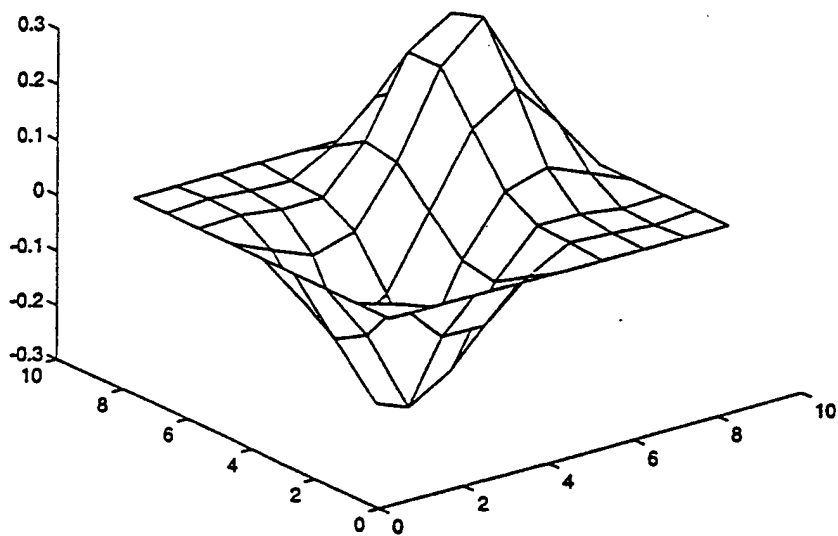


Fig. 4.31 The mode shapes of (0/90) clamped panel

2nd mode, Tem. Change=149.688 (deg. F)

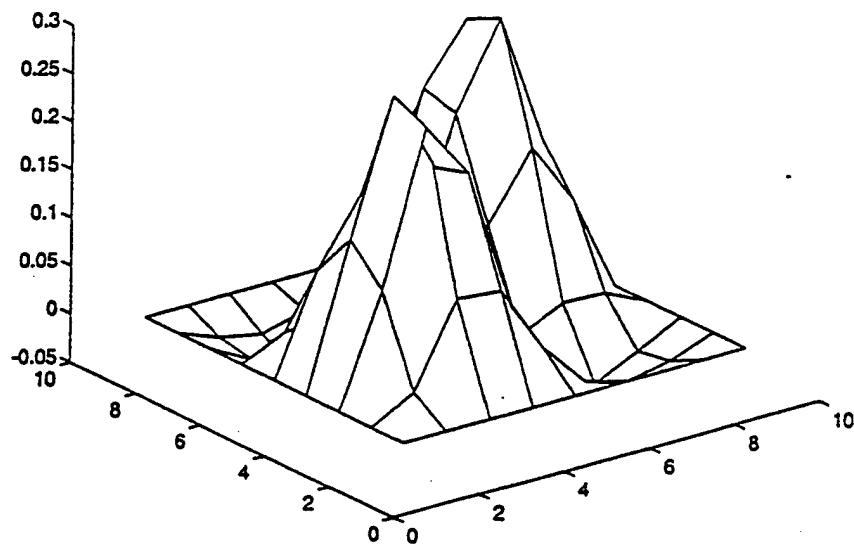


Fig. 4.31 Continued

3rd mode, Tem. Change=149.688 (deg. F)

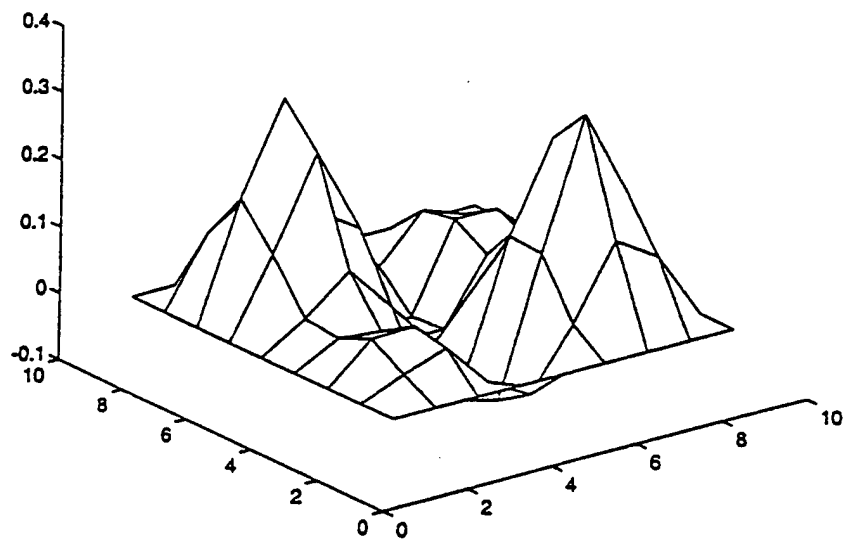


Fig. 4.31 Continued

4th mode, Tem. Change=149.688 (deg. F)

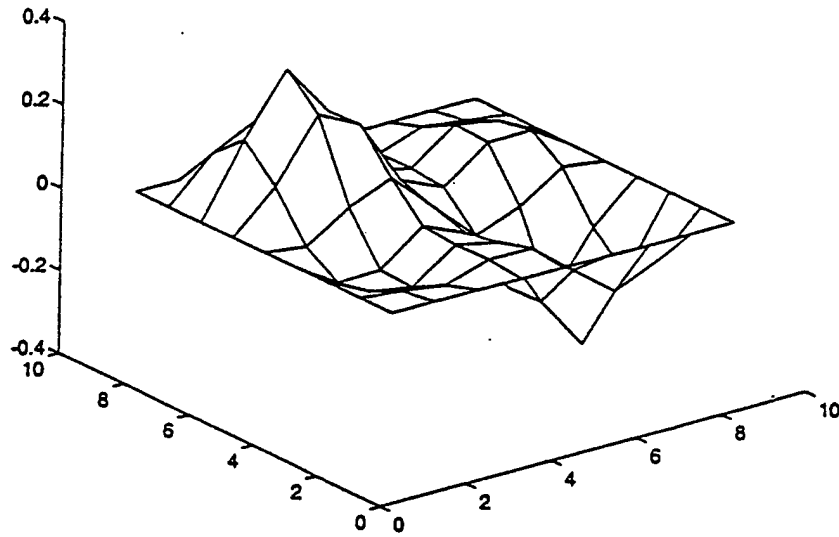


Fig. 4.31 Continued

5th mode, Tem. Change=149.688 (deg. F)

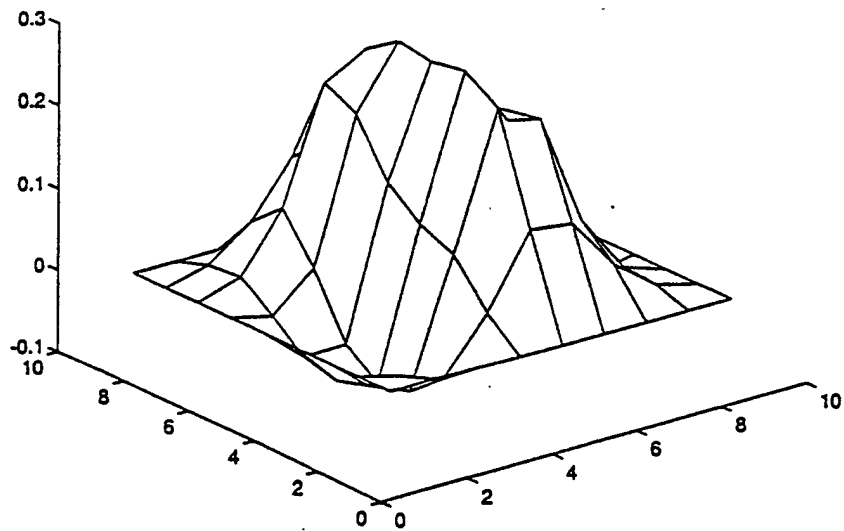


Fig. 4.31 Continued

6th mode, Tem. Change=149.688 (deg. F)

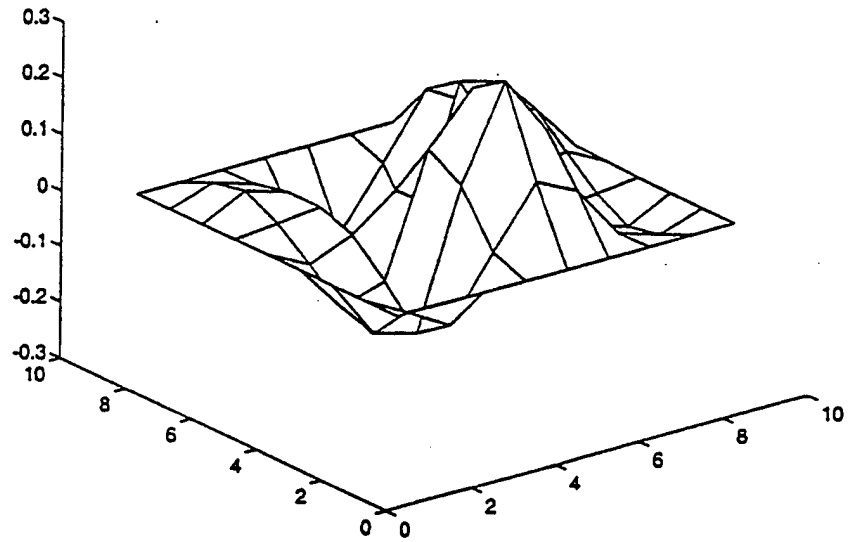


Fig. 4.31 Continued

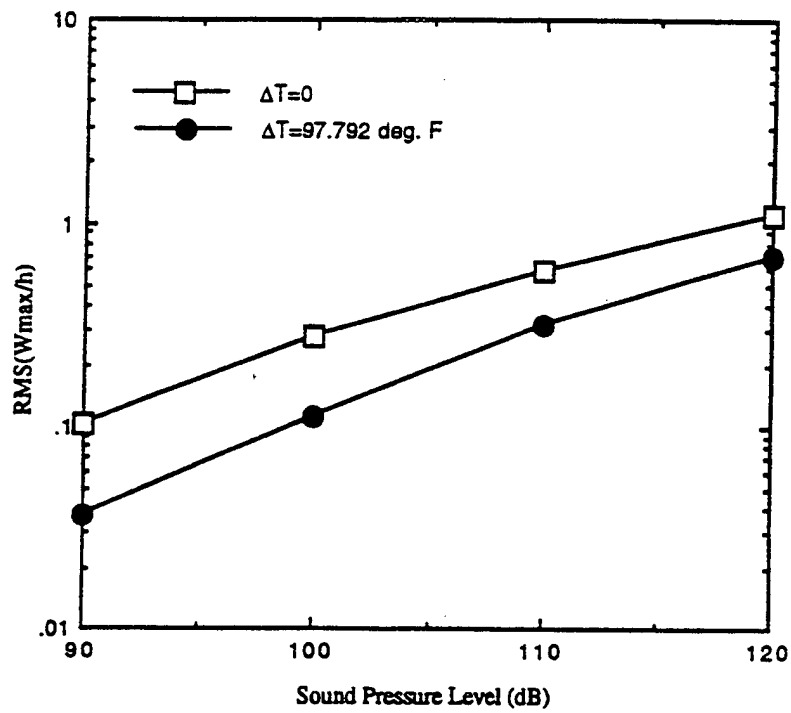


Fig. 4.32 RMS (Wmax/h) vs. SPL for the (0/90) panel

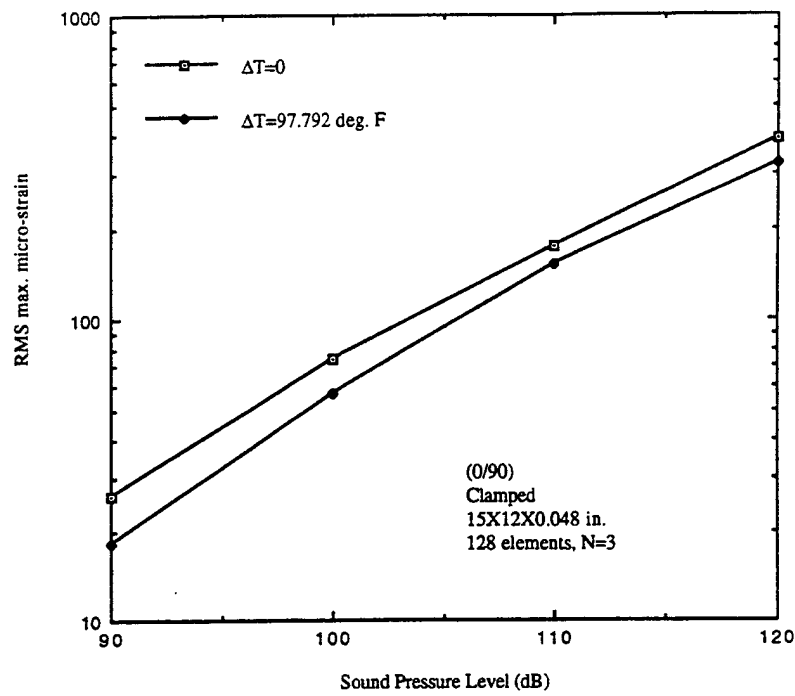


Fig. 4.33 RMS max. micro strain vs. SPL for the (0/90) panel

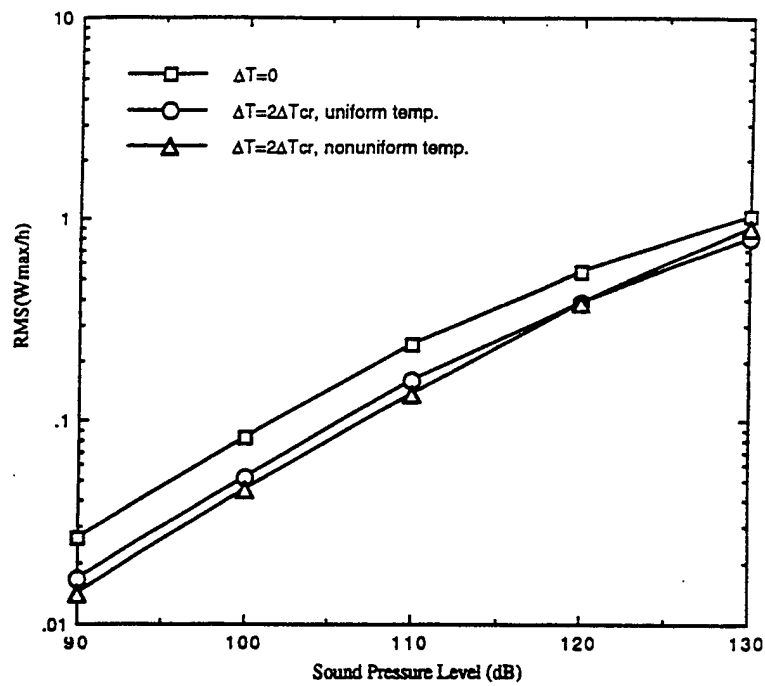


Fig. 4.34 RMS (Wmax/h) vs. SPL for a skewed panel

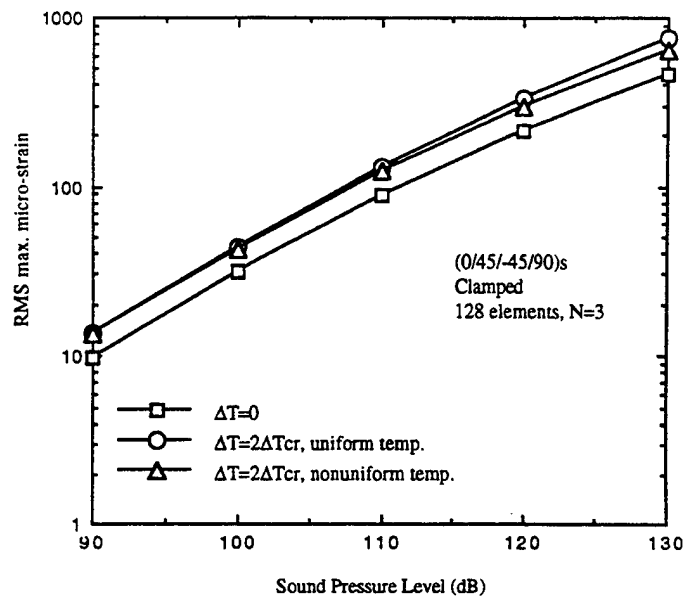


Fig. 4.35 RMS max. micro strain vs. SPL for a skewed panel

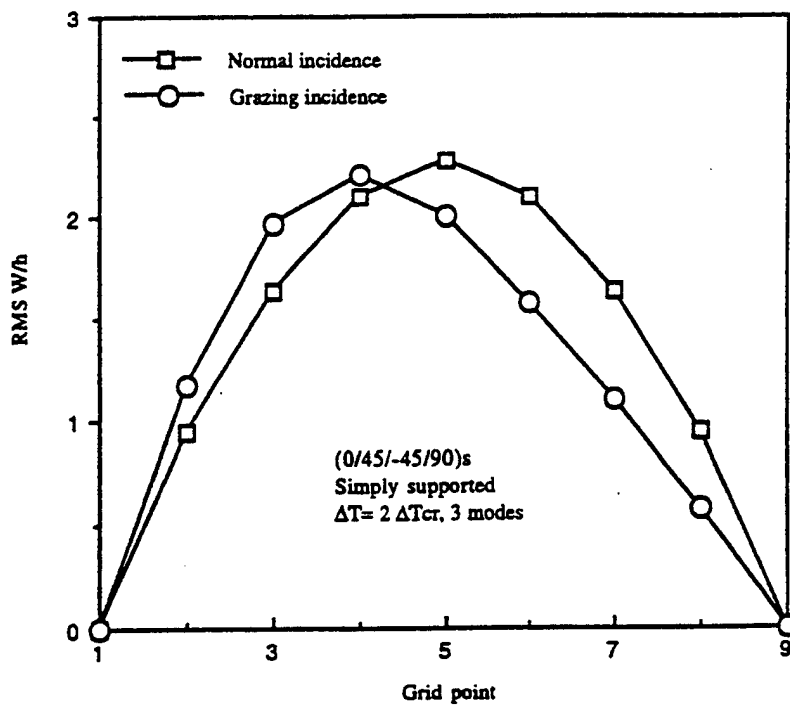


Fig. 4.36 Distributions of RMS W/h along the center line of the panel

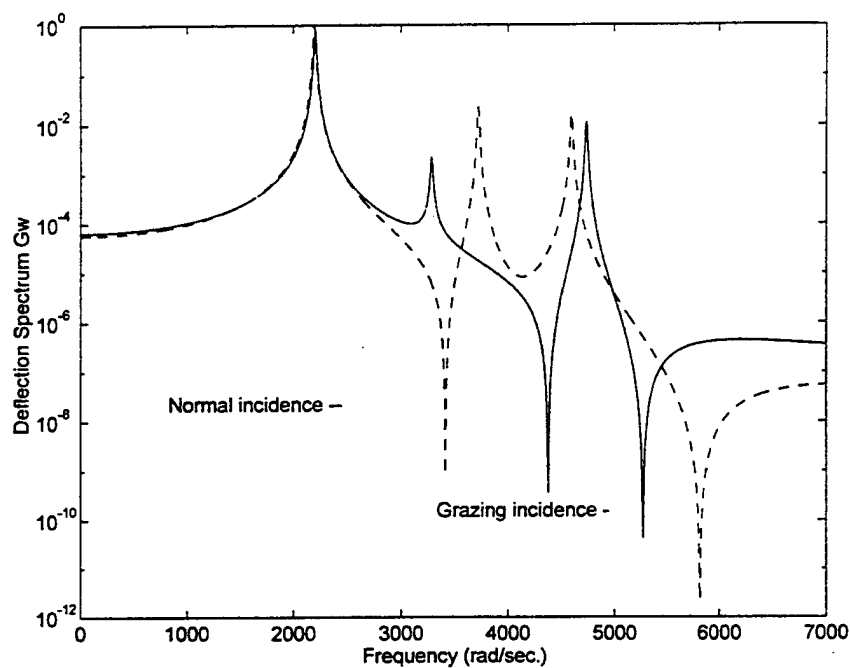


Fig. 4.37 The maximum deflection spectrum vs. frequency for the simply supported panel subjected to grazing wave

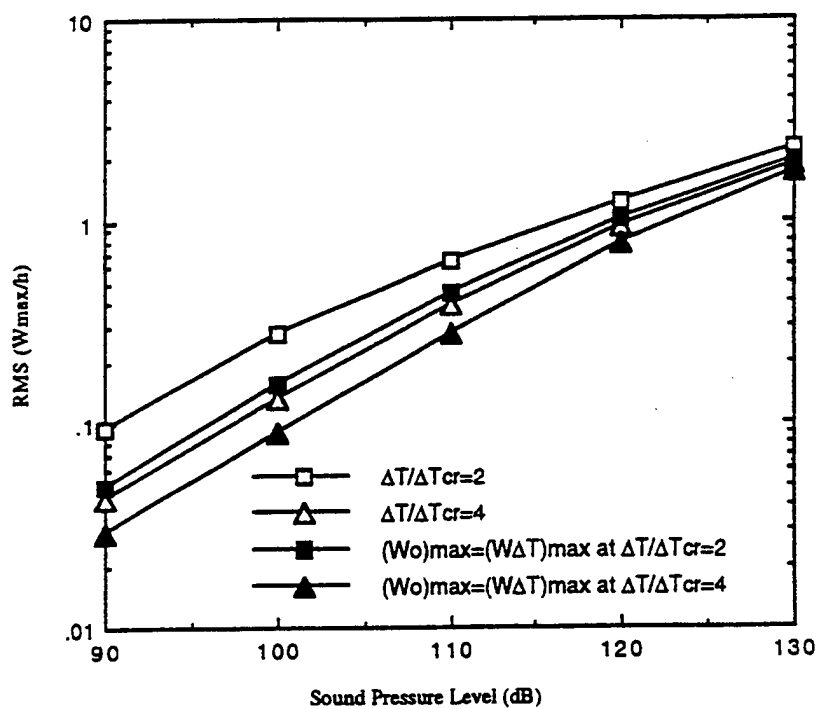


Fig. 4.38 RMS (W_{\max}/h) vs. SPL for the simply supported panel with initial deflection W_0

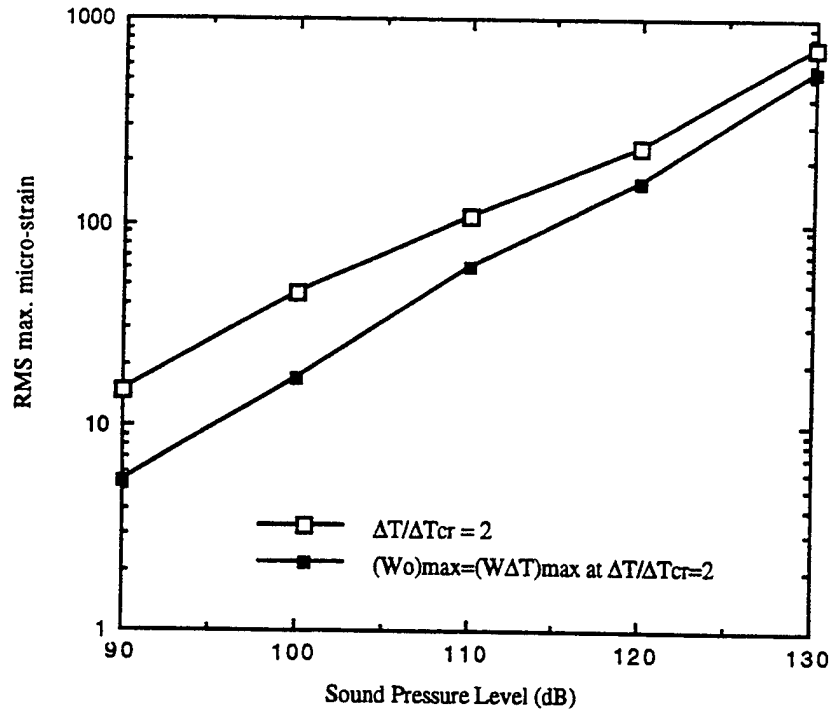


Fig. 4.39 RMS max. Micro-strain vs. SPL for the simply supported plate with initial deflection W_o

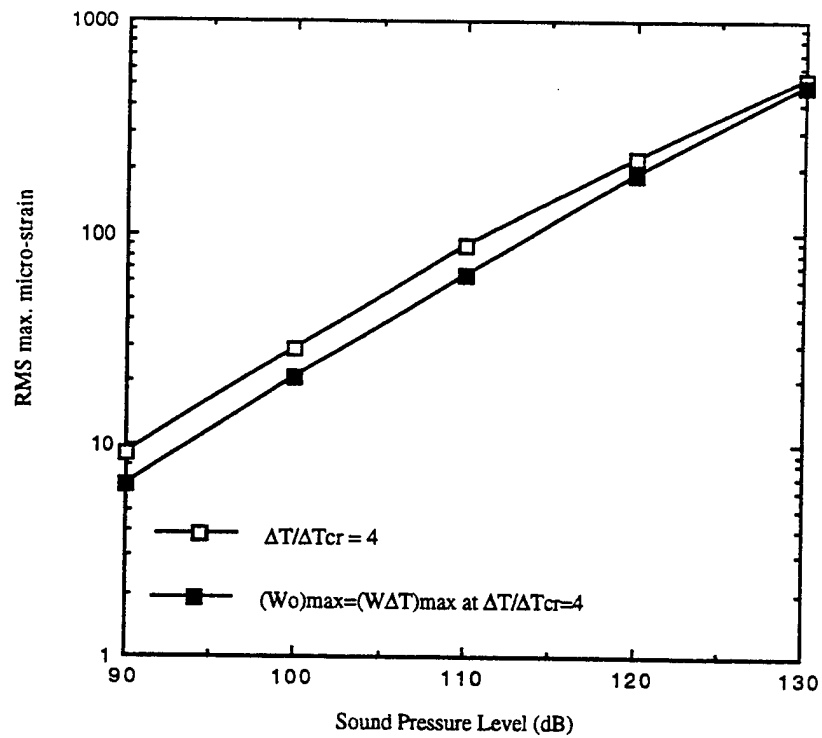


Fig. 4.40 RMS max. Micro-strain vs. SPL for the simply supported plate with initial imperfection W_o

Chapter 5

CONCLUSIONS

Using three-node Mindlin plate element with improved shear deformation, the governing nonlinear equations of motion have been derived for composite structures subjected to a combined acoustic/thermal loading. In order to simulate the acoustic waves in the progressive wave test facility, a grazing incidence wave model is used in the derivation. An innovative solution procedure has been created and the equations of motion were solved for applications of thermal postbuckling and large deflection random response of thermally buckled structures.

The critical temperature change that produced panel buckling was determined by the incremental equations of motion. The first buckling mode was used as the initial shape of the postbuckling solution. Newton-Raphson iteration method was used to solve for the deflections corresponding to a given temperature raise distribution. The extension and bending coupling makes the plate bending out of plane immediately when the plate is heated without prebuckling stage. The most interesting aspect of this study is the mode shape change. The described solution procedure can automatically obtains the mode changing in the postbuckling stage as long as the incremental step of temperature change is small enough, regardless of the presence of mechanical load.

In order to solve the system equation of motion, an innovative solution procedure is described. The response is assumed to be the sum of static component and dynamic component. Substituting the total displacements into the system equation of motion

and regrouping the terms, the equation is of the form $F(\{W\}_s) = G(\{W\}_t)$. The left-hand-side of the equation, $F(\{W\}_s)$, is independent of time t ; while the right-hand-side, $G(\{W\}_t)$, is time dependent. Therefore, the only possibility for both F and G to exist is that both F and G equal to zero, and the two equations are thus obtained. For the dynamic components, the modal transformation was used to reduce the number of equations. Then the equivalent linearization method is utilized to obtain the coupled linear equation. Finally, the modal transform was used to uncouple the equation of motion, and an iteration was used to obtain the random response.

The most significant contributions of the present study are the formulation and solution procedure, including grazing wave, of nonlinear modal equations used to describe the random response of composite structures to combined acoustic and thermal loads. These general equations are applicable not only to the present research, but also to other dynamic problems like gust response, buffet response of an aircraft. Comparing with the SeQuential Load method(SQL), this SiMultaneous Load method(SML) is much logical mathematically and straightforward, it is then easier to formulate nonlinear problems with combined loading. The solution procedure itself can take care of the inter-dependence between the thermal effects and the acoustic-structural response. In the SQL method engineering judgment is essential, otherwise some terms might be missed.

From the results, an interesting observation is that the antisymmetric modes participate in the response of the plate for grazing incidence acoustic wave. It is demonstrated that three or four modes will give converged RMS deflection. It is also found that the RMS maximum strain with temperature could be either smaller or larger than the one without temperature. This is due to that: (1) the temperature increases the thermal component, and (2) the thermal postbuckling deflection increases the nonlinear stiffness

which reduces the RMS deflection and it leads to smaller strain component. Uniform and nonuniform temperature distribution effect on random responses is investigated. The nonuniform temperature considered is that there is a temperature gradient along the edge of the plate. The results show that there is very little difference in random responses for the two temperature distributions studied. For plate with initial imperfection in deflection which has the same maximum deflection as the thermal postbuckling deflection, the plate with initial imperfection is stiffer and leads to smaller random responses.

Future improvements for grazing wave model and numerical integration methods are needed. The correlation study between numerical results and test results is very important if one wants to use this method to a practical problem.

REFERENCES

1. T.S. Atalik and S. Utku. "stochastic linearization of multi-degree-of-freedom nonlinear systems". *Earthquake Engineering and Structural Dynamics*, 4:411–420, 1976.
2. J. L. Batoz, K. J. Bathe, and L. W. Ho. "a study of three-node triangular plate bending elements". *International Journal for Numerical Methods in Engineering*, 15:1771–1812, 1980.
3. V. Birman and C. W. Bert. "buckling and postbuckling of composite plates and shells to elevated temperatures". *Journal of Applied Mechanics*, Vol. 60, pp. 514–519, 1993.
4. H. R. Busby and V. L. Weingarton. "response of nonlinear beam to random excitation". *Journal Engineering Mechanics Division, ASCE*, Vol. 99, pp.55–68, 1973.
5. C. T. Chen. "*Geometrically Nonlinear Random Vibrations of Structures*". PhD thesis, Purdue University, West Lafayette, IN, 1990.
6. C. T. Chen and T. Y. Yang. Geometrically nonlinear random vibrations of laminated composite plate. *Proceedings of the 8th International Conference of Composite Materials, Honolulu, HI*, July 15–19, 1991.
7. L. W. Chen and L. Y. Chen. "thermal postbuckling analysis of laminated composite plates by the finite element method". *Composite Structures*, Vol. 12, pp. 257–270, 1989.
8. L. W. Chen and L. Y. Chen. "thermal postbuckling behaviors of laminated composite plates with temperature-dependent properties". *Composite Structures Vol. 19*, pp.267–283, 1991.
9. R. Chen and Chuh Mei. "finite element nonlinear random response of beams to acoustic and thermal loads applied simultaneously". *Proceedings of 34th Structures, Structural Dynamics and Materials Conference*, AIAA-93-1427, 1993.
10. C. K. Chiang. "*A Finite Element Large Deflection Multiple-Mode Random Response Analysis of Complex Panels with Initial Stresses Subjected to Acoustic Loading*". Ph. D. Dissertation, Old Dominion University, Norfolk, VA., 1988.
11. B. Clarkson. "review of sonic fatigue technology". Technical report, NASA CR 4587, 1994.
12. B. L. Clarkson. "vibration of structures excited acoustically". *A lecture note at the University of Southampton*, 1986.

13. R. W. Clough and J. L. Tocher. Finite element stiffness matrices for analysis of plate bending. *Proc. Conf. on Matrix Methods in Structural Mechanics*, WPAFB, Ohio, 1965, pages 515–545, 1965.
14. N. N. Huang and T. R. Tauchert. “thermal buckling and postbuckling behavior of antisymmetric angle-ply laminates”. *Proc. Int. Symp. Composite Materials and Structures*, Beijing, People’s Republic of China, June 10–13, pp. 357–362, 1986.
15. C. Hwang and W. S. Pi. “nonlinear acoustic response analysis of plates using the finite element method”. *AIAA Journal*, Vol. 10, pp. 276–281, 1972.
16. J. Lee. “large-amplitude plate vibration in an elevated thermal environment”. *Applied Mechanics Review*, Vol. 46, No. 11., November, 1993.
17. L. Librescu, W. Lin, M. Nemeth, and Jr. Starnes, J. “effects of a thermal field on frequency-load interaction of geometrically imperfect shallow curved panels”. *Paper AIAA-94-1342 CP, Proceedings of the 35th AIAA/ASME/ASCE/AHS/ASC Structures, Structural Dynamics and Material Conference*, Hilton Head, SC, April 18–20, 1994.
18. L. Librescu and M. A. Souza. “postbuckling behavior of shear deformable flat panels under the complex action of thermal and in-plane mechanical loads”. *Proceedings of the AIAA/ASME/ASCE/AHS/ASC 32nd Structures, Structural Dynamics and Materials Conference*, AIAA Paper No. 91-0913, 1991.
19. J. E. Locke. “A Finite Element Formulation for the Large Deflection Random Response of Thermally Buckled Structures”. Ph. D. Dissertation, Old Dominion University, Norfolk, VA, 1988.
20. J. E. Locke and C. Mei. “a finite element formulation for the large deflection random response of thermally buckled beams”. *AIAA Journal*, Vol. 28, pp. 2125–2131, 1990.
21. C. Mei and C. B. Prasad. “effects of nonlinear damping on random response of beams to acoustic loading”. *Journal Sound Vibration*, Vol. 117, pp. 173–186., 1987.
22. C. Mei and C. B. Prasad. “effects of large deflection and transverse shear on response of rectangular symmetric composite laminates subjected to acoustic excitation”. *Journal Composite Materials*, Vol. 23, 1989, pp. 606–639.
23. C. Mei and H. F. Wolfe. “On Large Deflection Analysis in Acoustic Fatigue Design”. The Stephen H. Crandall Festschrift, Edited by I. Elishakoff and R. H. Lyon, Elsevier Science, 1986, pp. 279–302.

24. A. C. Meyers and M. W. Hyer. "thermally-induced geometrically nonlinear response of symmetrically laminated composite plates". *Composite Engineering*, Vol. 2, 1, pp. 3-20, January 1992,.
25. J. S. Mixson. "overview of acoustic fatigue activities at nasa langley research center". Technical report, AFWAL-TR-88-3034, Wright-Patterson AFB, pp. 573-591, July 1988.
26. A. K. Noor, J. H. Starnes Jr., and J. M. Peters. "thermo-mechanical postbuckling of multilayered composite panels with cutouts". *Paper AIAA-94-1367-CP, Proceedings of the 35th AIAA/ASME/ASCE/AHS/ASC Structures, Structural Dynamics and Material Conference, Hilton Head, SC*, April 18-20, 1994.
27. A. K. Noor and J. M. Peters. "multiple-parameter reduced based technique for bifurcation buckling and postbuckling analysis of composite plates". *International Journal for Numerical Methods in Engineering*, Vol. 19, pp. 1783-1803., 1983.
28. A. K. Noor, J. H. Jr. Starnes, and J. M. Peters. Thermoelastic buckling and postbuckling of multilayered composite panels. *33rd AIAA/ASME/ASCE/AHS/ASC Structures, Structural Dynamics and Materials Conference*, pp. 1052-1068, Dallas, TX, 1992.
29. D. B. Paul. Large deflections of clamped rectangular plates with arbitrary temperature distributions. Technical report, WPAFB, Ohio, AFFDL-TR-81-3003, Vol. I, Feb. 1982.
30. P. Pozefsky, R. D. Blevins, and A. L. Laganelli. "thermo-vibro-acoustic loads and fatigue of hypersonic flight vehicle structure". Technical report, AFWAL-TR-89-3014, Wright-Patterson AFB, February 1989.
31. C.B. Prasad and C. Mei. "multiple mode large deflection random response of beams with nonlinear damping subjected to acoustic excitation". AIAA 11th Aeroacoustics Conference, Paper 87-2712. Sunnyvale, CA, October 1987.
32. J.B. Roberts and P.D. Spanos. "random vibration and statistical linearization". *John Wiley & Sons, New York, NY*, 1990.
33. J. H. Robinson. "finite element formulation and numerical simulation of the large deflection random response of laminated composite plates". Master's thesis, Old Dominion University, Norfolk, VA, 1990.
34. J. H. Robinson. "variational finite element tensor formulation for the large deflection random vibration of composite plates". *32nd AIAA/ASME/ASCE/AHS/ASC Structures, Structural Dynamics and Materials Conference*, pp. 3008-3016, Baltimore, Maryland, 1991.

35. Lora Robinson, J. An accurate four-node stress plate bending element. *International Journal for Numerical Methods in Engineering*, pages 296–306, Vol. 14, 1979.
36. P. Seide and C. Adami. “dynamic stability of beams in a combined thermal-acoustic environment”. Technical Report AFWAL-TR-83-3027, WPAFB, OH, October 1983.
37. Gajbir Singh. Nonlinear bending, vibration and buckling of composite beams and plates. *Ph. D. Thesis, Department of Aerospace Engineering, Indian Institute of Technology Kanpur*, March 1993.
38. A. Tessler and T. J. R. Hughes. A three-node mindlin plate element with improved transverse shear. *Computer Methods in Applied Mechanics and Engineering*, pages 71–101, Vol. 50, 1985.
39. C. W. S. To. “random vibrations of nonlinear systems”. *The Shock and Vibration Digest*, Vol. 19, 1987.
40. R. Vaicaitis. “nonlinear response and sonic fatigue of surface panels at elevated temperatures”. *Workshop on Dynamics of Composite Aerospace Structures in Severe Environments, Southampton, UK*, July 1991.
41. R. Vaicaitis and R. Arnold. “time domain monte carlo for nonlinear response and sonic fatigue”. *13th AIAA Aeroacoustics Conference, Paper 90-3938, Tallahassee, FL*, October 1990.

APPENDICES

Appendix A

THE FORMULATIONS FOR $C_{\psi\psi ij}$'s

$$C_{\psi\psi 11} = \frac{1}{2}(y_{12}\xi_2 - y_{31}\xi_3)y_{23} \quad (\text{A.1})$$

$$C_{\psi\psi 12} = \frac{1}{2}(y_{23}\xi_3 - y_{12}\xi_1)y_{31} \quad (\text{A.2})$$

$$C_{\psi\psi 13} = \frac{1}{2}(y_{31}\xi_1 - y_{23}\xi_2)y_{12} \quad (\text{A.3})$$

$$C_{\psi\psi 14} = \frac{1}{2}(x_{13}\xi_3 - x_{21}\xi_2)y_{23} - \frac{1}{2}x_{21}\xi_1y_{31} + \frac{1}{2}x_{13}\xi_1y_{12} \quad (\text{A.4})$$

$$C_{\psi\psi 15} = \frac{1}{2}(x_{21}\xi_1 - x_{32}\xi_3)y_{31} - \frac{1}{2}x_{32}\xi_2y_{12} + \frac{1}{2}x_{21}\xi_2y_{23} \quad (\text{A.5})$$

$$C_{\psi\psi 16} = \frac{1}{2}(x_{32}\xi_2 - x_{13}\xi_1)y_{12} - \frac{1}{2}x_{13}\xi_3y_{23} + \frac{1}{2}x_{32}\xi_3y_{31} \quad (\text{A.6})$$

$$C_{\psi\psi 21} = \frac{1}{2}(y_{12}\xi_2 - y_{31}\xi_3)x_{32} - \frac{1}{2}x_{21}\xi_1y_{31} + \frac{1}{2}x_{13}\xi_1y_{12} \quad (\text{A.7})$$

$$C_{\psi\psi 22} = \frac{1}{2}(y_{23}\xi_3 - y_{12}\xi_1)x_{13} - \frac{1}{2}x_{32}\xi_2y_{12} + \frac{1}{2}x_{21}\xi_2y_{23} \quad (\text{A.8})$$

$$C_{\psi\psi 23} = \frac{1}{2}(y_{31}\xi_1 - y_{23}\xi_2)x_{21} - \frac{1}{2}x_{13}\xi_3y_{23} + \frac{1}{2}x_{32}\xi_3y_{31} \quad (\text{A.9})$$

$$C_{\psi\psi 24} = \frac{1}{2}(x_{13}\xi_3 - x_{21}\xi_2)x_{32} \quad (\text{A.10})$$

$$C_{\psi\psi 25} = \frac{1}{2}(x_{21}\xi_1 - x_{32}\xi_3)x_{13} \quad (\text{A.11})$$

$$C_{\psi\psi 26} = \frac{1}{2}(x_{32}\xi_2 - x_{13}\xi_1)x_{21} \quad (\text{A.12})$$

Appendix B

THE ELEMENT MATRICES

Linear stiffness matrix

$$[k]_{\psi} = \int_A [C_b]^T [D] [C_b] dA \quad (\text{B.1})$$

$$[k]_{\psi m} = \int_A [C_b]^T [B] [C_m] dA \quad (\text{B.2})$$

$$[k]_{m\psi} = \int_A [C_m]^T [B] [C_b] dA \quad (\text{B.3})$$

$$[k]_m = \int_A [C_m]^T [A] [C_m] dA \quad (\text{B.4})$$

Linear stiffness matrix due to $w_o(x,y)$

$$[k_o]_b = \int_A [C_{\psi b}]^T [\theta_o]^T [A] [\theta_o] [C_{\psi b}] dA \quad (\text{B.5})$$

$$[k_o]_{b\psi} = \int_A [C_{\psi b}]^T [\theta_o]^T [B] [C_b] dA + \int_A [C_{\psi b}]^T [\theta_o]^T [A] [\theta_o] [C_{\psi \psi}] dA \quad (\text{B.6})$$

$$[k_o]_{bm} = \int_A [C_{\psi b}]^T [\theta_o]^T [A] [C_m] dA \quad (\text{B.7})$$

$$[k_o]_{\psi b} = \int_A [C_b]^T [B] [\theta_o] [C_{\psi b}] dA + \int_A [C_{\psi \psi}]^T [\theta_o]^T [A] [\theta_o] [C_{\psi b}] dA \quad (\text{B.8})$$

$$\begin{aligned} [k_o]_{\psi} = & \int_A [C_{\psi \psi}]^T [\theta_o]^T [B] [C_b] dA + \int_A [C_b]^T [B] [\theta_o] [C_{\psi \psi}] dA \\ & + \int_A [C_{\psi \psi}]^T [\theta_o]^T [A] [\theta_o] [C_{\psi \psi}] dA \end{aligned} \quad (\text{B.9})$$

$$[k_o]_{\psi m} = \int_A [C_{\psi \psi}]^T [\theta_o]^T [A] [C_m] dA \quad (\text{B.10})$$

$$[k_o]_{m\psi} = \int_A [C_m]^T [A] [\theta_o] [C_{\psi\psi}] dA \quad (\text{B.11})$$

Linear stiffness matrix due to $\{N_{\Delta T}\}$

$$[k_{N\Delta T}]_b = \int_A [C_{\psi b}]^T [N_{\Delta T}] [C_{\psi b}] dA \quad (\text{B.12})$$

$$[k_{N\Delta T}]_{b\psi} = \int_A [C_{\psi b}]^T [N_{\Delta T}] [C_{\psi\psi}] dA \quad (\text{B.13})$$

$$[k_{N\Delta T}]_{\psi b} = \int_A [C_{\psi\psi}]^T [N_{\Delta T}] [C_{\psi b}] dA \quad (\text{B.14})$$

$$[k_{N\Delta T}]_{\psi\psi} = \int_A [C_{\psi\psi}]^T [N_{\Delta T}] [C_{\psi\psi}] dA \quad (\text{B.15})$$

Linear stiffness matrices due to $\{N_o\}$

$$[k_{N_o}]_b = \int_A [C_{\psi b}]^T [N_o] [C_{\psi b}] dA \quad (\text{B.16})$$

$$[k_{N_o}]_{b\psi} = \int_A [C_{\psi b}]^T [N_o] [C_{\psi\psi}] dA \quad (\text{B.17})$$

$$[k_{N_o}]_{\psi b} = \int_A [C_{\psi\psi}]^T [N_o] [C_{\psi b}] dA \quad (\text{B.18})$$

$$[k_{N_o}]_{\psi\psi} = \int_A [C_{\psi\psi}]^T [N_o] [C_{\psi\psi}] dA \quad (\text{B.19})$$

First-order nonlinear stiffness matrix

$$[n1]_{b\psi} = \int_A [C_{\psi b}]^T [\theta]^T [B] [C_b] dA \quad (\text{B.20})$$

$$[n1]_{bm} = \int_A [C_{\psi b}]^T [\theta]^T [A] [C_m] dA \quad (\text{B.21})$$

$$[n1]_{\psi b} = \int_A [C_b]^T [B] [\theta] [C_{\psi b}] dA \quad (\text{B.22})$$

$$[n1]_{\psi\psi} = \int_A [C_b]^T [B] [\theta] [C_{\psi\psi}] dA + \int_A [C_{\psi\psi}]^T [\theta]^T [B] [C_b] dA \quad (\text{B.23})$$

$$[n1]_{\psi m} = \int_A [C_{\psi\psi}]^T [\theta]^T [A] [C_m] dA \quad (B.24)$$

$$[n1]_{mb} = \int_A [C_m]^T [A] [\theta] [C_{\psi b}] dA \quad (B.25)$$

$$[n1]_{m\psi} = \int_A [C_m]^T [A] [\theta] [C_{\psi\psi}] dA \quad (B.26)$$

First-order nonlinear stiffness matrix due to $w_o(x,y)$

$$[n1_o]_b = \int_A [C_{\psi b}]^T [\theta]^T [A] [\theta_o] [C_{\psi b}] dA + \int_A [C_{\psi b}]^T [\theta_o]^T [A] [\theta] [C_{\psi b}] dA \quad (B.27)$$

$$[n1_o]_{b\psi} = \int_A [C_{\psi b}]^T [\theta]^T [A] [\theta_o] [C_{\psi\psi}] dA + \int_A [C_{\psi b}]^T [\theta_o]^T [A] [\theta] [C_{\psi\psi}] dA \quad (B.28)$$

$$[n1_o]_{\psi b} = \int_A [C_{\psi\psi}]^T [\theta]^T [A] [\theta_o] [C_{\psi b}] dA + \int_A [C_{\psi\psi}]^T [\theta_o]^T [A] [\theta] [C_{\psi b}] dA \quad (B.29)$$

$$[n1_o]_{\psi} = \int_A [C_{\psi\psi}]^T [\theta]^T [A] [\theta_o] [C_{\psi\psi}] dA + \int_A [C_{\psi\psi}]^T [\theta_o]^T [A] [\theta] [C_{\psi\psi}] dA \quad (B.30)$$

First-order nonlinear stiffness matrix due to $\{N_m\} (= [A] \{\epsilon_m^o\})$

$$[n1_{Nm}]_b = \int_A [C_{\psi b}]^T [N_m] [C_{\psi b}] dA \quad (B.31)$$

$$[n1_{Nm}]_{b\psi} = \int_A [C_{\psi b}]^T [N_m] [C_{\psi\psi}] dA \quad (B.32)$$

$$[n1_{Nm}]_{\psi b} = \int_A [C_{\psi\psi}]^T [N_m] [C_{\psi b}] dA \quad (B.33)$$

$$[n1_{Nm}]_{\psi} = \int_A [C_{\psi\psi}]^T [N_m] [C_{\psi\psi}] dA \quad (B.34)$$

First-order nonlinear stiffness matrix due to $\{N_b\} (= [B] \{\kappa\})$

$$[n1_{Nb}]_b = \int_A [C_{\psi b}]^T [N_b] [C_{\psi b}] dA \quad (B.35)$$

$$[n1_{Nb}]_{b\psi} = \int_A [C_{\psi b}]^T [N_b] [C_{\psi\psi}] dA \quad (B.36)$$

$$[n1_{Nb}]_{\psi b} = \int_A [C_{\psi\psi}]^T [N_b] [C_{\psi b}] dA \quad (\text{B.37})$$

$$[n1_{Nb}]_{\psi} = \int_A [C_{\psi\psi}]^T [N_b] [C_{\psi\psi}] dA \quad (\text{B.38})$$

Second-order nonlinear stiffness matrix

$$[n2]_b = \frac{3}{2} \int_A [C_{\psi b}]^T [\theta]^T [A] [\theta] [C_{\psi b}] dA \quad (\text{B.39})$$

$$[n2]_{b\psi} = \frac{3}{2} \int_A [C_{\psi b}]^T [\theta]^T [A] [\theta] [C_{\psi\psi}] dA \quad (\text{B.40})$$

$$[n2]_{\psi b} = \frac{3}{2} \int_A [C_{\psi\psi}]^T [\theta]^T [A] [\theta] [C_{\psi b}] dA \quad (\text{B.41})$$

$$[n2]_{\psi} = \frac{3}{2} \int_A [C_{\psi\psi}]^T [\theta]^T [A] [\theta] [C_{\psi\psi}] dA \quad (\text{B.42})$$

Linear stiffness matrix due to shear

$$[k_s]_b = \int_A [C_{\gamma b}]^T [A_s] [C_{\gamma b}] dA \quad (\text{B.43})$$

$$[k_s]_{b\psi} = \int_A [C_{\gamma b}]^T [A_s] [C_{\gamma\psi}] dA \quad (\text{B.44})$$

$$[k_s]_{\psi b} = \int_A [C_{\gamma\psi}]^T [A_s] [C_{\gamma b}] dA \quad (\text{B.45})$$

$$[k_s]_{\psi} = \int_A [C_{\gamma\psi}]^T [A_s] [C_{\gamma\psi}] dA \quad (\text{B.46})$$

Load vectors

$$\{p_{\Delta T}\}_m = \int_A [C_m]^T \{N_{\Delta T}\} dA \quad (\text{B.47})$$

$$\{p_{No}\}_m = \int_A -[C_m]^T \{N_o\} dA \quad (\text{B.48})$$

$$\{p_{\Delta To}\}_b = \int_A [C_{\psi b}]^T [\theta_o]^T \{N_{\Delta T}\} dA \quad (\text{B.49})$$

$$\{p_{Noo}\}_b = - \int_A [C_{\psi b}]^T [\theta_o]^T \{N_o\} dA \quad (\text{B.50})$$

$$\{p_{\Delta T o}\}_\psi = \int_A [C_{\psi \psi}]^T [\theta_o]^T \{N_{\Delta T}\} dA \quad (\text{B.51})$$

$$\{p_{Noo}\}_\psi = - \int_A [C_{\psi \psi}]^T [\theta_o]^T \{N_o\} dA \quad (\text{B.52})$$

$$\{p_{\Delta T}\}_\psi = \int_A [C_b]^T \{M_{\Delta T}\} dA \quad (\text{B.53})$$

$$\begin{aligned} \{p_p\}_b &= \int_A [H_w]^T p(x, y, t) dA \\ &= \frac{1}{2\pi} \int_{-\infty}^{\infty} P(\omega) e^{i\omega t} \int_A e^{-\frac{i\omega x}{a} \sin \lambda} [H_w]^T dA d\omega \\ &= \frac{1}{2\pi} \int_{-\infty}^{\infty} P(\omega) \{Y(\omega)\} e^{i\omega t} d\omega \end{aligned} \quad (\text{B.54})$$

$$\begin{aligned} \{p_p\}_\psi &= \int_A [H_{w\psi}]^T p(x, y, t) dA \\ &= \frac{1}{2\pi} \int_{-\infty}^{\infty} P(\omega) e^{i\omega t} \int_A e^{-\frac{i\omega x}{a} \sin \lambda} [H_{w\psi}]^T dA d\omega \\ &= \frac{1}{2\pi} \int_{-\infty}^{\infty} P(\omega) \{Y_\psi(\omega)\} e^{i\omega t} d\omega \end{aligned} \quad (\text{B.55})$$

(For Eqs. (2.107) and (2.108) see Ref.[Clarkson])

Mass matrix

$$[m]_b = \int_A [H_w]^T \rho h [H_w] dA \quad (\text{B.56})$$

$$[m]_{b\psi} = \int_A [H_w]^T \rho h [H_{w\psi}] dA \quad (\text{B.57})$$

$$[m]_{\psi b} = \int_A [H_{w\psi}]^T \rho h [H_w] dA \quad (\text{B.58})$$

$$[m]_\psi = \int_A [H_{w\psi}]^T \rho h [H_{w\psi}] dA \quad (\text{B.59})$$

$$[m]_m = \int_A ([H_u] + [H_v])^T \rho h ([H_u] + [H_v]) dA \quad (\text{B.60})$$

LIST OF SYMBOLS

a, b	lengths of a plate
$[A],[B],[D]$	laminate extensional, extension-bending and bending stiffnesses
c	acoustic wave traveling speed
$[C]$	the matrices relating slope and curvature with displacements
E	Young's modulus
$E[]$	expected value
$\{e\}$	linearization error vector
$\{f\}, \{\tilde{f}\}$	modal force vector of coupled and uncoupled modal equations
$\{g(\{q\})\}$	the stiffness term of the modal equations of motion
G	shear modulus of the materials
$H_j(\omega)$	single degree of freedom transfer function
$[H]$	shape function matrices
h	thickness of plate
$[K]$	linear stiffness
$\{M\}$	resultant moments per unit length acting on a laminate
$[M]$	mass matrix
$\{N\}$	resultant forces per unit length acting on a laminate
$[N1], [N2]$	the first and second order nonlinear system stiffness matrices
$\{P\}$	nodal load vector
$\{q\}$	coupled modal coordinate vector
$[Q]$	lamina reduced stiffness
$\{R\}$	resultant shear forces per unit length acting on a laminate
t	time
u, v	inplane displacement
w	lateral displacement
x, y, z	Cartesian coordinates
Greek Symbols	
α	thermal expansion coefficient and shear correction factor
ΔT	temperature distribution
$\{\epsilon\}, \{\gamma\}$	strain vector

ζ	damping ratio
η	uncoupled modal coordinates
$\theta, [\theta]$	acoustic wave incident angle, and as defined in Eq. (2.26)
$[\phi]$	modal matrix
ψ_x, ψ_y	rotations of the normal around x and y axes due to bending only
Ω	equivalent linear frequency
ω_n	linear frequency of the deformed structure
Subscripts	
b	bending
m	membrane
N _b	stiffness matrices due to {N _b }
N _m	stiffness matrices due to {N _m }
N _o	stiffness matrices due to {N _o }
N _{ΔT}	stiffness matrices due to {N _{ΔT} }
o	quantity related with initial displacement
T	tangent stiffness
ΔT	thermal